Forschungszentrum Karlsruhe
Technik und Umwelt

Wissenschaftliche Berichte
FZKA 5756

PREMIX, Documentation of the Results of Experiments PM01 to PM06

F. Huber, A. Kaiser, M. Steinbrück, H. Will

Institut für Reaktorsicherheit
Projekt Nukleare Sicherheitsforschung

März 1996

Forschungszentrum Karlsruhe
Technik und Umwelt

Wissenschaftliche Berichte

FZKA 5756

PREMIX, Documentation of the Results of Experiments PM01 to PM06

F. Huber
A. Kaiser
M. Steinbrück
H. Will

Institut für Reaktorsicherheit

Projekt Nukleare Sicherheitsforschung

Forschungszentrum Karlsruhe GmbH, Karlsruhe
1996

Als Manuskript gedruckt

Forschungszentrum Karlsruhe GmbH
Postfach 3640, 76021 Karlsruhe

ISSN 0947-8620

Abstract

A series of so-called PREMIX experiments is being performed in which the mixing behaviour is investigated of a hot alumina melt which is discharged into water. The tests are part of a multi-lateral programme carried out in support of the licencing procedure of future light water reactors (LWR). The programme, which aims at the safety of the reactor, includes relevant experiments and the numerical simulation by computer codes. The parameters of the first experimental series were: melt masses of 10 and 20 kg, released through nozzles of 40 and 56 mm in diameter, respectively, the type of melt discharge, a slender size of the water pool, and the degree of sub-cooling. The phenomena of mixing can well be described by means of both high speed and video films and a variety of measurements. The results show that it is the period up to about 0.4 to 0.5 s in which the decisive processes of premixing occur.

The very first material release generally occurs as single droplets. In three of the first six tests, a more or less compact stream of melt formed soon after that. In the other tests, the spray-type discharge of melt continued. A funnel-shaped interaction region is formed in the water pool. Its radial and axial growth rates are determined by the discharge mode and mass flux of the melt. A vapour explosion did not occur. The test results are well suited to be used in the verification and validation of computer models.

The results of the measurements and the post-test examination of the debris give an indication of a possible inherent limitation of the masses involved in premixing. Consequently, the probability of a steam explosion to occur would also be limited. This limitation is anticipated to occur in two stages: (1) The bulk portion of the water is displaced far enough by the growing interaction region and is, by this process, prevented from taking part immediately in the thermal interaction. Vapour is the continuous phase in the interaction region. (2) In case of a compact melt stream, the major part of the melt quickly flows down through the interaction region. The fragmentation and heat transfer processes are by far not finished when the melt arrives at the bottom where it cumulates.

PREMIX,
Dokumentation der Ergebnisse der Versuche PM01 bis PM06

Zusammenfassung

In einer Reihe von Versuchen, den sogenannten PREMIX-Experimenten, wird der Ablauf des Vermischungsvorgangs untersucht, der nach dem Einleiten einer heißen Aluminiumoxidschmelze in Wasser beginnt. Die Versuche sind Teil eines multi-lateralen Programms, das die Lizensierung künftiger Leichtwasserreaktoren (LWR) unterstützt. Dieses Programm, das auf die Sicherheit des Reaktors gerichtet ist, umfaßt sowohl aussagefähige Experimente als auch die numerische Simulation eines Unfallablaufs durch Rechenprogramme. Die Parameter der ersten Versuchserie waren: Schmelzemassen von 10 und 20 kg, die aus Öffnungen mit einem Durchmesser von 40 bzw. 56 mm flossen, die Form des Schmelzestroms, eine schlanke Gestalt des Wasserbehälters und das Maß der Wasserunterkühlung. Der Ablauf der Vermischung wird durch Filmaufnahmen (Hochgeschwindigkeits- und Videofilme) sichtbar gemacht und ist durch eine Vielfalt an Meßsignalaufzeichnungen nachvollziehbar. Es zeigt sich, daß die entscheidenden Vermischungsvorgänge nach etwa 0,4 bis 0,5 Sekunden abgeschlossen sind.

Das erste Schmelzematerial tritt gewöhnlich als Einzeltropfen aus. In dreien der ersten sechs Versuche entsteht kurz danach ein mehr oder weniger kompakter Schmelzestrahl, in den anderen drei Versuchen ein Sprühstrahl. Im Wasser bildet sich eine trichterförmige Interaktionszone aus, deren axiale und radiale Wachstumsrate vom Massenfluß der Schmelze bestimmt werden. Eine Dampfexplosion trat nicht auf. Die Versuchsergebnisse sind für die Verifizierung und Validierung von Computermodellen gut geeignet.

Die Meßergebnisse und die Nachuntersuchung der Fragmente geben einen Hinweis auf eine mögliche Selbstbeschränkung der an der Vorvermischung beteiligten Massen (Schmelze und Wasser). Diese würde wiederum die Wahrscheinlichkeit vermindern, daß eine Dampfexplosion auftritt. Die Selbstbeschränkung könnte in zwei Phasen ablaufen: (1) Die Hauptmasse des Wassers wird durch das Anwachsen der Interaktionszone weit genug von deren Innerem und damit vom Interaktionszentrum ferngehalten. Die kontinuierliche Phase in der Interaktionszone ist Dampf. (2) Bildet sich ein kompakter Schmelzestrahl aus, fließt der Hauptteil der Schmelze rasch durch die Interaktionszone nach unten. Die Fragmentierung und die Wärmeübertragung sind bei weitem noch nicht beendet, wenn die Schmelze den Boden erreicht und dort kumuliert.

Table of Contents

List of the Tables

List of the Figures

1. Introduction

Future nuclear power stations in Germany will be licenced only if proof can be provided that the consequences of all severe reactor accidents are restricted to the reactor building itself /1/. This rule entails precautionary design measures and plausible engineering judgments that are based on both relevant experiments and the numerical simulation by computer codes. The tests reported herein are part of an experimental programme designed to contribute to these goals.

Investigations of severe accidents in light-water reactors (LWR) show that a melt-down of the core may occur due to a loss of coolant /2/. It is expected that the corium melt is at first retained by crusts. These crusts may break due to decay heat generation, allowing the melt to drain downward into the lower calotte of the pressure vessel. This cavity is still filled with water at or near saturation conditions. The melt will possibly be released in the form of streams created by the holes of the lower grid plate. A typical diameter of the holes is 80 mm. Though precautionary design measures are undertaken to make this scenario unlikely, the probability has to be taken into consideration of a steam explosion to occur during the penetration of the melt into the water.

A hot melt which is poured into water will undergo coarse fragmentation due to hydro- and thermodynamic interactions. Coarse mixing is indispensable for an energetic steam explosion. Both the masses and the actual conditions (i. e. the temperatures or the degrees of fragmentation and dispersion) of the materials involved define the starting conditions and, by this, the energetics of a steam explosion.

Research work in this field is done at several laboratories /3-5/. It also includes the development of computer codes (e.g. IVA-KA, cf. /4/) which are used to describe the multi-phase interaction of a hot melt and water. Information is still needed about the phenomena that dominantly control the premixing for an effcient verification of the various computer models. Furthermore, quantitative results are required for code validation, such as pressure build-up, steam production rate, growth of the interaction region, and masses involved. Code development at FZK is done within a collaboration of two groups at the INR and IRS institutes.

PREMIX is the name of an experimental FZK/IRS programme in which the mixing behaviour is investigated of a hot alumina melt which is discharged into water. The reason why we use a simulating material are strong safety directions which make tests with "real" melt materials, i. e. corium, extremely difficult and expensive. By using simulating materials, we are following common experiences.

Those tests, if performed in a proper parameter range (e.g. temperature, melt masses), are deemed to be well suited for the investigation of the questions put. Computer codes that have been verified by those experiments will take over afterwards the task of providing the proof necessary for licencing.

Of course, tests with melt masses in the order of several tons can not be performed. The main goals of the first series of experiments that was carried out with 10 and 20 kg of melt are:

- *To demonstrate the feasibility of the test procedure.* Although the design of the melt generator was tested in advance, proof had to be provided of making available the desired melt mass within the time scheduled.
- *To prove the applicability of the experimental apparatus.* Prior to the performance of tests with larger melt masses knowledge is required about both the suitability of the test apparatus and the reliability of the instrumentation.
- *To demonstrate the good chance of reaching the final goal.* This goal is premixing of a hot melt in a water pool without the occurrence of a steam explosion. In persuing this goal, the various parameters have to be altered to find out their influence on the test results.

This step is necessary prior to the start of a second, more expensive series of experiments in which larger melt masses (20 to 50 kg) are applied. It should be mentioned, again, that the investigation of the steam explosion itself is not a goal of these experiments.

In the present report, five tests with 10 kg and one test with 20 kg of melt are documented. The data should primarily be regarded as a source for the development of computer codes.

2. Experimental set-up and test procedure

A vertical cylindrical vessel (PREMIX test vessel) is the major part of the test apparatus (Fig. 2.1). Four venting pipes and a gas supply system are connected to the top of the vessel. The test apparatus is housed in the so-called FAUNA pressure vessel. This large containment is a protective barrier against the consequences of a steam explosion. The main components inside the PREMIX test vessel are the water pool in the lower part, the melt generator in the upper part, and the gas compartment (short: gas space) which comprises the space between the water surface, the melt generator, and the vessel wall. The cameras are mounted at the

outer periphery of the FAUNA vessel. The registration units and controllers are housed in an adjacent building. The various parts are described in detail in the following sub-sections.

2.1 Melt generation

For obvious reasons, the material used to simulate the corium melt should be a metal oxide. We use an alumina melt which is generated by a thermite reaction:

$$8\,Al + 3\,Fe_3O_4 \rightarrow 4\,Al_2O_3 + 9\,Fe + 3732\,J/g$$

The large exothermic energy would lead, for the stoichiometric mixture, to a temperature which is calculated to be well above the boiling temperature of iron. This is about 3020 K at standard pressure. To prevent boiling and, subsequently, a even more violent chemical reaction, 4% of mass of alumina are added to the stoichiometric mixture:

$$8\,Al + 3\,Fe_3O_4 + xAl_2O_3 \rightarrow (4 + x)Al_2O_3 + 9\,Fe$$

$$215{,}76\,g + 694{,}56\,g + 36{,}41\,g \rightarrow 444{,}17\,g + 502{,}56\,g$$

Such a composition will theoretically result in a temperature of 3050 K. It is known, however, that even in the equilibrium state, such a reaction does not reach completeness. Furthermore, the aluminium partly evaporates during the reaction. Comparisons of results from a computer programme which calculates chemical equilibrium and of post experiment investigations of the reactants show that the incompleteness of the chemical reaction is about 5 to 10% (see section 3.3). The temperature calculated under this condition is about 2780 K. Part of the enthalpy is lost to the crucible. Because of the high temperature of the melt, part of the liner of the crucible melts and is mixed to the melt. This part in general is magnesia. Taking this loss into account, the actual melt temperature is estimated to be about 2600 K.

The melt temperature was measured by use of a pyrometer in pretests and has been measured since test PM03. These measurements indicate that a value of 2600 K for the melt temperature is, in fact, the best estimate.

The reaction products, alumina and iron, separate during the reaction due to their different densities. This effect is used to keep the iron in the generator and to release only the oxidic melt into the water pool. Because of the incompleteness of the separation a small portion of iron is still remaining in the oxide melt frac-

tion, however. From post test examinations of the debris (cf. section 3.3) the following melt composition is supposed to be given:

Al_2O_3	81 %
FeO	10 %
MgO	6 %
Fe	3 %

The melt generator is shown schematically in Fig. 2.2. In principle, it is a closed vessel whose top is connected to a gas supply and venting system. The outlet nozzle and a small annular compartment designated to collect the separated iron are connected to the bottom of the crucible. Both the outlet nozzle and the small compartment are closed by metallic foils, initially. Three sensors (D1 - D3) are installed at various axial positions in the outlet nozzle to detect the passage of the melt.

The walls of the generator and the small container are protected against melt attack by a liner consisting of mainly magnesium oxide.

The thermite reaction is started at the top of the mixture by means of four electrical igniters. The generator is vented during the reaction to allow the smoke generated by the evaporation of impurities and the adsorbed gas to escape without notable pressure increase.

The signal from the D1 melt detector indicates the arrival of the melt front at the bottom of the generator. At this time, the annular foil melts through. The iron which has been largely separated from the alumina flows into the small container. The thermite reaction proceeds into the nozzle. After a preset delay time which is started by the signal of the D1 melt detector, the valve in the venting pipe is closed and that of the gas storage tank is opened.

When the melt front in the nozzle reaches the D2 melt detector, the high speed cameras and part of the data recording systems are started. One to two seconds later, the melt reaches the lower foil which is destroyed within less than one millisecond. The melt release starts. This event is indicated by the D3 melt detector. The signal is used to start the fast transient recorders.

The output capacity of the melt generator described is just under 10 kg of oxide melt. It can be increased up to 20 kg by increasing the height of the generator.

2.2 Test apparatus

As mentioned, the test apparatus consists of a cylindrical part and four venting tubes (Fig. 2.3). The vessel is 700 mm in diameter and 3000 mm in height. It is closed except for the venting tubes. The four tubes are 100 mm in diameter and act as exits for the steam generated during the interaction. The test vessel has rows of plain glass windows at the front and at the rear which extend over almost the whole axial height. They enable both illumination of the interaction region by backlight and high-speed photography. Furthermore, six round glass windows are mounted laterally on both sides.

The vessel is partitioned in height (two parts) due to manufacturing reasons. The horizontal partition plane defines the origin of the axial z-coordinate. All axial coordinates given in the figure and mentioned in the text are related to this plane. For example, the melt release mouth is at +113 mm, the water level was at -85 mm in the first experiment.

An intermediate bottom plate (fragment catcher) is mounted inside the apparatus whose axial height is one of the test parameters. It defines the distance by which the melt can penetrate into the water. In tests PM02 to PM06, the bottom was mounted at -1800 mm and was equipped with a grid which enables the collection of particles at well defined radial and azimuthal positions.

A small external loop which contains an electrical heater, a pump, and a filter is connected to the water pool. Together with heaters fixed to the outer surface of the apparatus, the loop allows to establish the desired water temperature. All parts of the test vessel located above the water level are heated to a temperature which exceeds the saturation temperature by about 15 K in order to prevent steam condensation.

2.3 FAUNA vessel

The 220 m^3 FAUNA pressure vessel, formerly used for experiments on sodium fires and concrete interaction, is used as an outer container. It has a design pressure of 1 MPa. This feature allows to perform experiments at higher system pressures later on. It is expected that a higher system pressure will essentially influence the interaction of a hot melt and water. The tests described in the present report were performed at ambient pressure only.

2.4 *Instrumentation*

The test apparatus is extensively instrumented with various types of measuring devices. Part of the instrumentation, mostly thermocouples, is used in the performance of the experiment. The instrumentation (cf. Table 2.1) consists of the following parts.

- Pressure transducers are distributed over the axial height of the vessel measuring in the water pool as well as in the gas/steam space. The sensitive areas of the probes are mounted flush with the inner surface of the vessel. Generally, piezo-electric pressure transducers were applied which record the dynamic pressure. The absolute pressure was additionally recorded from test PM04 on by a strain gauge pressure transducer.
- The absolute pressure and the temperature are measured in the venting lines. Both values are used in the calculation of the steam quality.
- The driving pressure measured in the thermite generator is also used to determine the duration of melt release.
- The melt temperature is measured by a pyrometer. Although the measurement is disturbed soon after the melt release by smoke and steam, it gives sufficient information. The pyrometer pre-settings are calibrated on the basis of experiences gained from several pre-tests.
- The steam flow meters mounted in the venting tubes are of the vortex type. They are the fastest acting flow meters known. The calibrated output signal is proportional to the flow velocity. Unfortunately, the flow meters are very sensitive to a change in the phase of the fluid. This can occur, in the actual case, when the steam flow changes into a two-phase flow with water droplets.
- Level indicators record the rise of the water level at four (in PM01 at two) positions, thereby giving additional information on the flatness of the water surface. These probes only measure the "net water column", this means that gas or steam bubbles contained in the water do not contribute to the signals.
- Several lances positioned at various axial levels protrude from the vessel wall into both the water and the gas space (Fig. 2.3). The lances are equipped with up to eight void sensors and with a thermocouple at their ends. The sensors are mounted at equal radial distances and indicate whether there is water or no water at the location of the sensor tips.
- High-speed photography is used to register the phenomena of the experiment. The self-illumination of the melt is superabundant for exposure of the

films. Strong back-lightening allows to distinguish on the films between bubbles, liquid droplets, and melt droplets. This is mainly true for the outer region of the projected interaction region. Normally, three cameras are operated with 2000 frames/s while different kinds of films (black and white or colour) and filters are used and various image areas are chosen.

- Up to two video cameras are used additionally to the film cameras. Especially, they allow a quick look on events occurring during the test, and they observe areas that are not covered by high speed photography.

More details concerning the instrumentation, especially the qualification of the measuring devices in meeting the requirements, are given in Appendix A.

Besides the instrumentation listed, there are also measuring devices around the melt generator as described in section 2.1. These are mostly used to check the correct burning of the thermite and to trigger both the pressurisation of the reaction vessel and the start of the registration units (see section 2.6). Knowledge about the time history of the chemical reaction allows to estimate the physical properties of the melt at its first contact with the water.

2.5 Experimental conditions and test procedure

The experimental conditions are summarized in Table 3.1 together with some calculated data. The conditions comprise both preset and measured data. Preset data are: the composition and mass of the thermite mixture, the driving pressure inside the melt generator, the water temperature, and the height of the outlet nozzle above the water surface. Variations in the latter value are due to varying losses of water occurring during the heat-up period prior to the test. Variations in the duration of melt release are inherent to the stochastic course of the thermite reaction.

The test is started by igniting the thermite. The generation of the melt is described in detail in section 2.1. A piece of information should be given here already. As a matter of fact, the melt-through of the foil in the outlet starts locally; therefore, the initial melt release occurs as droplets and as small jet. The full size of the jet, i. e. the approximate internal diameter of the nozzle, is reached after some tens of milliseconds.

2.6 Data evaluation procedure

2.6.1 Data recording and processing

The signals of the measuring devices are amplified and converted to normalized signals, typically being 0 to 10 V corresponding to a preset range. These data are registered by transient recorders, analog tape recorders, digital data tape and data logger. All registrating units including the high speed cameras are synchronized by the aid of a real time online clock.

The start of the registration units is performed partly by hand (analog tape), partly automatically by specific events (transient recorders, digital data tape, data logger and cameras).

To prevent a loss of data the most important signals are picked up twice. The expected information could generally be obtained though, in a few cases, data were lost by failure of a measuring device or a registration unit.

2.6.2 Data evaluation procedure

All experimental data collected have to be considered together in order to get a clear picture of the course of events that have taken place in an experiment. The pressure time histories, the spatial growth of the multiphase interaction zone, the water level increase, and the flow rate of the steam which leaves the interaction zone are the major sources of information for a data base that can also be used for computer code verification. To make the comparison of the various tests easier, zero time in the data evaluation is defined as the instant when a substantial mass of molten material the first time hits the water surface. Single leading drops are not taken into consideration.

The interaction zone is defined as the region outside which, laterally and downwards, only liquid water is present (Fig. 2.4). The upper boundary of the interaction region is given by the water level. It is assumed that the water rises in form of an annulus close to the vessel wall and that the surface is plane. This assumption was verified in all tests to be valid in general.

The volume of the interaction region can be written as the sum of three partial volumes, given by the following equation:

$$V_I = V_{v,I} + V_{\ell,I} + V_{m,I} \qquad (2.1)$$

where $V_{v,I}$ and $V_{\ell,I}$ are the volumes of vapour (i. e. steam) and liquid water, respectively; $V_{m,I}$ is the volume of the melt.

V_I and $V_{m,I}$ can be determined from the measurements, the volume of the vapour by use of a second equation:

$$V_{v,I} = \Delta L\, A_V - V_{m,I} + V_{v,exit}\, \frac{\rho_v}{\rho_\ell} \qquad (2.2)$$

This equation is obtained from a balance of the volumes of the water and melt involved in the thermal interaction, by neglecting small contributions. A comprehensive deduction is given in Appendix B. The first summand in eq. (2.2) is the product of the water level increase and the cross sectional area of the water pool. The third summand accounts for the volume of the steam that has left the test vessel through the venting pipes. This summand does not play an important role in the first period of the experiment as the quotient ρ_v/ρ_ℓ is very small.

The progress of the interaction zone into the water pool and the increase of the water level can be seen in the video recording and film takes. Information about the level increase is also obtained from the level measurements. Alternatively, the development of the interaction zone can be constructed by use of the information given by the characteristic changes in the void and temperature signals. An example is given in Fig. 3.2;15 which shows the void signals obtained from the uppermost lance positioned in the water pool.

The pictures provided by video recording only draw a two-dimensional image. The void measurement is equally unable to provide a really three-dimensional picture because of the limited number of sensors. As a first approximation, rotational symmetry of the interaction boundary related to the vessel axis is therefore assumed in the calculation of the volume of the interaction region.

The evaluation based on void sensor signals is performed by use of the MATHCAD computer software [6]. Various measured data are taken as an input. A short description of the procedure is given in Appendix C.

2.6.3 Post-test debris recovery and methods of analysis

The fragmented debris produced during the melt-water interactions were gathered as complete as possible. The grid inside the intermediate bottom allowed to evaluate distributions in mass and particle size. However, it was obvious from visual inspection that there was no significant local distribution neither in mass or in particle size, so this investigation was performed just at one test.

After drying, the debris were separated by sieve analysis into size fractions. For that purpose, a vibrating apparatus and a stack of 8 sieves with opening 10 mm, 5 mm, 2 mm, 1 mm, 500 µm, 250 µm, 125 µm and 63 µm were used. The debris of test PM01 were partly separated into magnetic and non-magnetic particles by means of a permanent magnet and later on analysed individually.

The debris were examined by light optical microscopy and scanning electron microscopy (SEM) to define the shape and the structure. For cross-sectional photos, the samples were cut with a diamond saw, embedded into a two-component epoxy resin under vacuum (to fill the pores), and ground/polished down to 1 µm.

The chemical composition was determined by energy dispersive X-ray spectroscopy (EDX) and X-ray fluorescent analysis (XFA). EDX spectroscopy allowed to make point analyses on phases identified with the electron microscope. XFA delivers more integral results. For that method, representative samples were powdered and, after separation of metal particles, molten with a special salt mixture. The SEM/EDX investigations were performed at the University of Karlsruhe (Laboratorium für Elektronenmikroskopie) and the XFA analyses were done at the Institut für Materialforschung (IMF-I) at FZK.

X-ray diffraction (XRD) was used to determine the phase composition of various debris of tests PM01, PM02 and PM06. This study could be carried out in the XRD laboratory of the IMF-I institute. Again, only representative samples were examined, which were powdered and measured with Cu-K_α-radiation from $2\theta = 10°$ to $2\theta = 70°$ (step size: 0.02°, measuring time: 3 s). For qualitative phase analysis, the yielded diagrams were compared with corresponding JCPDS-files (Joint Commitee on Powder Diffraction Standards).

Furthermore, the density of the particles was determined by the buoyancy method with an analytical balance. For that purpose, only unbroken debris (with a closed shell) of different sizes were taken to avoid penetration of water into the particles.

The measurement of the liquidus and solidus temperature of the oxidic slag by differential thermal analysis (DTA) failed, probably because of too a small energetic effect on the melting of the slag. Therefore, the melting point (or range) was estimated by remelting tests performed with some specimen in a high temperature furnace step by step at intervals of 50 K. These investigations were performed by the Frauenhofer-Institut für Keramische Technologien und Sinterwerkstoffe (IKTS), Dresden.

Up to now, the debris produced in tests PM01 and PM02 was analysed very extensively, whereas only a few methods were applied to analyse the fragments of PM03 to PM06. As the thermite generation was identical for all tests, the properties of the corresponding debris were shown to be quite similar. Of course, if there is need, further investigations will be done.

3. Test Results and Discussion

As an introduction, the general course of events during a test is given. Afterwards, the six single tests are described in detail and the results are discussed of the post-test debris examination. The chapter is closed by summarising the experimental experience.

3.1 General course of the interaction

As outlined before, the very first material release occurs in the form of single droplets which are followed by a shower of droplets. Soon after that, a more or less compact stream of melt flows out. The velocity of the leading drops is much higher than that of the stream; it can be estimated from the film pictures. The discharge velocity of the compact stream is calculated by use of a small computer programme to be about 6 m/s. The result of the calculation is checked by comparison with the duration of melt release which can be estimated from the film takes and pressure measurements.

On hitting the water surface, the melt particles are strongly decelerated. Initially, a shallow interaction zone is formed, whose boundary can easily be seen on the films. The succeeding mass of melt penetrates into the water at axial rates of up to 4 m/s. The comparison of this value with the calculated one (6 m/s), leads to the conclusion that the melt stream is largely fragmented in its leading part. A funnel-shaped channel is formed and the displaced water causes the pool level to increase.

The evaporation rate, which is very low initially, increases steeply after about 100 ms. This behaviour is due to both the increasing rate of melt entering the interaction region and the advancing fragmentation process.

The water level rises slowly at the beginning of interaction. A little later than the evaporation rate, it increases rapidly, by this contributing to the pressure increase in the gas room. Finally, the water hits against the top of the test vessel. The impact is not violent because of the two-phase nature of the rising water. Water also penetrates into the steam venting lines causing the steam velocity to slow down markedly.

The last period of the experiment is characterized by continuous violent boiling coming from the fragmented alumina settled on the bottom plate.

3.2 Test results

For each test, the course of events is described and the relevant signals recorded are shown. Information of a higher grade obtained by the combination of a variety of signals is also included for four tests. The starting conditions are listed in Tab. 3.1.

3.2.1 Test PM01

Data registration was triggered only about 200 ms after the first melt particles had penetrated into the water. This happened due to an unexpectedly slow increase of the trigger D2. About 3.5 kg of melt had already entered the interaction region at that time.

Fig. 3.2;1 and 3.2;2 show the pressure time histories measured in the gas room and underneath the water surface, respectively. It should be mentioned that the amplitudes recorded by the piezo pressure transducers are too low in this test and the following two tests. Nevertheless, the pressure readings are shown because the characteristic changes in the profiles help to identify the course of events.

The measurement of one of the three well-operating vapour flow meters is given in Fig. 3.2;3 as an example. The signals of the flow meters are nearly identical. The flow rate shows three relative maxima, as the pressure curves do, with a maximum flow rate of 0.7 m^3/s. The reading shows a strong oscillation, which is attributed to the effect of water drops hitting the vortex bar of the measuring instrument. The signal decreases to zero at about 0.75 s, probably because the flow contained too large a volume fraction of water droplets. The total flow rate was estimated by extrapolating the sum of the three measurements available and integrated (see Fig. 3.2;4).

The signals of the two level indicators available in this test show similar behaviour among each other (Fig. 3.2;5) thus indicating that the water surface rose evenly. The maxima are in phase with those of the pressure measurements. As a matter of fact, the level measured is smaller than the true level of the water surface if there are steam bubbles mixed in the rising water. The reason is that the measuring device sums up only the liquid portion across the measured length. This find-

ing is supported by the measurements of the void sensors also mounted in the gas room from test PM03 on.

The time histories of the volume of the interaction region and of the volume that corresponds to the level swelling are shown in Fig.3.2;6. The information was obtained by the evaluation of video pictures (see section 2.6.2) since no void measurements were available in test PM01. The measuring tips had been eroded by the demineralized water. The difference of both curves is equal to the volume of liquid water drops in the interaction zone, if it is assumed that the contributions of both the steam and the melt are negligible (compare the expositions given in Appendix B).

The figure shows that, up to about 0.160 s, the volume fraction of the water in the interaction region is small; afterwards, it increases markedly. This result is supported by the film pictures. The melt is seen to fall like a stone into the water initially, producing a relatively narrow interaction region. Afterwards the interaction becomes more violent. Steam generation and water under-mixing increase, enhancing in turn the violence of the interaction. The variations in time of the partial volumes of the interaction region are shown in Fig. 3.2;7.

The evaluation of the volumes of water, steam and melt includes an error (about $\pm$ 5 %) because of the assumptions made. At any rate, the tendency depicted in the graphs should be secure.

A loss of 62 dm^3 in the water volume was stated after the test. This volume exceeds by far the volume that could be evaporated theoretically by the enthalpy of the melt. This means that liquid water was expelled through the venting pipes as droplets. Evidence for this is also given by the readings of the flow meters as mentioned before. The drop in the flow meter signals coincides with the maximum of the water level measurement. These events are observed in all following test.

3.2.2 Test PM02

The second experiment was performed with the same parameters as PM01 except for those of the water. Special attention was paid to a safe triggering of the recording system, so that data are available also for the time prior to melt release.

The water was heated to boiling conditions. Due to the experiences of the first test normal drinking water was used instead of demineralized water. This condition entailed another disadvantage, however. During heating-up, calcium carbonate precipitated which acted as nucleons for tiny vapour bubbles. Thereby,

stray light prevented neither details of the thermal reaction nor the extension of the interaction region to be visible in the film takes and video recording.

Figs. 3.2;8 and 3.2;9 show the time histories of the pressures measured at seven different axial positions in the gas space. The pressures start to rise at 0.08 s. The pressure maxima are as low as in PM01.

The pressure recorded in the water is given in Fig. 3.2;10. The pressure profile is very similar to and the amplitude is as low as those measured in the gas room.

The flow meter signals are similar in their shapes and amplitudes. One signal is shown in Fig. 3.2;11. The flow rate starts to rise at 0.105 s, i. e. earlier than in PM01. It reaches about the same maximum value as in PM01. The measurement is disturbed at 0.6 s, a little earlier than in PM01. The integrated flow rate and the steam velocity are shown in Figs. 3.2;12 and 3.2;13, respectively. The level measurements presented in Fig. 3.2;14 show that the water rises evenly.

From this test on, data are available from the void sensors. Examples are given in Fig. 3.2;15. As outlined previously, the signals are used to construct the development of the interaction region in axial and radial directions. The result of the evaluation which also includes the time histories of

- the speed of penetration,
- the melt volume entering the interaction region,
- the total and partial volumes, and
- the volume fractions

is shown in Figs. 3.2;16 - 3.2;21.

The progression of the interaction boundary into the water pool (Fig. 2.2;16) seems reliably represented by the isochrones up to about 400 ... 500 ms. After that time, the information obtained from the void sensors becomes unclear. This is valid for all experiments. The reason is that the displaced water moving upward at the periphery of the interaction region becomes permeated with steam bubbles, which had originated from lower parts of the interaction region. The extension of the interaction region can no longer be determined in the sense of the original definition.

The rate by which the melt front penetrated downwards in the centre of the vessel is illustrated in Fig. 3.2;17. The data which are obtained from the thermocouples and the innermost void sensors show a rather steady progression. The dia-

gram on the right hand side gives approximate values for the velocity of penetration.

To properly evaluate the total volume and the partial volumes of the interaction region, especially in the initial phase, the volumetric flow of the melt had to be approximated by a function which is shown in Fig. 3.2;18. The steam that leaves the test vessel (labeled as "vexit" in Fig. 3.2;20) proves to be negligible in the calculation of the three partial volumes. The upper limit of the interaction region and with it the total volume can be reliably determined only up to about 300 - 350 ms. After that time, the rising water penetrates into the gap between the melt generator and vessel wall. The boundary between the water which will occupy the outer part of the annular cross section and the steam flow can no longer bedetermined exactly.

In the discussion of the averaged volume fractions of the melt, liquid water, and steam inside the interaction zone (Fig. 3.2;21), one should keep in mind that:

(i) The measurement of level increase, which initially gives very low signals, has been approximated in its first part by a smooth curve. This curve, labelled with "ΔL" in Fig. 3.2;19, starts from zero level, increases slowly, and joins the measurement about at the start of the very steep level increase (90 ms).

(ii) The mass of melt entering the interaction region is represented in the calculation by an equation of fourth degree (compare Appendix C).

Anyhow, the result seems quite reasonable. Let us start the discussion with the melt: The scattered melt drops hit the water surface and produce steam whose volume is smaller than that of the melt. The melt volume fraction is relatively important at the beginning, but soon decreases to insignificant values due to the rapid growth of the interaction region. The vapour volume fraction decreases with the melt volume fraction initially. Consequently, the liquid volume fraction increases and takes on very large values. These large values are due to the widespread (horizontal) area of interaction formed at the start. After about 100 ms, the fractions of the vapour and the liquid run in opposite directions taking on quite different values; in this context, the large value of the vapour volume fraction is remarkable.

3.2.3 Test PM03

The third experiment was performed with a subcooling of 5 K to investigate the influence of subcooling on the delay time between the events "first material pen-

etrates the water surface" and "onset of pressure increase". The other parameters (see Table 3.1) were identical to those of tests PM01 and PM02.

The melt release started in the form of drops as usual. Soon afterwards, a compact stream established. About 3 ms after the stream had reached the water surface it became blasted along its way down through the gas room. The reason is not yet clear. It may be that gas was enclosed in the melt and expanded, or a small amount of nonreacted thermite was released with the melt and reacted later on. An indication of the latter assumption may be the comparatively short time interval between the D2 detector signal and the start of melt release.

From this experiment on, the melt temperature was measured (Fig. 3.2;22). The pyrometer sensing spot was positioned at - 65 mm, i.e. a short distance above the water surface. The initial temperature spikes are caused by leading melt drops. The signal rises several milliseconds after the first melt/water contact (t = 0). This means that the very first melt drops probably bypassed the sensing spot which is about 10 mm in diameter. The peak temperature was 2473 K. Since the pyrometer always measures the surface temperature, the bulk temperature should have been higher. After the fourth signal peak, the measurement was obviously disturbed by steam and by the impact of melt, which eventually destroyed the lenses of the system.

Because of the spray-type material release, the energy input per unit of time into the water was larger than in the experiments before. In fact, it was planned to vary this parameter later in the PREMIX test series, but not in this experiment.

The violence of reaction or, to be more precise, the growth rate of the interaction region was larger than in the preceding tests as one can see in the measurements of the

- pressures (Figs 3.2;23 and 3.2;24),
- steam flow and steam volume (Fig. 3.2;25), and
- level increase (Fig. 3.2;26).

The larger initial enthalpy input per unit of time is also visible in Fig. 3.2;27 where the growth of the interaction region and the time history of the liquid volume fraction (both evaluated from video pictures) are shown together with the results of the two preceding tests.

The development of the interaction region evaluated from the void signals is drawn in Fig. 3.2;28 (the presentation has to be confined to time 300 ms because the void sensors mounted below level -465 mm had failed just before the start of

the test). The growth rate is markedly larger, especially in radial direction, if it is compared with that of PM02 (Fig. 3.2;16). This result is attributed to the spray-type melt discharge in test PM03.

The low pressures measured in the first three experiments gave rise to the performance of separate calibration tests (see Appendix A).

3.2.4 Test PM04

In this test the conditions of PM03 were repeated: subcooling of 5 K and 10 kg of melt at about 2600 K. The measurements are given in Figs. 3.2;29 to 3.2;35. From this test on, the setting of the pressure transducers is correct.

The relatively high pressure values measured in the gas space after time 0.2 - 0.3 s are puzzling because they are not reflected in corresponding reactions of the water level and steam flow rate. The inspection of the high speed colour films revealed that a portion of nonreacted thermite was released at 0.065 s. At that time, a compact stream of melt had just formed at the nozzle outlet and a significant amount of melt had already entered the interaction region. The thermite reacted suddenly, caused a burst of the melt stream, and produced a cloud of hot smoke. Presumably, this event has caused the steep increases in the gas pressure measurements.

The evaluation of the measurements by the MATHCAD procedure (progression of the interaction region, rate of penetration, etc.) are shown in Figs. 3.2;36 to 3.2;41. The scattered discharge of the melt obviously influences the development of the interaction region. The comparison with the result of test PM02 (Fig. 3.2;16) shows that the rate of growth in radial direction is much larger in test PM04. The penetration velocity (Fig. 3.2;37) and the time histories of the volume fractions (Fig. 3.2;41) are comparable to those in test PM02 (see Figs. 3.2;17 and 21, respectively).

The results of the calibration tests (compare Appendix A) led to the additional application of a strain-gauge pressure transducer. Fig. 3.2;31 shows that all pressure signals agree exactly up to 0.280 s. The differences after that time are most probably due to both local effects (such as the different distances from the interaction region) and differences in the performance characteristics which are inherent in the piezo pressure transducers. The result gives evidence of the reliability of the measurements.

3.2.5 Test PM05

The measurements of the melt temperature, pressures, steam flow rates and level changes are available from the beginning. They are given in Figs. 3.2;42 to 3.2;48. Unfortunately, no video and film takes are available for this test because an unexpected course of the thermite reaction caused a mess in the trigger chain (compare Appendix D). Only one video camera, applied in this test for the first time to observe the outlet of a venting tube, operated correctly. The test results are discussed in the following. Because of the lack of visual information, zero time in this test is set arbitrarily.

In order to have a link to earlier pressure transducer operation, one amplifier (PK10 in Fig. 3.2;44) was set as in the first three tests The comparison is among the signals show that only the absolute values are much too small whereas the pressure fluctuation frequency is correct.

The steam volume flow (Fig. 3.2;46) increases about 0.04 s later than the pressure. Again, the flow rate signals decrease considerably long before the time when the pressures reach their maxima. This behaviour was also observed in the preceeding tests. On the other hand, the video film shows steam leaving the venting tubes for several seconds. From time 0.77 s on, water is seen to drain down the outlet part of the tube. It is assumed that a two-phase flow containing very fine droplets had been formed even much earlier. These droplets are not visible in the steam flow whose temperature was 373 K.

The level meters reach a maximum of 550 mm at about 0.4 s. Taking into account the measuring principle of the probe, it is assumed that the water front reached the entrances of the venting tubes just at that time.

The amount of water that drained out of the venting tubes is estimated to be a few liters. The major portion of the water loss, which is estimated to be about 78 dm^3, was obviously transported with the steam as droplets. If a homogeneous two-phase mixture is assumed, the average water fraction was $0.25 \cdot 10^{-3}$.

Although no visual information is available of the course of events, all measurements indicate a blasted melt release. It was decided to perform no post-test investigation, at least for the present.

3.2.6 Test PM06

The main differences in the test conditions compared to the foregoing experiments are as follows:

- The melt mass to be discharged was doubled. To keep the time of melt release approximately constant, the cross section of the outlet orifice was increased.
- Water separators were introduced in the venting pipes. These are barrels, having a cross section about 25 times larger than that of the venting tubes. They are equipped with baffles forcing the steam flow to change its direction twice by about 90°. The retained water is collected after the test.

The measurements shown in Figs. 3.2;49 to 3.2;55 indicate that the course of events was quite similar to those of the preceding tests. The melt temperature was 2500K (see Fig. 3.2;49). The maximum pressures (Figs. 3.2;50 and 3.2;51) underneath and above the water were 1.0 and 1.5 bar, respectively.

The progression of the interaction region, the rate of penetration, the melt flow, the time histories of the total and partial volumes, and the change in the volume fractions are shown in Figs. 3.2;58 to 3.2;63. The results of test PM06 can be best compared with those of PM02 because of a similar type of melt release.

The larger melt flow rate has an effect on the rate of melt penetration (compare Figs. 3.2;58 and 3.2;16). As reflected in the r-z profiles, the speed of axial penetration is not affected up to about 0.250 s. After that time, the axial penetration rate even increases in PM06 whereas it remains approximately constant in PM02. On the other hand, different growth rates of the interaction region can be stated in the radial direction from the beginning of interaction. The vessel wall is reached by the interaction boundary much earlier in the test with the larger mass flow rate.

The time history of the volume fractions in PM06 is different from that in PM02 in two items (compare Figs. 3.2;63 and 3.2;21):

1.The initial period, in which the liquid fraction increases, is shorter in PM06 (the low starting value, Ω0.1, is due to numerical effects resulting from the assumptions made).

2.The volume fractions of the vapour and the liquid approach average values of about 0.5 each after about 200 ms. I.e., the liquid fraction takes on larger values in PM06 than in PM02. This finding is in agreement with the larger growth rate in radial direction occurring from the beginning of interaction (see before). Presumably, this result is correlated with different time histories of the fragmentation processes: A thicker melt jet will fragment, on average, into larger particles which travel longer distances, also in radial direction, before they reach their final sizes.

The pressures above the water surface were significantly higher than those measured below in all preceding tests. Three possible effects could be the reason for this difference: the release of hot gases, radiation, and water impact. In an attempt to separate these effects, three of the pressure transducers were protected by a perforated cap and one was connected to the vessel wall by an elbow pipe filled with water. As one can see, these gauges approximately show the same values; i.e., the actual reason for the pressure difference cannot be stated yet.

It was in this test for the first time that the pressure in the test vessel increased so fast that it exceeded the driving pressure for a short period of time (see Fig. 3.2;52). Note that the piezo measurements, PK05 and PK09, fade; they should be as large as PK07. Of course, the sudden step in the driving pressure at 0.6 s can only occur after the melt has passed the nozzle. It seems that the melt release had just been finished when the pressures intersected. The duration of melt release is therefore deduced to be 0.60 s. The calculation in which a constant pressure difference is assumed predicts 0.50 s.

The steam flow rate is given in Fig. 3.2;53. Its average is higher by about 25% than in the preceding tests which were performed with half the melt mass. A second maximum in the flow rate formed at about 2.9 s (Fig. 3.2;54) was never recorded in former tests. This result is probably due to the new water separators which allow a consistent flow measurement for a period of time which is much longer than before. The integrated flow rate shows that this second maximum gives a larger contribution to the total steam volume measured compared to the first one. The steam velocity is depicted in Fig. 3.2;55. It reached a maximum of 140 m/s.

The meaning of the first flow maximum can be identified by the comparison of various measurements as given in Fig. 3.2;57. It seems that the leading flow increase is due to hot gas released with the melt. The gas expands and leaves the gas room by the venting pipes, together with the steam.

The integrated flow rate gives a total steam volume of 9 m^3 at the end of the first 10 seconds. This number is small compared with the volume of steam that can theoretically be generated by the melt (60 m^3, corresponding to 36 kg as listed in Table 3.2). On the other hand, the video film shows that the major part of the steam was released in that period of time.

A volume of about 0.071 m^3 of water was retained in the four water separators. About double this value, $\approx$0.135 m^3, was transported with the steam as droplets.

If a homogeneous two-phase mixture is assumed, the average water fraction is calculated to be $0.35 \cdot 10^{-3}$.

3.3 Post-test debris analysis

The appearance of the debris is very similar in all tests. It consists mainly of particles which are more or less spherical, grey in colour and sometimes a little bit rosty due to the presence of metallic iron. The surface of the debris is dense and smooth like a shell. The vast majority of the debris apparently solidified before reaching the bottom of the interaction vessel. In the test with 20 kg of melt, a small but significant amount of the melt froze on the bottom sticking together as a cake.

Some broken particles give the impression that most of the debris have a hollow or at least very porous structure. As an example, the debris as collected after test PM02 is shown in Fig. 3.3;1.

Some debris particles have a hole (cf. Fig. 3.3;2) which obviously was formed during the fragmentation process. Such hollow spheres are found above all among the smaller particles. Furthermore, it turns out that the larger the particle size the larger is the deviation from an ideal spherical shape.

3.3.1 Particle size distribution

The particle size distribution was determined for the tests PM01 - 04 and PM06. The results are compiled in Table 3.3;1 and summarised in Fig. 3.3;3. All tests with 10 kg show rather similar values. (1).

(1) One should not overvalue the difference found between PM01 on the one hand and PM02 - PM04 on the other. The larger debris of the first test was separated by means of self-made sieves (5,10 mm) whereas, starting with PM02, a complete sieve stack conforming to standards was used.

The fraction of debris particles larger than 10 mm is significantly larger in test PM06. This result may partly be due to the inclusion of the particles stuck together at the bottom of the test vessel. About 90 mass-%, or less, of the debris were larger than 2 mm in diameter. Table 3.3 also shows that the smaller particle fractions can not be neglected because they give a superproportional contribution to the overall surface. The mass mean diameter ranges from about 7 to 12 mm, the surface specific Sauter mean diameter, 6 V/A (with V=volume, A=surface), was found to be in the range between about 4 and 6 mm. The largest values are obtained for test PM06 performed with 20 kg.

Figure 3.3;4 presents views of typical nonmagnetic particles selected from the size fractions larger than 125 µm. The debris of the smaller size (< 5 mm) is almost ideally spherical, indicating that the particles had solidified before they reached the walls or the bottom plate.

It should be mentioned that part of the debris agglomerated and increased the larger-size fractions on the one hand, and larger fragments broke and entered smaller-size fractions on the other. Both effects which influence the result for a fraction, each in an opposite direction, can hardly be estimated. Up to now, the results of the sieve analysis have not been corrected.

Finally, it should be mentioned that a small part of the debris was entrained with the steam and transported out of the test vessel. These particles were not available for the sieve analysis in the tests PM01 - 04. In test PM06, such particles were caught in the water separator and were included in the sieve analysis.

3.3.2 Microscopy

Cross-sectional views of debris of different sizes are shown in Figs. 3.3;5 to 3.3;7. It seems to be obvious that the porosity of the particles is increasing with increasing debris size. Figure 3.3;8 shows one of the magnetic particles. A core of iron is completely surrounded by oxide material. No interactions took place between these two phases. The iron on the edge of an oxidic sphere (Fig. 3.3;9) was partly oxidised due to the reaction with water.

SEM investigations with high magnifications showed that the oxide phase is very uniform and homogeneous in most of the particles. Only small amounts of other phases were found apart from the main phase (see chapter 3.3.4)

3.3.3 Density

The density of about 40 particles each of various size was determined for the PM01 and PM02 debris. Every particle was checked with a magnet whether it was ferro-magnetic (iron inside !) or not. The results are summarised in Fig. 3.3;10. For both tests, the density of the debris was found to be between about 3.2 and 2.1 g/cm^3; it decreases with increasing particle size. This is conform with the impression obtained by microscopy.

A strong scatter was observed when analysing the magnetic particles. High density values were caused by large iron contents. The very low densities found for some particles may result from hydrogen production due to the reaction of iron and water during the fragmentation process leading to inflated debris.

Actually, such hollow particles with a hole as shown in Fig. 3.3;2 were found above all among the magnetic debris.

The high porosity (or low density, respectively) of the debris partly can be explained by a considerable volume shrinking of about 20 % during freezing of molten alumina /8/. Due to the cooling of a molten droplet from the outside, an outer solid shell is formed at first. This shell defines the shape of the debris and contains liquid oxide at the beginning, which shrinks at the phase transition solid/liquid, thus, creating pores. Because the ratio of surface to volume decreases with increasing diameter of a particle, larger particles have lower densities.

3.3.4 Chemical composition

The chemical composition of the debris produced in test PM01 was determined by energy dispersive X-ray spectroscopy while the samples were being photographed with the scanning electron microscope. A typical spectrum is shown in Fig. 3.3;11. In this way, a number of analyses of the "main phase" was obtained which were averaged to give the values compiled in Tab. 3.3;2. Apart from this main phase consisting of Al_2O_3, FeO, MgO, and MnO, a minor phase with large contents of SiO_2 and CaO was found in some samples.

Furthermore, the metal phase (Fig. 3.3;8 and 3.3;9) was analysed to be pure iron.

The compositions of one debris (10 mm) of test PM01 and of various debris produced in test PM02 were analysed by X-ray fluorescent analysis, which allowed to obtain a more integral measurement. As described above, the metal phase was separated after pulverization of the samples. The metal which was again analysed to be pure iron amounted to about 3-5 mass-%. The composition of the oxide phase in PM02 is very similar to that of PM01, as can be seen in Tab. 3.3;2.

Theoretically, the only products of the thermite reaction according to eq. (3.1) are alumina and iron.

$$10\,Al + 3\,FeO + 3\,Fe_3O_4 + x Al_2O_3 \rightarrow (5 + x)\,Al_2O_3 + 12\,Fe \qquad (3.1)$$

The left hand side of eq. (3.1) gives the composition of the thermite mixture used in all PREMIX tests. A portion of 4 mass-% of alumina was added to the stoichiometric mixture (corresponding to $x = 0{,}463$) in order to decrease the temperature of the melt and, thus, the potential of iron evaporation.

If the reaction does not go to completeness, e.g., due to local evaporation of aluminium eq. (3.2) can be written as:

$$(10 - z)\ Al + 3\ FeO + 3\ Fe_3O_4 + x\ Al_2O_3 \rightarrow (5 + x - \frac{z}{2})\ Al_2O_3 + (12 - \frac{3}{2}z)\ Fe + \frac{3}{2}z\ FeO \qquad (3.2)$$

And further, because Al_2O_3 and FeO tend to form a mixed oxide, namely hercynite:

$$(10-z)\ Al + 3\ FeO + 3\ Fe_3O_4 + x\ Al_2O_3 \rightarrow (5 + x - 2z)\ Al_2O_3 + (12 - \frac{3}{2}z)\ Fe + \frac{3}{2}z\ FeAl_2O_4 \qquad (3.3)$$

Equations (3.2) and (3.3) deliver an explanation for the FeO content found in the oxide phase. They can be used to calculate the conversion ratio of the thermite reaction from the results of chemical analysis, and vice versa. The presence of considerable amounts of oxygen gas during the thermite reaction, which would lead to similar effects, could be excluded.

The occurrence of MgO in the oxid phase is caused by partial solution and/or melting of the liner of the melt generator which consists mainly of MgO (93 %). The small part of MnO found in the debris is probably added by the producer of the thermite mixture which is normally used for welding of railroad rails to improve the quality of the steel.

3.3.5 Phase composition

X-ray diffraction was employed to determine the phase composition of the debris. Figures 3.3;12 and 3.3;13 show the X-ray diffraction patterns of several samples from PM01 and PM02.

The only phase which could be identified in all samples, even in the magnetic ones, is a cubic spinel phase with a lattice parameter of about a_o = 0,799 nm. This phase is a solid solution between γ-Al_2O_3 and the ternary oxides $FeAl_2O_4$ (hercynite), $MgAl_2O_4$ (spinel), and $MnAl_2O_4$ (galaxite), all crystallising in the cubic spinel structure.

Taking the compositions (in mol-%) given in Tab. 3.3;2 and the lattice parameters of the compounds (γ - Al_2O_3: 0.790 nm, $FeAl_2O_4$: 0.815 nm, $MgAl_2O_4$: 0.808 nm, and $MnAl_2O_4$: 0.826 nm) and applying Vegard's law, the theoretical lattice

parameter of the spinel phase can be calculated. The calculation gives $a_o = 0.799$ nm which is the same value as found experimentally.

Some of the X-ray diagrams show one or two additional peaks ($2\theta = 56.3°$ and 33,6°) which have not been identified yet.

3.3.6 Estimation of the liquidus temperature

The freezing temperature of the molten debris was estimated by remelting some samples of the tests PM01 and PM02 under Helium atmosphere. All samples remained unmolten at 2073 K. The visual inspection of the samples after heating up to 2123 K showed that they were molten.

Therefore, the freezing temperature of the debris is within the range of 2073 and 2123 K.

3.3.7 Estimation of temperature and enthalpy of the melt at release

The computer code equiTherm /9/ was used to determine the temperature and the enthalpy of the melt at the time of release /10/.

In principle, this code allows to calculate chemical equilibria of multi-component multi-phase mixtures at a given temperature and pressure. For the special purpose of calculating the temperature of the melt after thermite reaction (the adiabatic temperature of the reaction), the starting parameters were varied as long as, firstly, the calculated composition of the oxidic melt corresponded to the values obtained by chemical analyses, and, secondly, the energy balance of the whole process was zero.

Based on calculations with a heat conduction programme, the energy losses to the liner are assumed to be 3.2 MJ. Furthermore, a certain amount of MgO dissolved from the injector liner was included into the calculations. The presence of MnO was neglected.

As described above, the presence of FeO within the oxide melt is caused by an incomplete thermite reaction probably due to the evaporation of aluminium. Therefore, the parameter z defined in eq. (3.2) was varied between 0 and 0.1.

Some results of the calculations are compiled in Tab. 3.3;3.

The best agreement between calculation and chemical analysis was found for a degree of reaction between 92.5 and 95 %. This corresponds to a melt temperature of about 2500 - 2600 K and an enthalpy of about 3.9 MJ/kg.

3.4 *Summary of experimental experience*

During the design phase of PREMIX, it was not easy to predict the measuring ranges of the data. Results reported from other experimental programmes (see e.g. reference 5) were taken into account as far as possible. More often than not, different materials, geometries, and temperature ranges have been applied in those tests. From the present point of view, it can be stated, however, that the assumptions made to reach the experimental goal were largely correct. The experiences made with the various kinds of measurement are summarised as follows (for details see Appendix A).

The amplifier setting of the (piezo) **pressure transducers** applied in the first three tests proved to be inadequate because it provided too small signal amplitudes. It had been chosen under the assumption that the thermal interaction was rather violent. Comparison of measurements, simultaneously performed with an alternative (strain gauge) system and with altered amplifier settings, showed good agreement. From the fourth test on, correct pressure measurements have been obtained with an altered amplifier setting. Since the occurrence of a vapour explosion cannot totally be excluded in the PREMIX experiments, two pressure transducers are always operated with a much larger pressure range.

The steam flow meters have been chosen because of their fast response ability. The measuring principle was qualified in pretests. The sensibility of the flow meters on the entrainment of water droplets in the steam flow proved to be unexpectedly high, however. Marked signal decreases always started to occur when the water level had reached the lower ends of the venting pipes. We believe that the water drops disturb the formation of flow vortices. When the volume fraction of the droplets exceeds a certain value, the signal amplitude seriously decreases.

On the other hand, the amount of water that is transported by the steam out of the tests section is unexpectedly large. Water separators mounted in the venting pipes upstream of the steam flow meters extend the period of time (from 0.4 to about one second) in which a rather undisturbed flow rate measurement is possible. After one second, the period of interest is finished.

The **water level probes** are capacitive sensors consisting of an electric coil housed in a steel tube. The rising water level increases the wetted length of the probe and causes a variation in frequency. A quasi steady-state calibration procedure was applied to establish the relation between the level increase and the frequency measurement. As a matter of fact, the measuring errors are relatively large at the beginning of the tests, i.e., when the level increases are very small. To

obtain consistent results in the evaluation of both the volume of the interaction region and the volume fractions, the measurement has to be replaced in its initial part (up to 120 ms) by a smooth, slowly increasing curve which joins the starting point of steep level increase.

When starting the design of the test apparatus, we were not sure whether the thermal interaction would proceed more in axial or in radial direction at the leading edge of the melt jet. The results show that the axial growth rate is larger than the radial one, i.e., the decision to build a slender test vessel turns out to be correct. Additional effects are introduced by the type of melt discharge. E.g., the initial growth rate in radial direction is faster in case of a spray-type melt discharge than in case of a compact melt stream. In any case, it is not possible to predict the mode of melt discharge. Anyhow, two major types of melt discharge (compact stream and spray flow) anticipated to occur in a reactor accident have been represented in our tests.

Though reservations exist as for the accuracy of some of the measurements, the experimental data obtained are regarded to be well suited for the verification of computer models. The high-speed and video films provide additional information.

4. Summary and Conclusions

Six experiments have been carried out to date in which an alumina melt of 2600 K was discharged into water. The major test parameters were:

- melt masses of 10 and 20 kg,
- no sub-cooling and moderate sub-cooling, and
- the type of melt release.

The third parameter was not intended initially. It resulted from an irregularity occurring during the melt generation process. This deviation from the "normal" procedure points to the difficulty generally encountered to repeat a certain set of parameters exactly in another experiment. It is therefore necessary to perform numerous experiments and put together the various results afterwards.

The phenomena of mixing can well be described by means of visual recording (high speed photography and video) and the measurements of pressures, water level increase, steam production and the local changes of phase (liquid to steam and vice versa) both in the water pool and the gas room. The results show that it is the period up to about 0.4 to 0.5 s in which the decisive processes of premixing occur that determine whether or not there is an energetic thermal interaction. The time history of these processes is known to decide on the energetics set free in case of a steam explosion.

The very first material release occurs as single droplets that are followed by a shower of droplets. In three of the six tests, a more or less compact stream of melt formed soon after that. In the other tests, the spray-type discharge of melt continued.

When hitting the water surface, the melt particles are strongly decelerated. Initially, a shallow interaction region is formed. The succeeding mass of melt penetrates into the water at an axial rate of up to 3 to 4 m/s. This means that the melt stream that leaves the nozzle at an average speed of 6 m/s is fragmented at its leading edge at once. A funnel-shaped interaction region is formed, and the displaced water causes the water level to rise. The water level eventually hits on the top of the test apparatus. The water also penetrates into the steam venting pipes. The last period of an experiment is characterised by continuous violent boiling produced by the alumina particles which are accumulated on the intermediate bottom plate.

The small number of tests that have been performed until now, in concurrence with the difficulty mentioned in reproducing the parameters, makes a

comparison of the results more difficult. Nevertheless, the effect of one important test parameter, namely the melt mass flow rate, on the test results can be recognised. Moreover, the effects of two other parameters, the water sub-cooling and the mode of melt release, can be observed.

- In case of the larger melt flow rate, the speed of *axial* penetration is not affected during the first period of time, i.e. up to about 0.250 s. After that time, the axial penetration rate even increases in this case, whereas it remains approximately constant in the cases of lower mass flow rate. On the other hand, a larger growth rate of the interaction region can be stated in the *radial* direction in case of the larger melt flow rate already from the beginning of interaction. Another effect can be stated: the steam flow rate was about 25% larger in the case of the larger (i.e. double) melt flow rate.
- In case of a spray-type melt discharge, the initial growth rate of the interaction region in radial direction is much larger than in case of a compact stream (the melt flow rates being the same). On the other hand, the axial penetration velocities and the time histories of the volume fractions in both cases are comparable. In search for the reason for the spray-type melt discharge, it was found that a relatively high pressure existed in the gas room and that a small portion of thermite, obviously nonreacted, was released at 0.065 s.
- It is known from experience that sub-cooling influences only the first period of interaction. The degree of sub-cooling applied (2.5 K) seems to cause a larger steam production rate. This result may partly be due to the simultaneous occurrence of a spray-type melt discharge. Another effect can be stated which is connected to the steam production rate: the larger the subcooling, the faster is the water level increase. On the other hand, the maximum level measured is smaller in the tests with larger subcooling. This shows that the rising water contained a larger fraction of bubbles. The interaction can be described as more violent.

As for the mean volume fractions evaluated for the interaction region, the following information was gained. Showing a decreasing tendency at the start, the steam volume fraction soon increases due to both the increasing rate of melt entering the interaction region and the advancing fragmentation process. In the cases of a compact melt stream, the volume fractions of steam and liquid take on approximately constant values after about 0.2 s, while a comparatively large steam fraction can be stated for the smaller melt mass. Large steam volume

fractions were also measured in the middle and at the end of the 0.4-second time period in the case of a spray-type melt discharge.

Of course, the mean volume fractions give only a limited information. More detailed information, e.g. about the radial and axial distributions of the steam and water fractions for a given time, is expected to be obtained from the evaluation of the void signals which is still going on. Furthermore, the evaluation of the film pictures will enable a comparison with the results obtained from the void signals.

The pressure in the water pool was relatively small. The maxima did not exceed 1.0 bar. In all tests the pressures measured above the water surface were markedly higher than those measured in the water. Two processes are considered to be responsible for the difference: the release of hot gases from the source during melt release and thermal radiation from the melt.

The post test examination of the debris showed that part of the mass had reached the bottom still in a molten condition. In particular, this is true for the test with the larger melt flow rate where a portion of 47% of the large particle size (>10 mm) reached the pool bottom. This means that, on arrival of the melt at the bottom, the heat transfer process which is tightly connected to the fragmentation process is less advanced in case of a larger melt flow rate.

Considering the kind of melt used, the rather small melt masses applied, the geometrical conditions chosen, the small number of tests performed until now, and the status of evaluation which is still incomplete, the following *preliminary conclusions* can be drawn:

The test results are well suited for the identification of the physics that dominate the mixing. They can therefore be used for code verification. Moreover, they give an indication for a possible inherent limitation of the masses involved in premixing. Consequently, the thermal energy which is transformed into mechanical work in the case of a steam explosion will also be limited. It is anticipated that this limitation may occur in two stages:

1. Upon impact with water, the leading edge of the melt is fragmented and an interaction region is formed in which steam, melt fragments, and water particles are mixed. The bulk portion of the water is displaced far enough by the growing interaction region and is, by this process, prevented from taking part in the thermal interaction.

2. In case of a compact melt stream, the major part of the melt quickly flows down to the bottom of the pool through the interaction region. Under this

condition, the fragmentation and heat transfer processes are not finished when the melt arrives at the bottom.

The first item seems to be relevant in the reactor case where an immediate radial displacement of the water would take place due to the presence of the grid plate. Evidence for a behaviour as described in the second item is found in the test with the larger mass flow rate. Here, a considerable part of the melt reached the bottom of the water pool in a molten state and the fragmentation was very coarse. This means that only part of the energy stored in the melt was transferred during the passage through the actual interaction region. On the other hand, in case of a spray-type melt discharge, the melt particles had been solidified to a very high degree when they reached the bottom.

The tests will be continued next by varying the following, more relevant parameters: larger melt masses, a much smaller height of melt fall (a few millimeters only), and a smaller depth of the water. The other parameters, like a larger subcooling, and an increased ambient pressure, will be investigated afterwards.

5. Literature

/ 1 / H. H. Hennies, B. Kuczera,
Kooperative Weiterentwicklung der LWR-Sicherheitstechnik
(Cooperative Development of the LWR-Safety Technology, in German)
FZK-Nachrichten 4/95, pp. 246 - 255

/ 2/ Gesellschaft für Reaktorsicherheit mbH (GRS),
Deutsche Risikostudie Kernkraftwerke, Phase B,
Verlag TÜV Rheinland GmbH, Köln, 1990

/ 3/ G. Berthoud, Progress made in the area of molten fuel coolant interaction, Proceedings of the FISA-95 Symposium, EU Research of Severe Accidents, pp. 117-139, Luxemburg, November 20 - 22, 1995

/ 4/ H. Jacobs et al., Studies of principal processes during melt-water premixing, ibid., pp. 165-183.

/ 5/ D. Magallon et al., High temperature melt-water mixing: Results and calculations of FARO, PREMIX and MIXA experiments, ibid., pp. 140-164.

/ 6/ B. Paláncz, M. Jordán, Gy. Koczka, E. Strausz
Evaluation and Analysis Method for "PREMIX" Experiments on Molten Fuel Coolant Interaction, Part 2, Document 21.52-116-2/2, Institute for Electrical Power Research Co., Budapest, May, 1995

/ 7/ H. Will, unpublished report, 1995

/ 8/ P. Tyrolerova, W.-K. Lu, Volume Change on Freezing of Al_2O_3,
J. Am. Ceram. Soc., **52**, 77, 1969

/ 9/ Computerprogramm equiTherm, Dr. W. Schmidt,
VCH Scientific Software, Münster, 1993

/10/ M. Steinbrück, unpublished reports, 1995

Acknowledgement

This work is performed under the sponsorship of and partly funded by the European Community, SIEMENS, and a consortium of german utility companies.

The authors express their thanks to all colleagues who have contributed to perform the experiment, to evaluate the results, to the interpretation and conclusion, and to write this report.

Table 2.1: Instrumentation; characteristic data and number of probes and recording devices that worked properly

		PM01	PM02	PM03	PM04	PM06
Pressure transducers						
in water		4	3	5	5	5
Range of measurement	MPa	0.5	0.5	0.5	0.5	0.5
Transfer frequency	kHz	63	22	22	22	22
in gas volume		5	7	5	5	6
Range of measurement	MPa	0.5	0.5	0.5	0.5	0.5
Transfer frequency	kHz	63	22	22	22	22
Level indicators		2	4	4	4	4
Flow meters		3	4	4	3	4
Lances with void sensors						
in water pool		0	10	4	8	8
in gas room		0	0	2	2	5
High speed camera		2	1	2	3	3
Video camera		1	2	2	2	2

Table 3.1: Experimental conditions

		PM01	PM02	PM03	PM04	PM06
MELT						
mass						
nominal	kg	10	10	10	10	20
found after the test	kg	9.32	9.44	9.19	9.05	20.16
temperature						
measured with pyrometer	K	-	-	2473	2600	2500
recalculated from post experiment findings	K	2600	2600	2600	2600	2600
driving pressure difference						
preset	MPa	0.080	0.080	0.080	0.080	0.080
measured	MPa	0.078	0.085	0.085	0.075	0.092
outlet diameter [1]	mm	45	45	45	45	60
height of fall	mm	198	163	180	185	198
velocity						
leading drops	m/s	8.5	8.4	3.0	5.3	∽ 10
compact stream (calculated)	m/s	6.35	6.3	6.3	6.3	6.35
duration of release	s	0.565	0.45	1.20	1.09	0.57
WATER						
characteristic property		demineral.	drinking	demineral. +salt	demineral. + salt	demineral. + salt
temperature	K	371	373	368	368	371
subcooling	K	2.5	0	5	5	2
mass	kg	712	750	745	743	720
initial level	mm	- 87	- 55	- 67	- 72	- 82
depth till bottom	mm	1560	1590	1580	1570	1560

[1] In fact, the real diameter diminishes by about 4 - 5 mm due to crust formation

Table 3.2 Test results

PREMIX experiment no		1	2	3	4	5 [1]	6
Water sub-cooling	K	2.5	0	5	5	5	2
Melt							
Mass discharged	kg	9.323	9.435	9.189	9.055	≈ 9	20.158
Principal kind of release	-	compact	compact	spray	spray	-	compact
First temperature increase	s	-	-	0.014 [2]	- 0.017 [3]	- 0.081 [2]	0.016 [2]
Marked pressure increase	s	0.220	0.080	0.060	0.090	- 0.052	0.125
Steam production							
Start of flow increase	s	0.218	0.105	0.070	0.084	- 0.025	0.072
Maximum flow rate	m^3/s	2.70	3.00	3.80	3.30	3.90	5.00
Loss of water	dm^3	62	80	89	73	104	246
Mass of water that could be evaporated by the melt	kg	17.5	18	17	17	17	36
Characteristics of interaction region							
Rate of axial progression	m/s	1.5 - 3	1.5 - 3	1.5 - 2	1 - 3	-	1.5 - 3
Remarks		[4]	[4]	[4]		no films	

1) Arbitrary zero time for PM05

2) Pyrometer just above the water surface

3) Pyrometer 135 mm above the water surface

4) Pressure measurements not reliable

Tab. 3.3; 1: Results of the sieve analysis. The various shares within the size spectrum are correlated with the fractions of total mass and total surface of debris

Opening of mesh [mm]	Mass-% / Surface-%				
	PM01	**PM02**	**PM03**	**PM04**	**PM06**
10	21.3 / 5.5	32.2 / 8.2	38.9 / 13.8	37.2 / 12.3	46.8 / 15.7
5	42.7 / 22.1	35.5 / 19.4	35.8 / 25.4	36.2 / 24.0	33.2 / 25.0
2	24.4 / 27.1	21.9 / 25.6	19.5 / 29.5	19.9 / 28.2	14.8 / 27.9
1	8.1 / 21.1	6.9 / 18.7	4.2 / 14.8	4.7 / 15.6	3.7 / 13.7
0.5	2.7 / 14.0	2.5 / 13.8	1.2 / 8.3	1.5 / 9.8	1.1 / 8.1
0.25	0.6 / 6.6	0.7 / 7.6	0.3 / 4.0	0.4 / 5.5	0.3 / 4.1
0.125	0.1 / 2.7	0.2 / 3.5	0.1 / 3.5	0.1 / 2.5	0.1 / 2.6
0.063	< 0.1 / 1.0	0.1 / 3.2	< 0.1 / 0.7	< 0.1 / 2.1	< 0.1 / 2.9
Mass Mean Diameter [mm]	7.4	8.9	9.3	9.1	11.6
Sauter Mean Diameter [mm]	3.9	4.1	5.3	5.0	5.6
Overall Mass [kg]	9.323	9.435	9.189	9.055	20.158
Overall Surface [m^2]	4.8017	4.6116	3.4644	3.6493	7.1610

Tab. 3.3; 2: Chemical composition of the debris produced in tests PM01 and PM02

Test	Oxide	Mass-%	At-%	Mixed Oxide	Mass-%	At-%
PM01 (a)	Al_2O_3	81.3	71.2	Al_2O_3	48.4	59.6
	FeO	12.4	15.4	$FeAl_2O_4$	29.9	21.6
	MgO	5.6	12.5	$MgAl_2O_4$	19.9	17.5
	MnO	0.6	0.9	$MnAl_2O_4$	1.8	1.3
PM01 (b)	Al_2O_3	81.0	69.9	Al_2O_3	46.6	57.3
	FeO	10.3	12.7	$FeAl_2O_4$	25.1	18.1
	MgO	5.6	16.5	$MgAl_2O_4$	26.8	23.6
	MnO	0.7	0.7	$MnAl_2O_4$	1.4	1.0
PM02 (b)	Al_2O_3	82.4	71.0	Al_2O_3	48.9	59.2
	FeO	9.1	11.1	$FeAl_2O_4$	21.9	15.6
	MgO	7.9	17.2	$MgAl_2O_4$	27.8	24.2
	MnO	0.6	0.7	$MnAl_2O_4$	1.4	1.0

a) Results obtained by EDX

b) Results obtained by XFA

Tab. 33; 3: Temperature, enthalpy, and chemical composition of the oxide melt at release time calculated with equiTherm (1)

Starting Assumption	T_{melt} [K]	ΔH [MJ/kg]	Chemical Composition [Mass-%]		
			Al_2O_3	$FeAl_2O_4$	$MgAl_2O_4$
100 % Al reacted	2730	4.4	75.7	4.3	20.1
95 % Al reacted	2579	4.0	59.2	21.4	19.4
92.5 % Al reacted	2506	3.9	50.5	31.0	19.0
90 % Al reacted	2437	3.7	41.1	40.3	18.6
92,5 % Al reacted no heat losses	2604	4.0	50.5	31.0	19.0

(1) A more detailed discussion of the chosen parameters and the equiTherm code are given in /10/

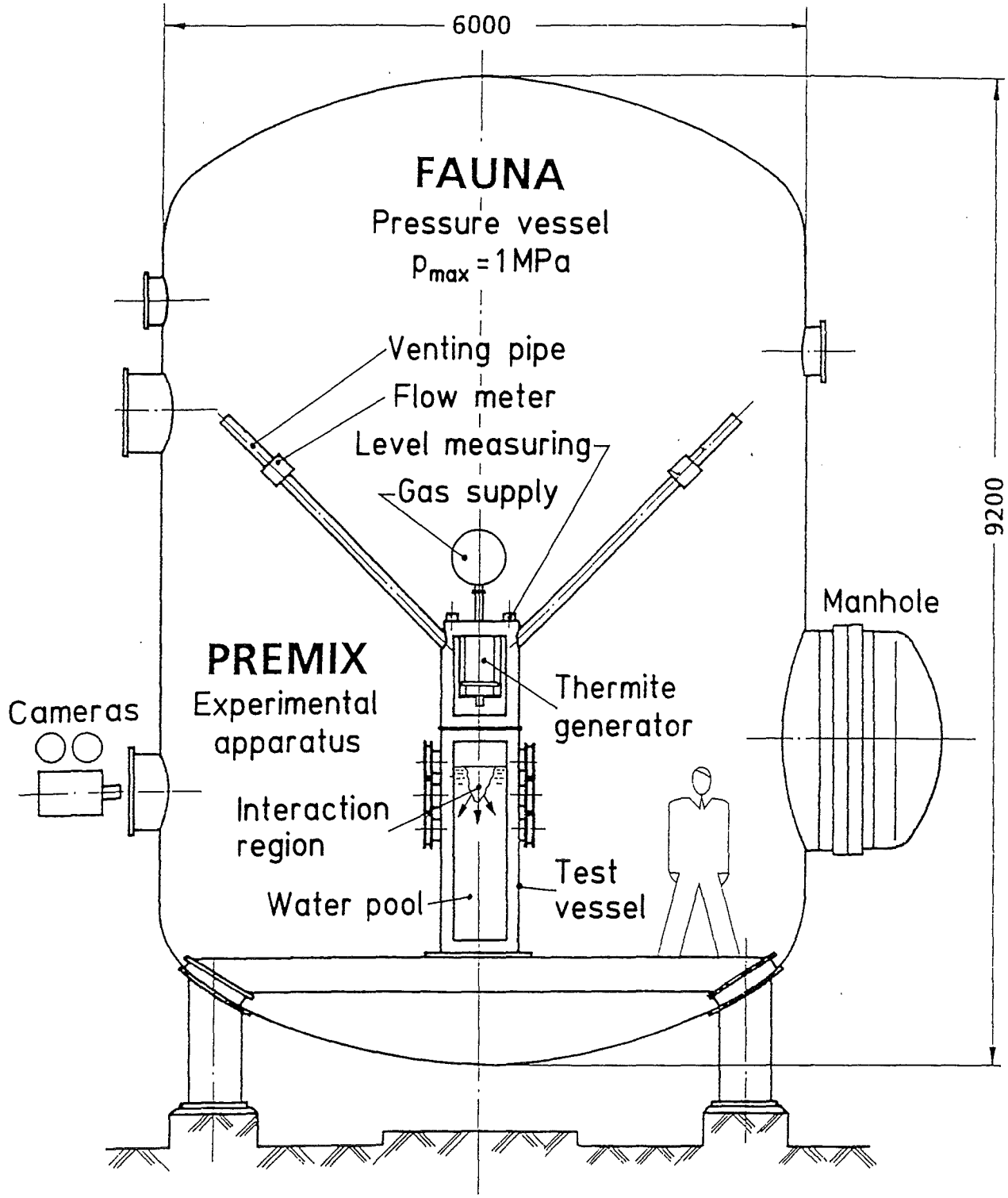

Fig. 2.1 **PREMIX** experimental facility, schematically

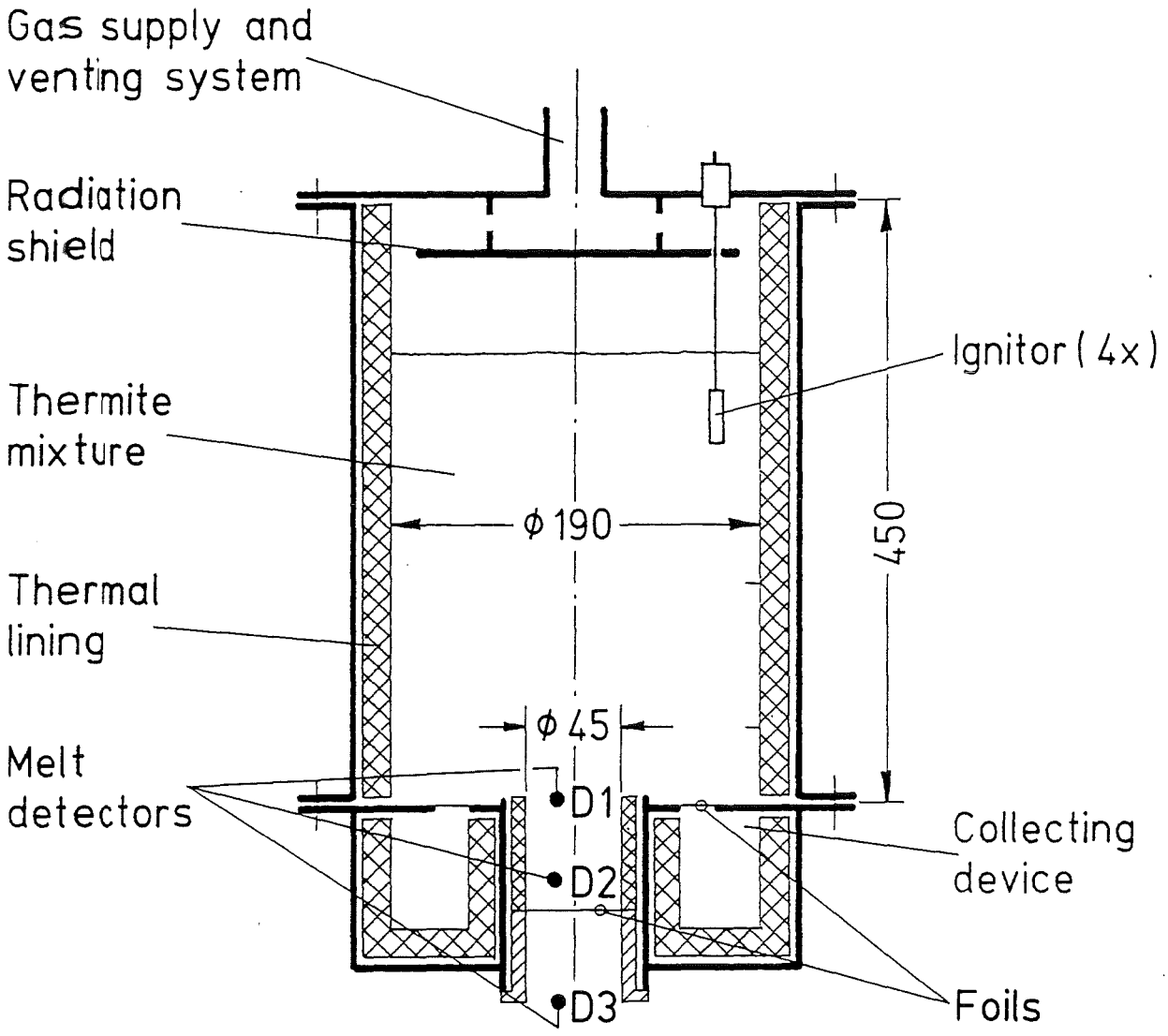

Thermite charge 19 kg / 9.5 dm^3

Melt (Al_2O_3) available 9 kg / 3.3 dm^3

Fig. 2.2 PREMIX melt generator, type 10 kg

IRS 9472395

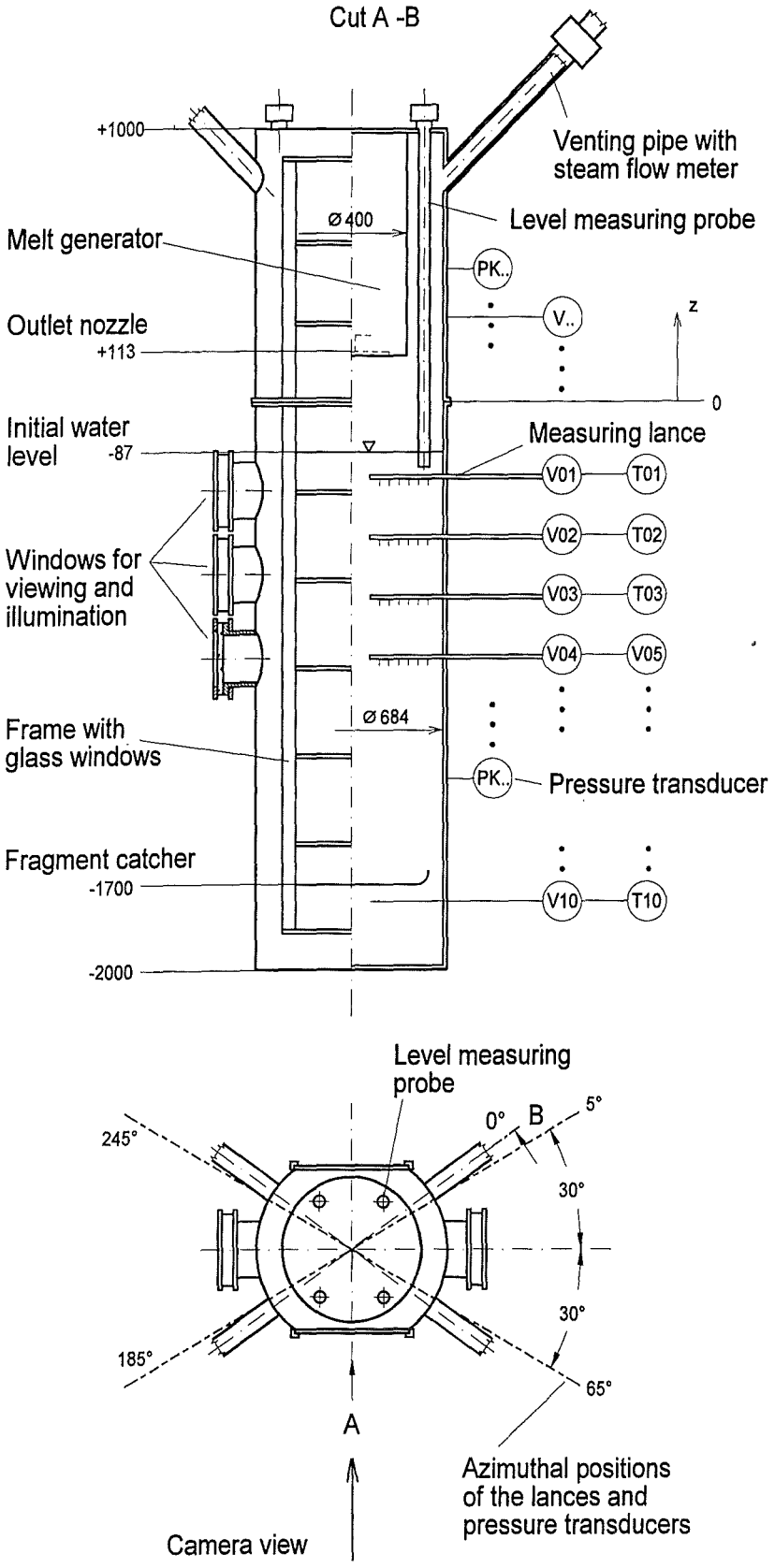

Fig. 2.3: Test apparatus

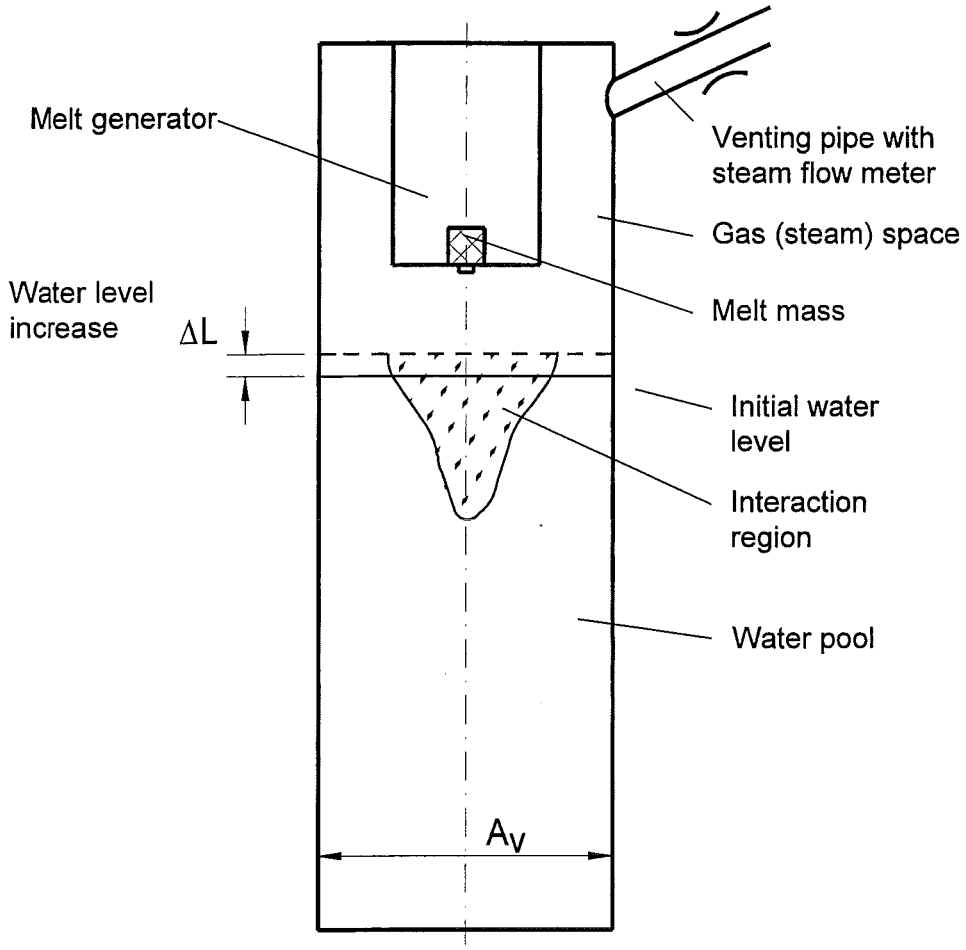

Fig. 2.4: Situation around the interaction region, schematically.
A_V = area of cross section

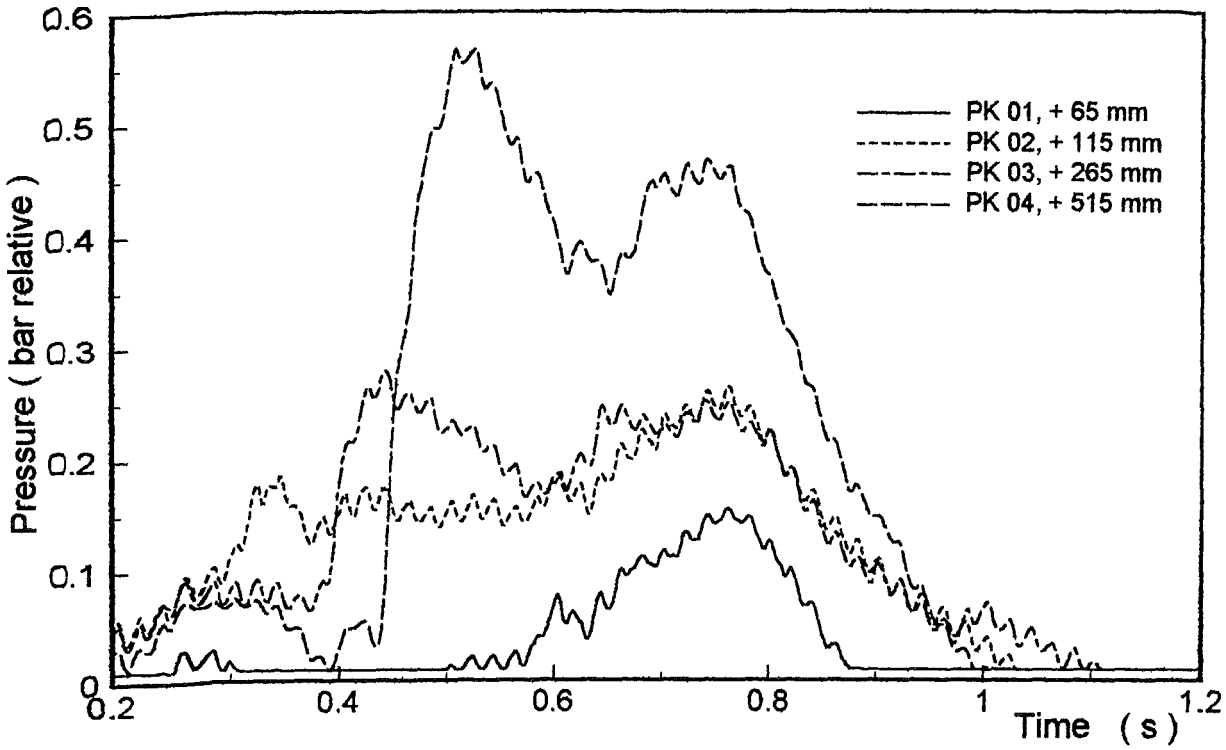

Fig. 3.2;1: PM01, Pressures above the water level

DRUCK1 | 8.12.1995

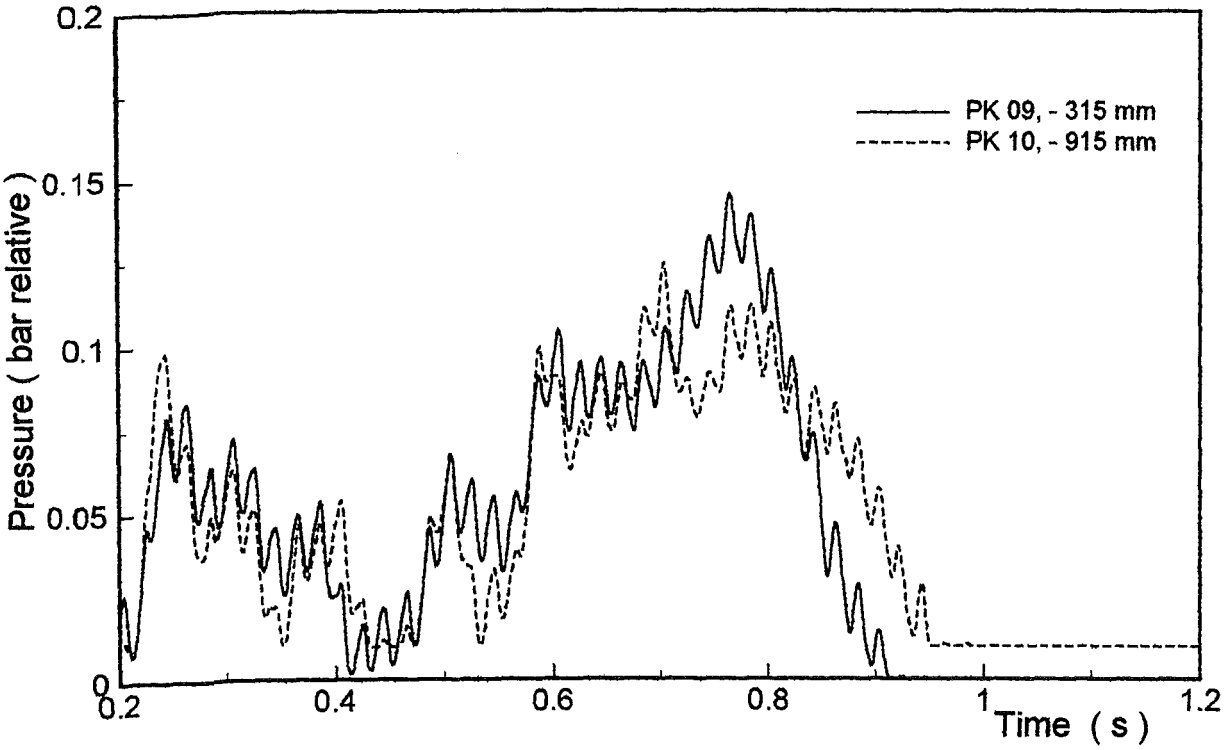

Fig. 3.2;2: PM01, Pressures underneath the water level

DRUCK2 | 8.12.1995

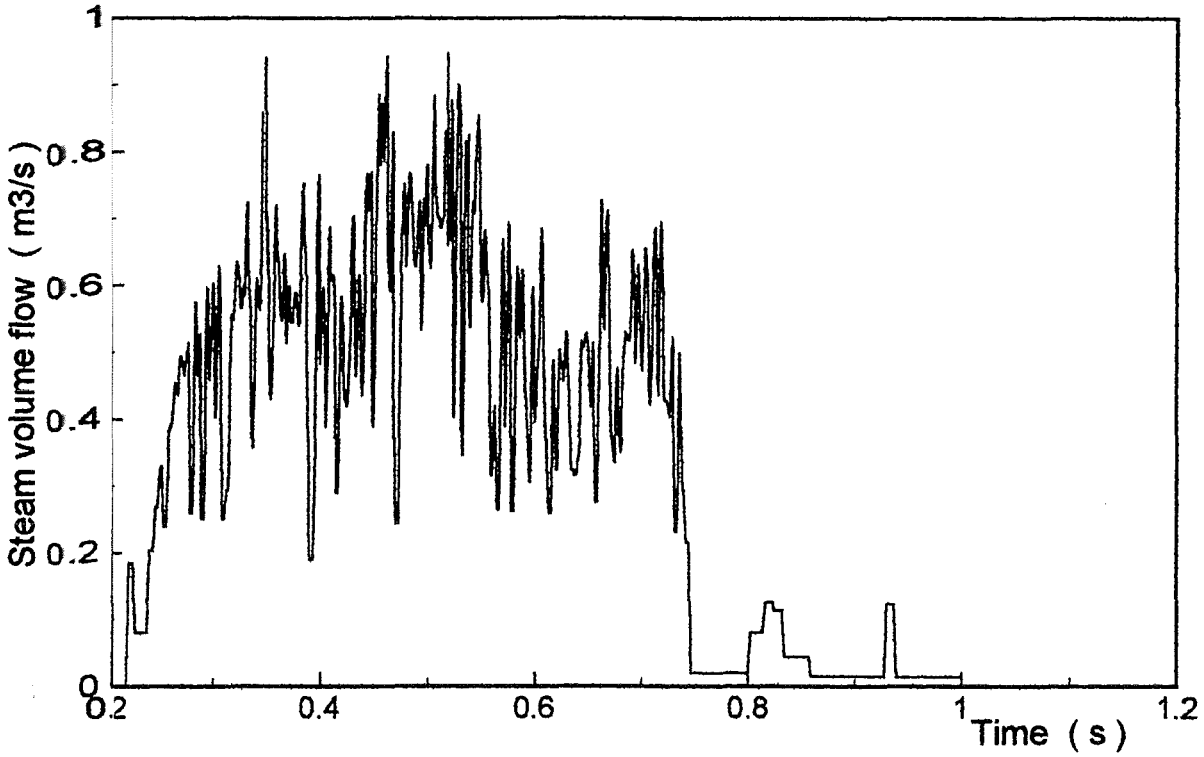

Fig. 3.2;3: PM 01, Steam flow (F02)

FLOW | 8.12.1995

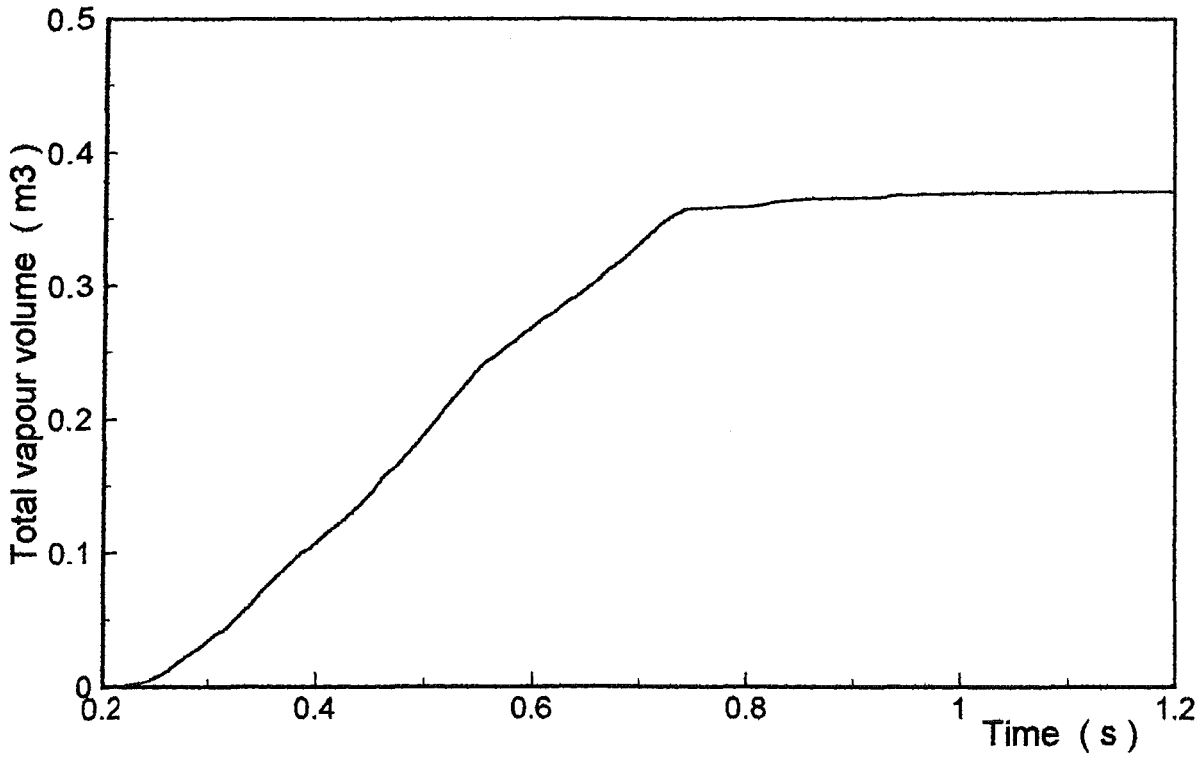

Fig. 3.2;4: PM 01, Integrated total vapour flow

DURCHSAT | 8.12.1995

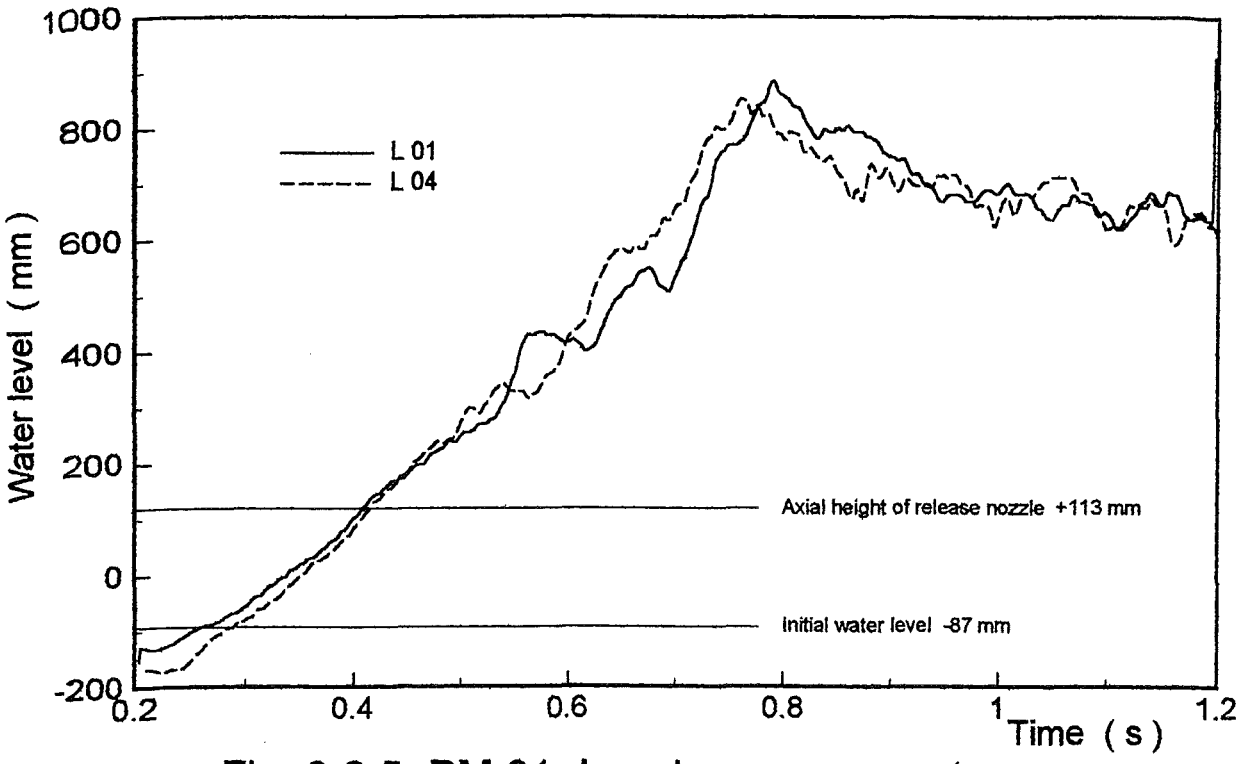

Fig. 3.2;5: PM 01, Level measurement

LEVEL | 8.12.1995

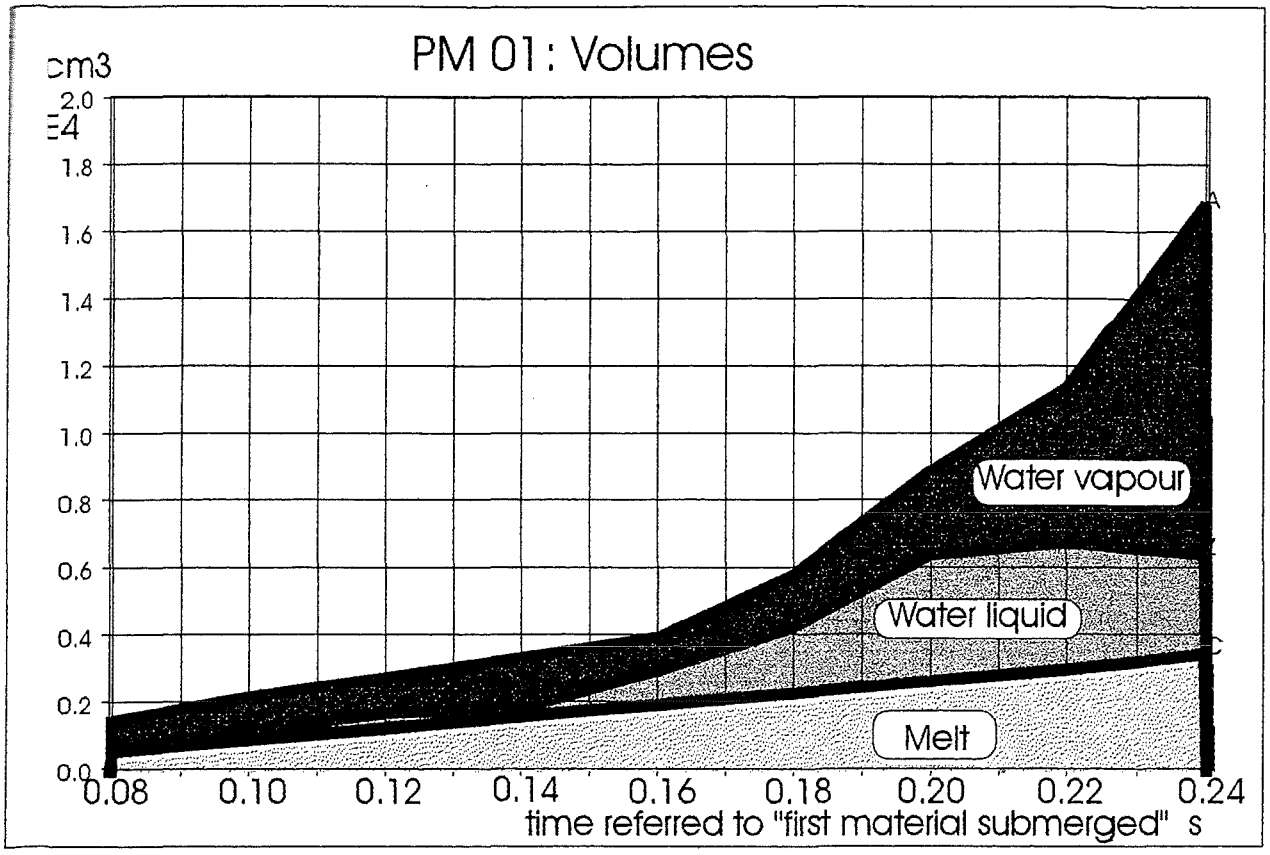

Fig.3.2;6: PM01 Volume of the interaction region and volume related to level increase

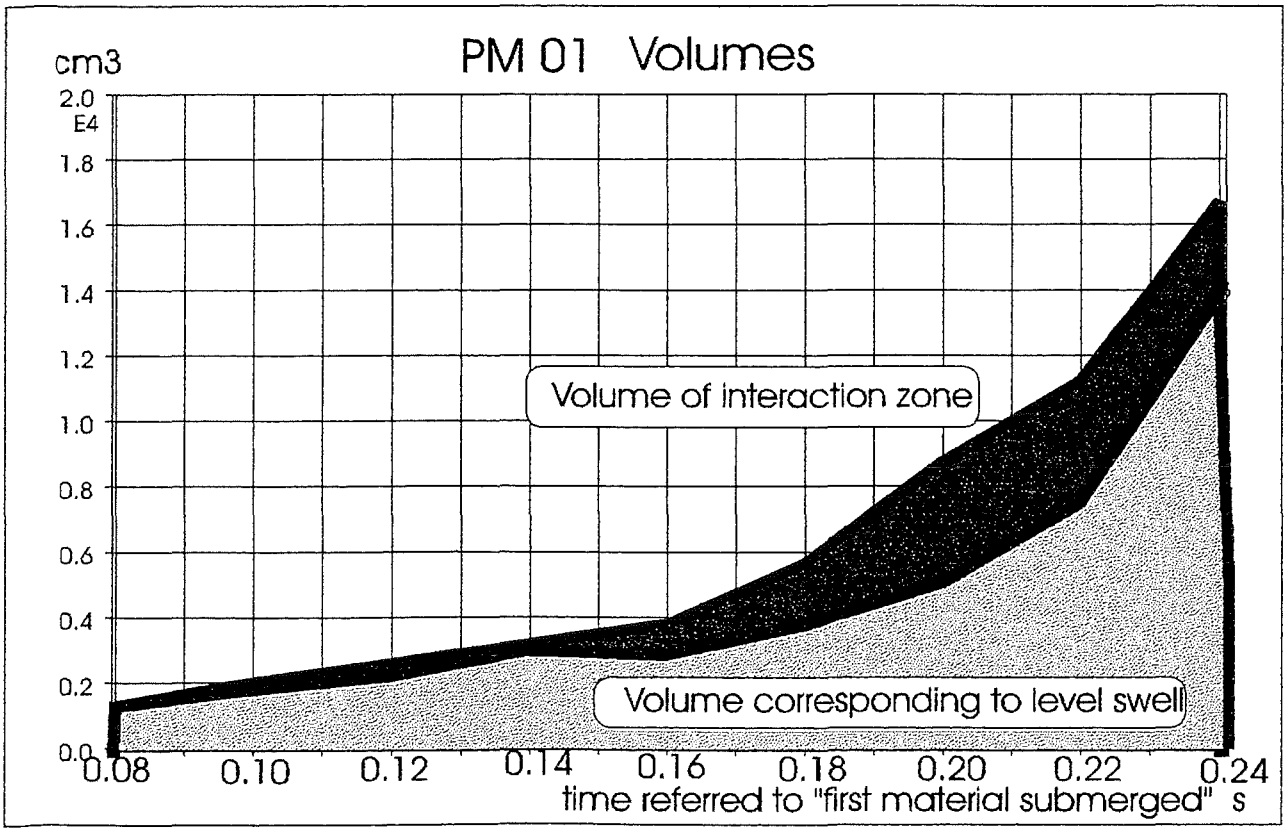

Fig. 3.2;7: PM01 Partial volumes of the interaction zone

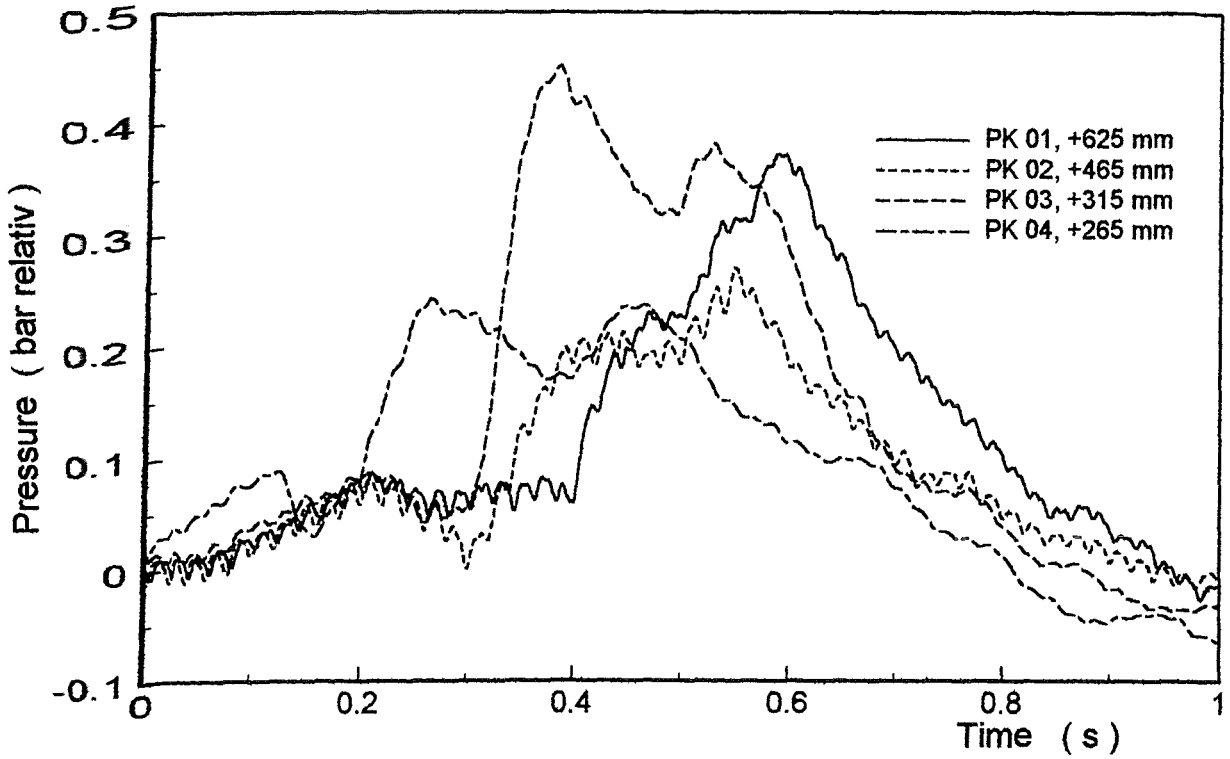

Fig. 3.2;8: PM 02, Pressures above water level (part 1)

DRUCK1 | 8.12.1995

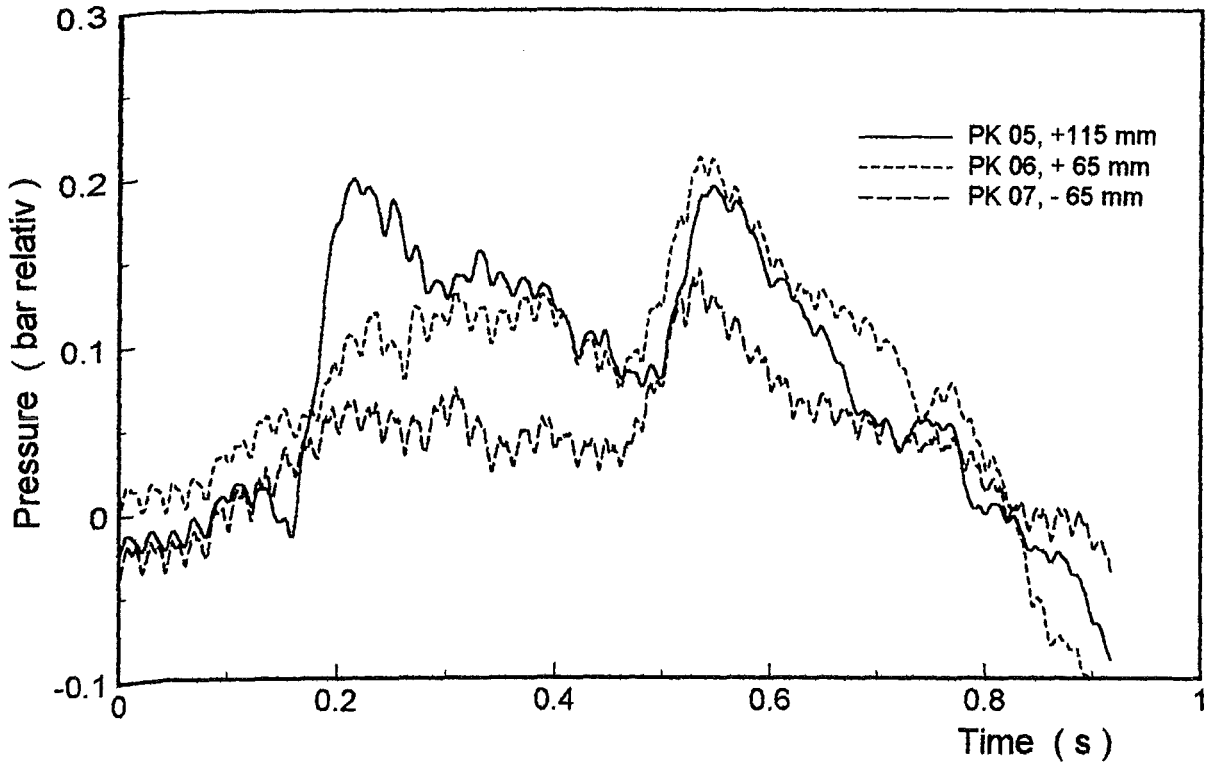

Fig. 3.2;9: PM 02, Pressures above water level (part 2)

DRUCK2 | 8.12.1995

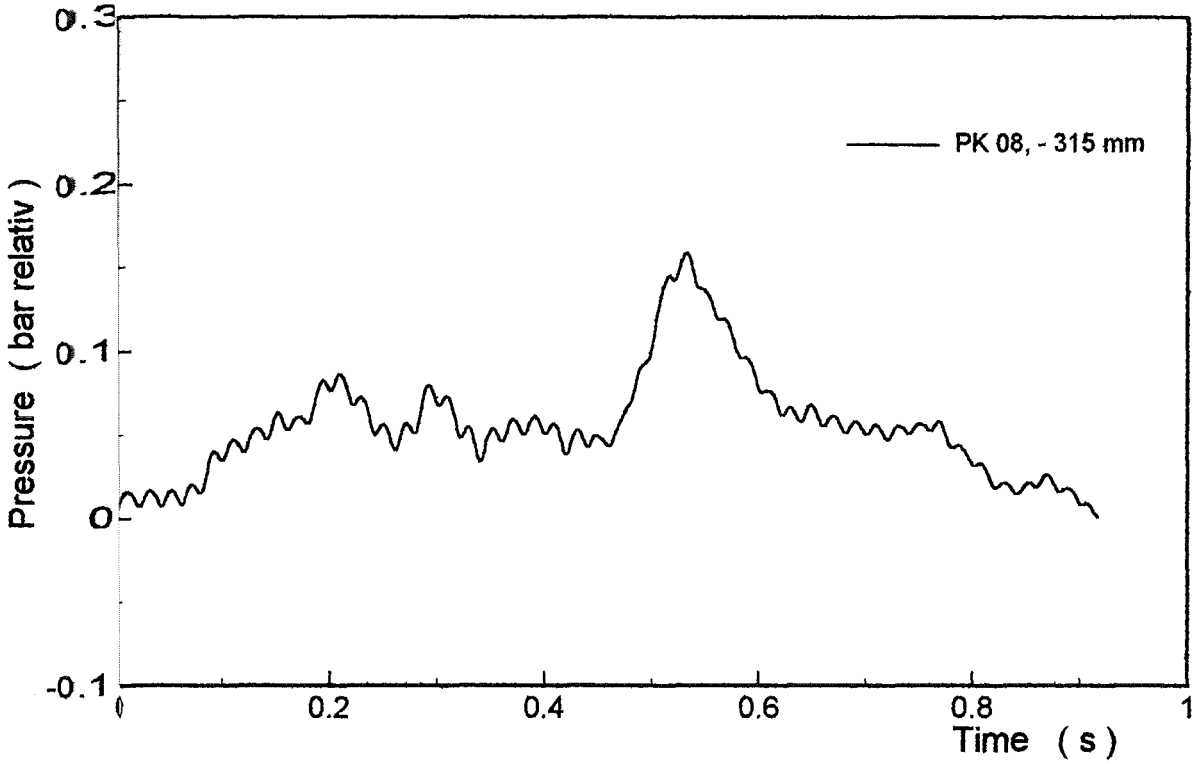

Fig. 3.2;10: PM 02, Pressure underneath the water level

DRUCK3 | 8.12.1995

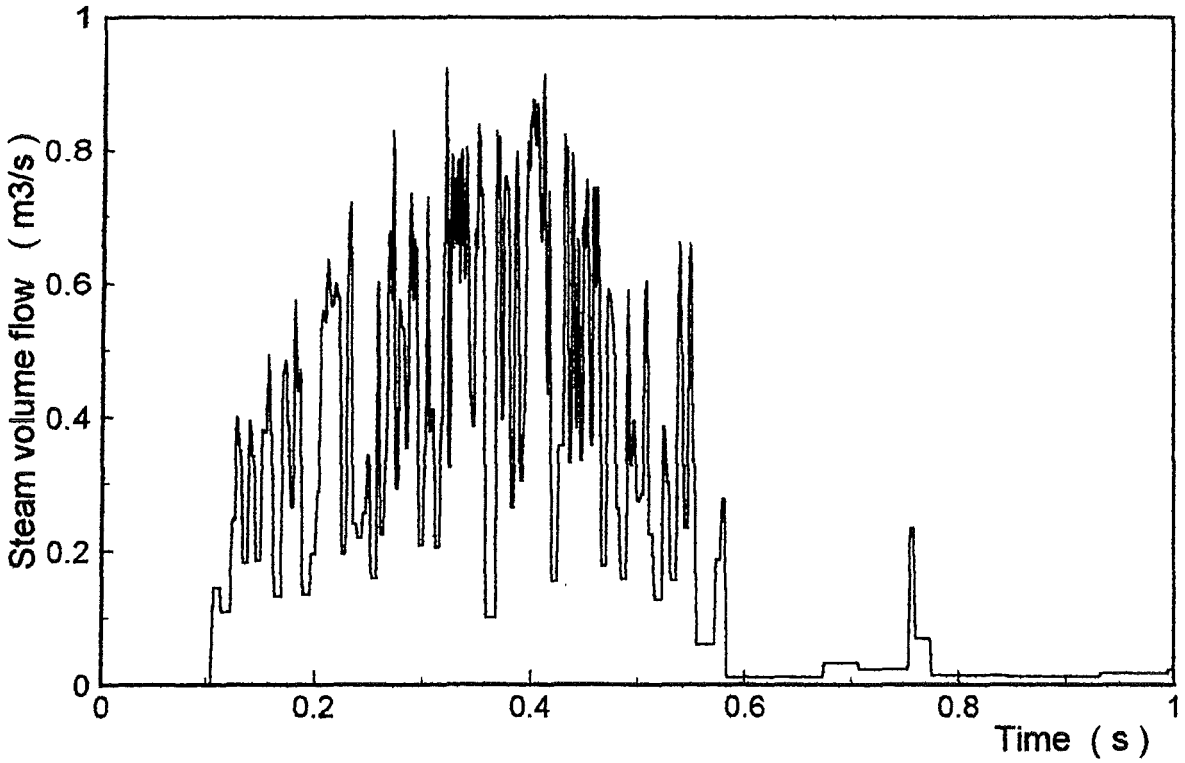

Fig. 3.2;11: PM 02, Steam flow rate (F01)

FLOW | 8.12.1995

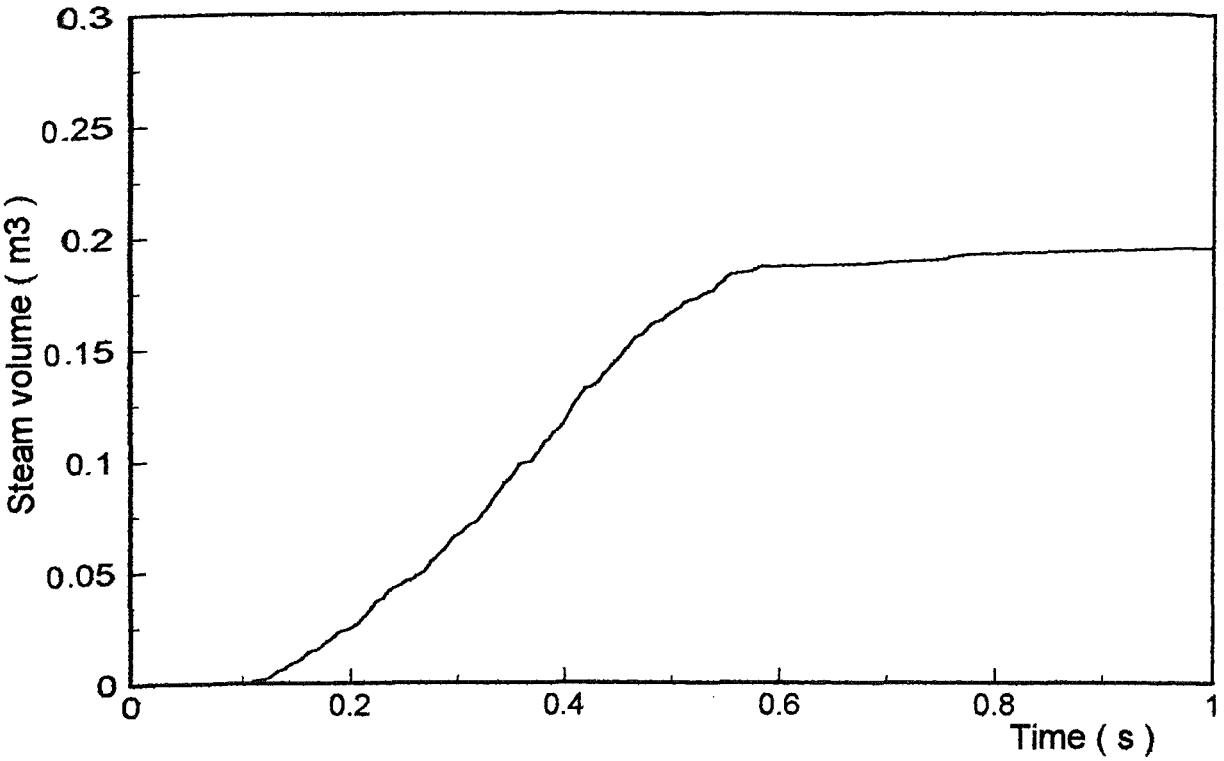

Fig. 3.2;12: PM 02, Integrated vapour flow (F01)

VOLUME | 8.12.1995

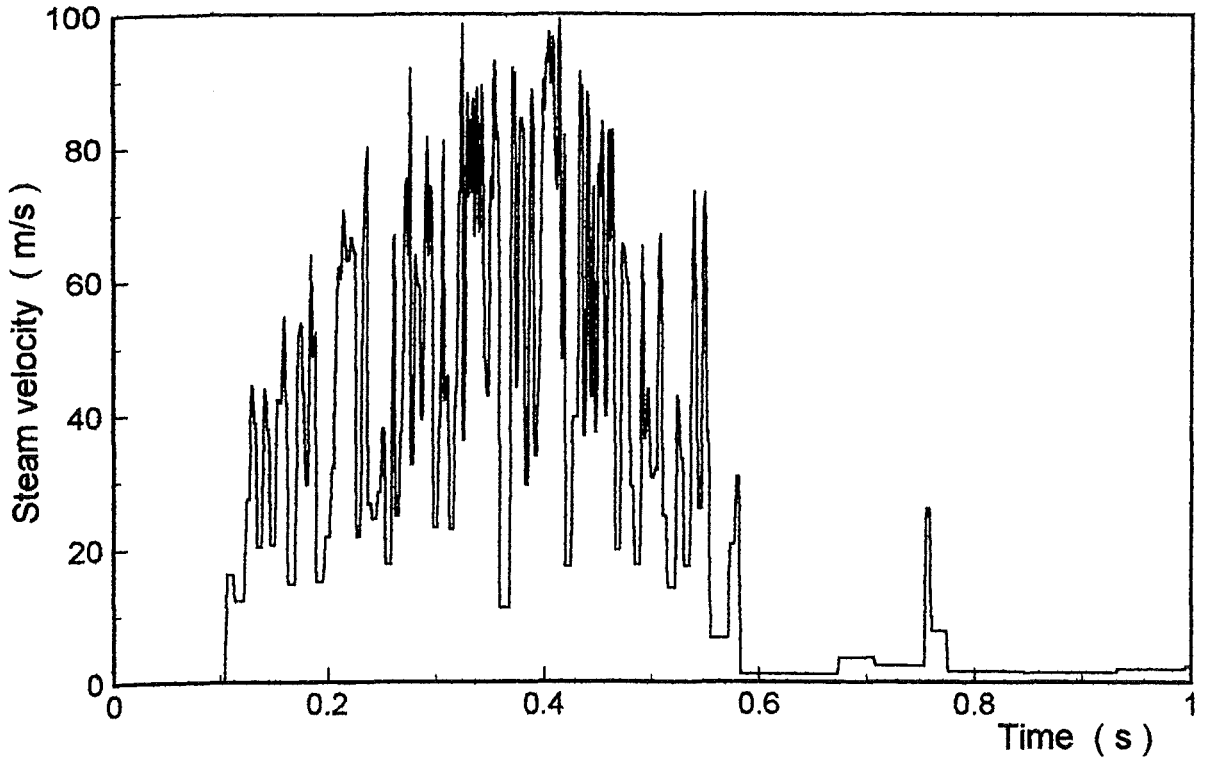

Fig. 3.2;13: PM 02, Steam velocity (F01)

VELOCITY | 8.12.1995

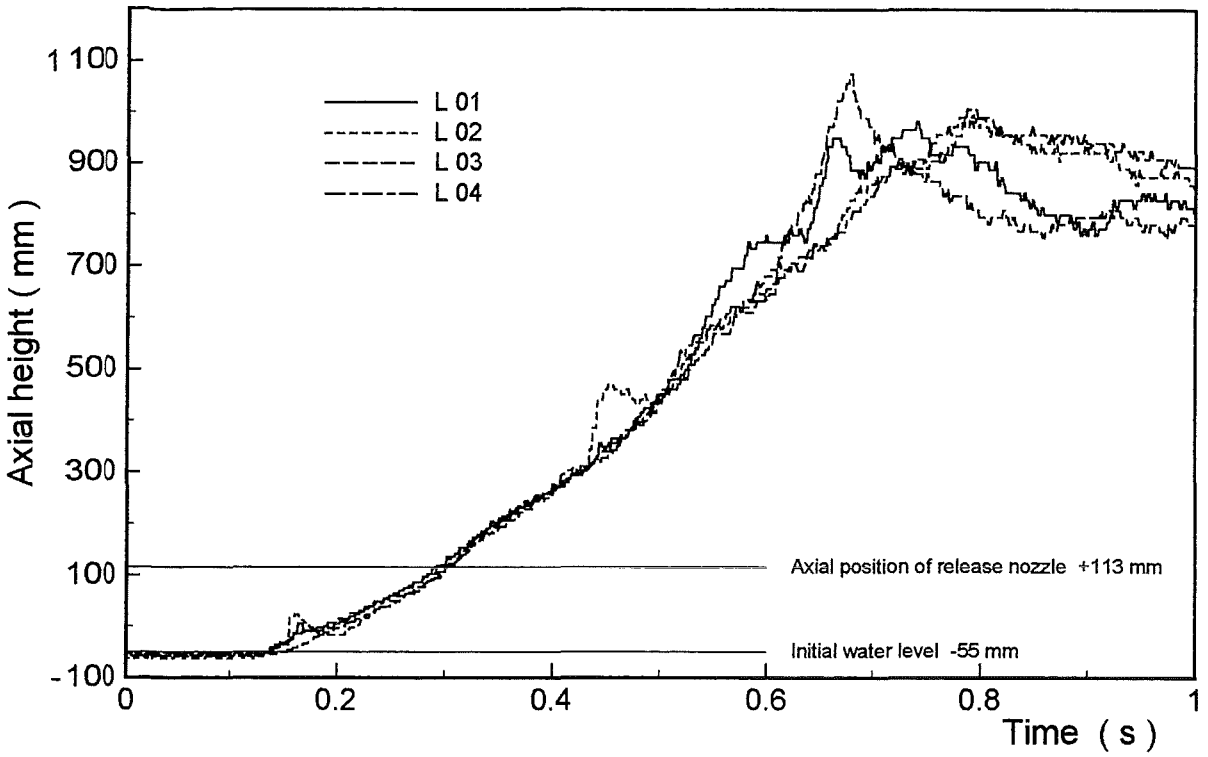

Fig. 3.2;14: PM 02, Level measurement

LEVEL | 8.2.1996

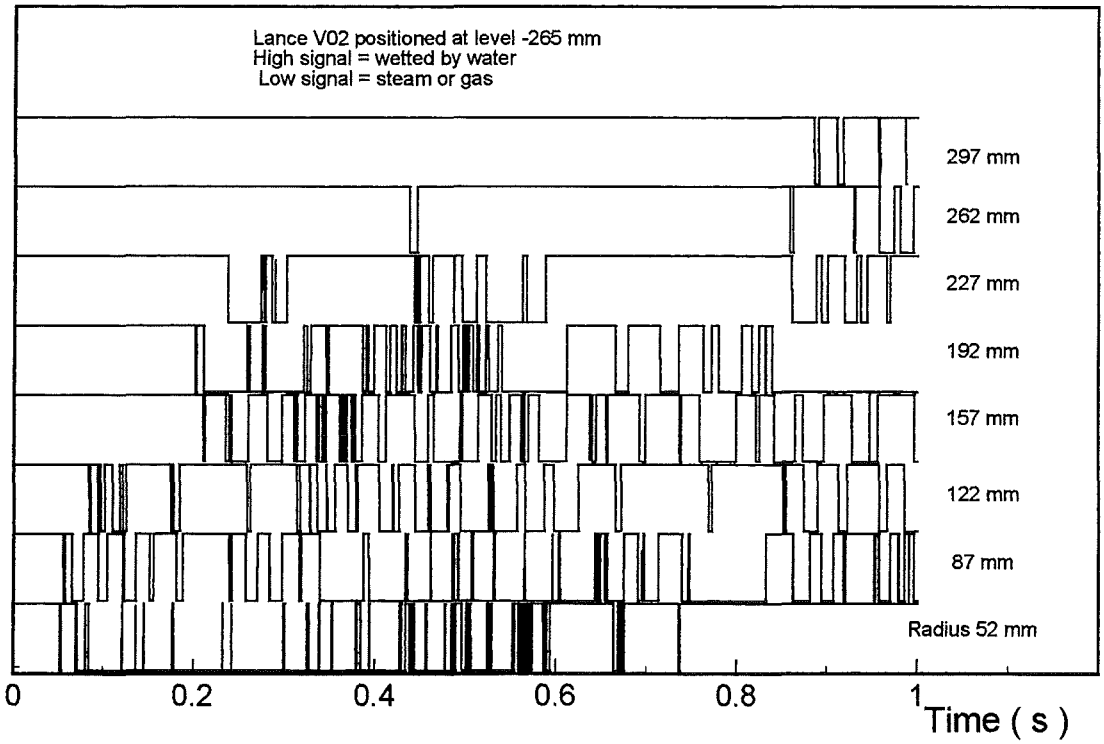

Fig. 3.2;15: PM 02, Void sensor signals (z = 115 mm)

VOID | 8.2.1996

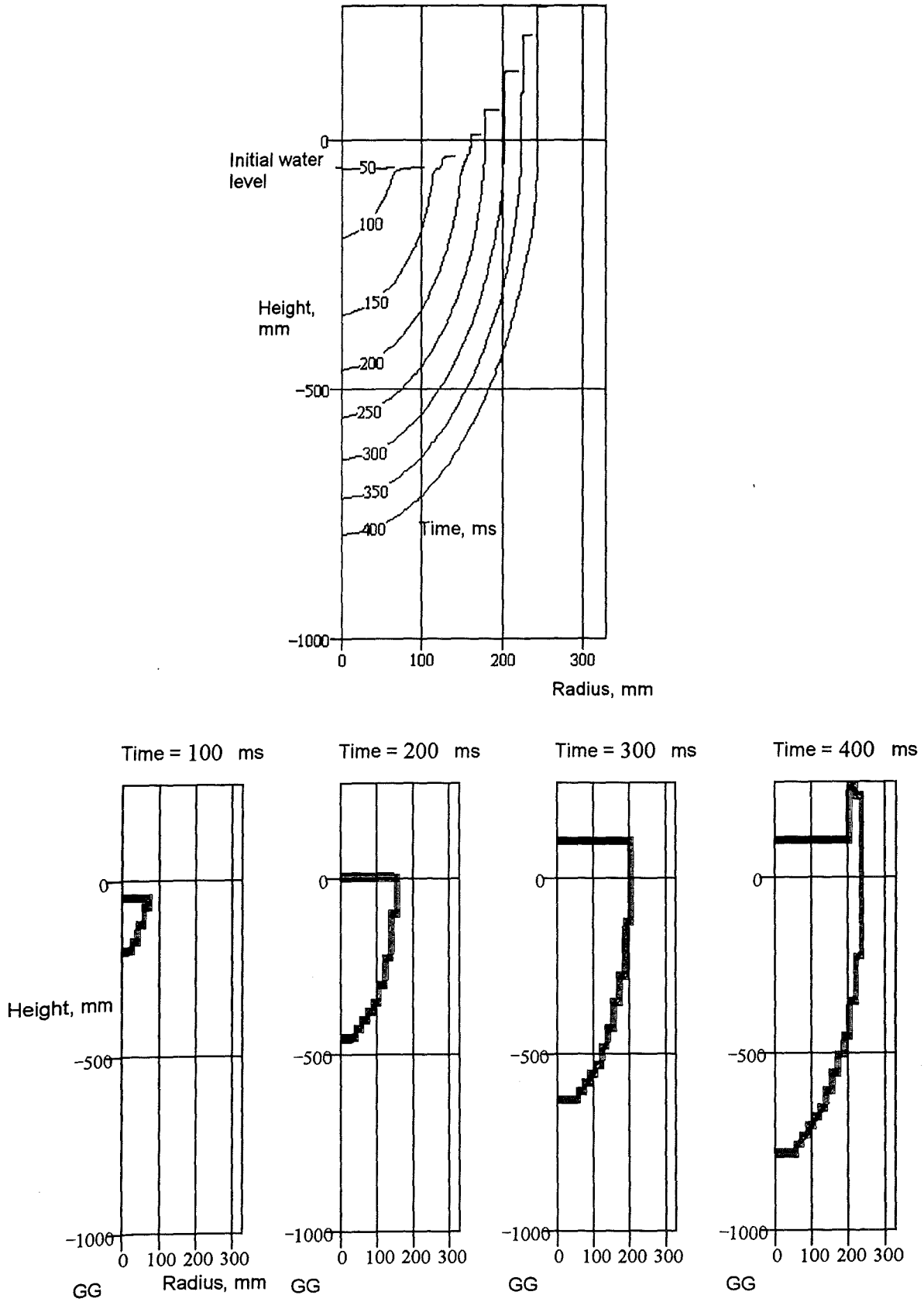

Fig. 3.2;16: PM02. Progression of the interaction region with the time as a parameter. The level of the rising water is indicated at the upper ends of the isochrones by a short horizontal stroke (upper graph). The series of graphs in the lower part gives the boundaries of the interaction region as used in the calculation of the volume.

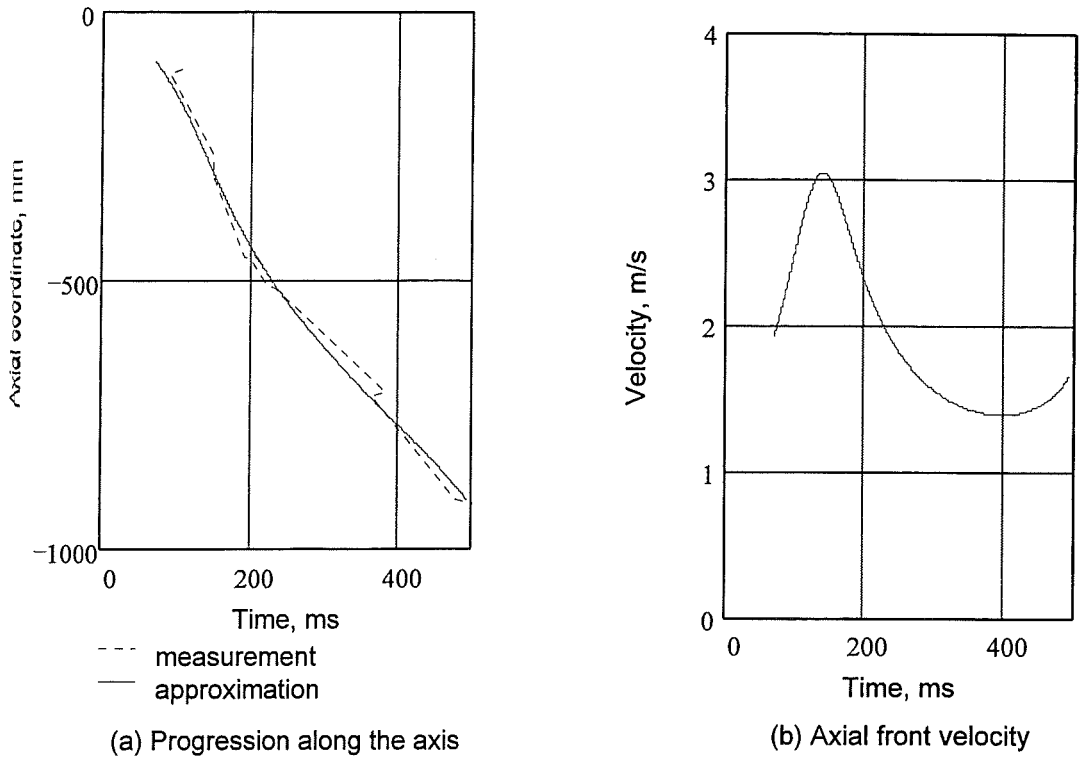

(a) Progression along the axis

(b) Axial front velocity

Fig. 32;17: PM02. Progression of the interaction region along the vessel axis (a) and derived velocity (b). The measurement is approximated by a funtion of fourth order (method of least squares).

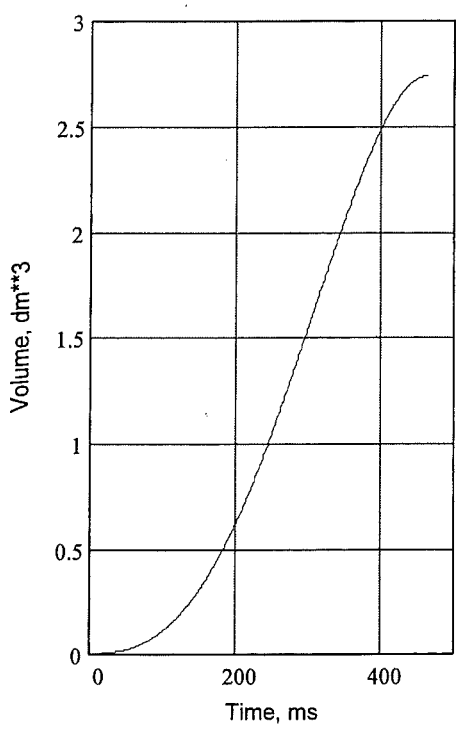

Fig. 3.2;18: PM02. Function assumed to describe the volume flow of the melt entering the interaction region.

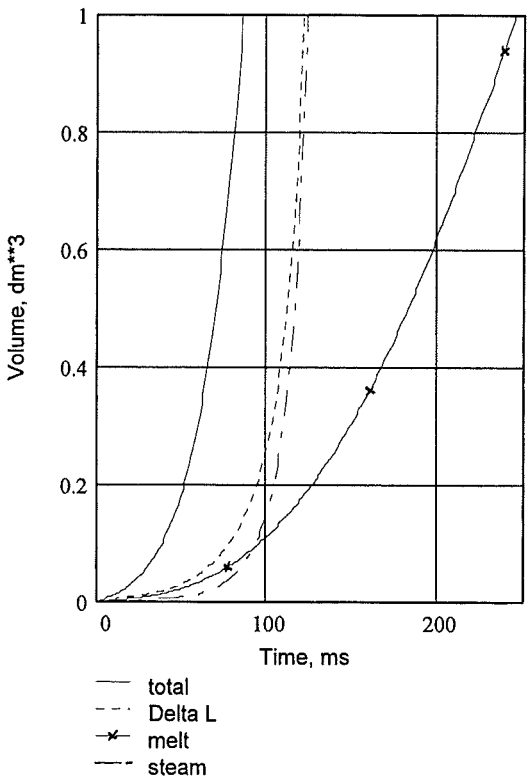

Fig. 3.2;19: PM02. Volumes as approximated for the initial period of time.

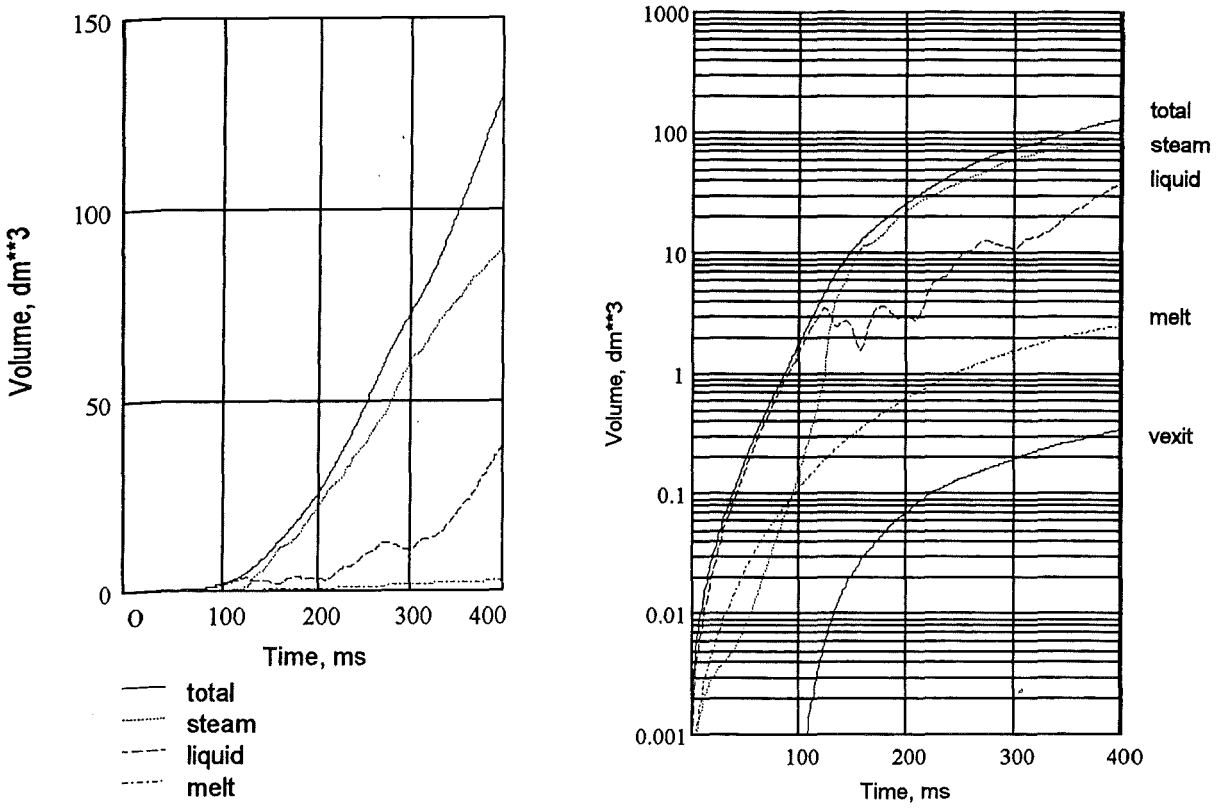

Fig. 3.2;20: PM02. Total volume and partial volumes of the interaction region. The curve labelled with vexit illustrates the small contribution of the outgoing steam

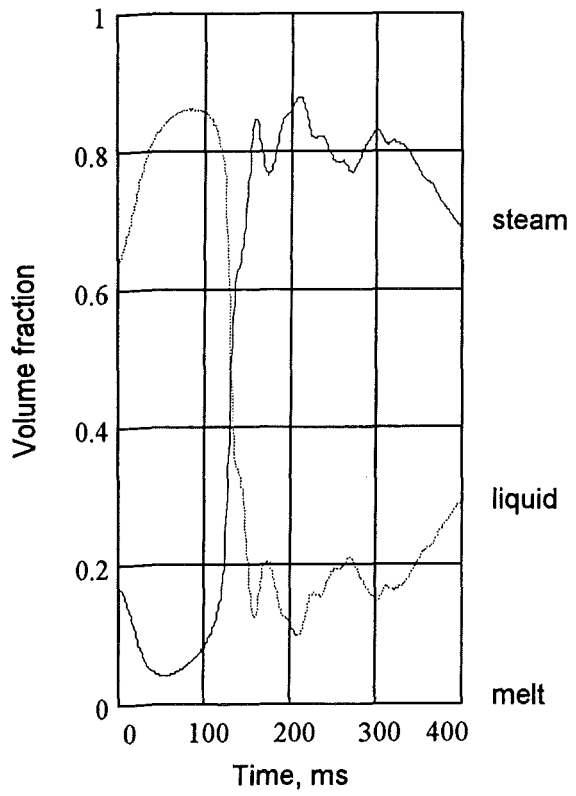

Fig. 3.2;21: PM02. Volume fractions of the three partial volumes.

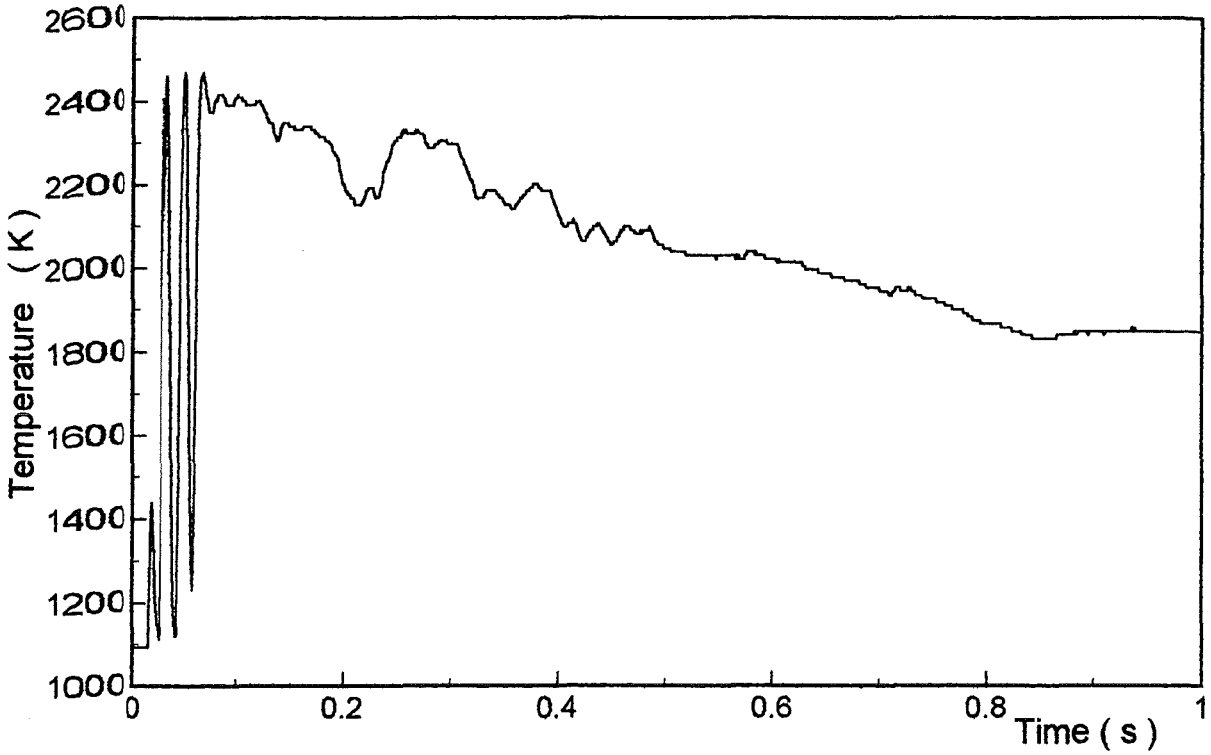

Fig. 3.2;22: PM03, Melt temperature

PYRO | 13.12.1995

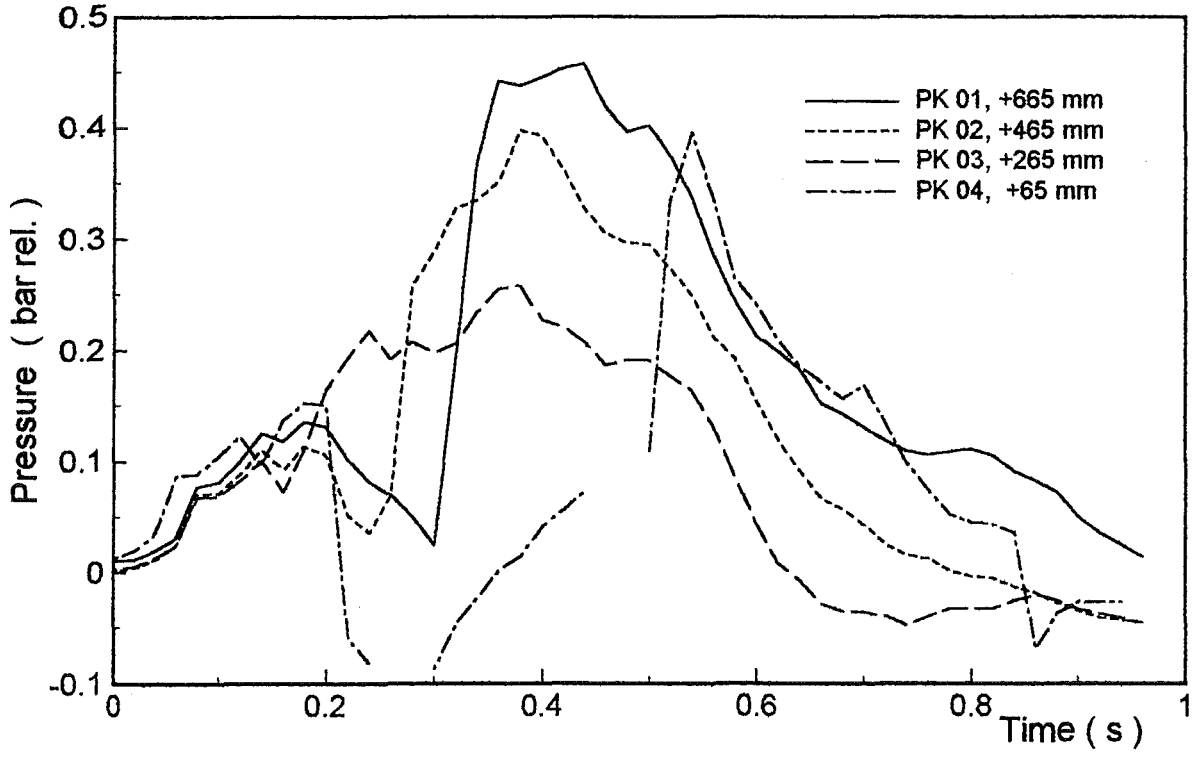

Fig. 3.2;23: PM03, Pressures above the water level

DRUCK1 | 13.12.1995

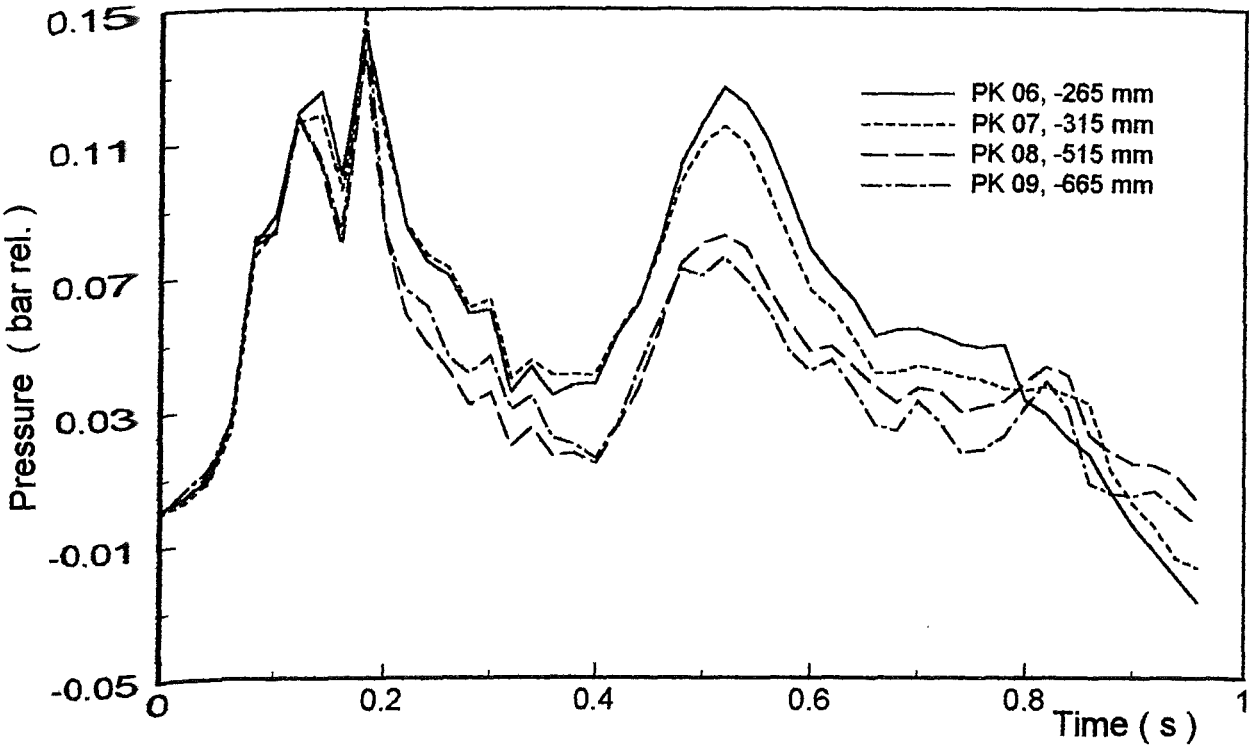

Fig. 3.2;24: PM03, Pressures underneath the water level

DRUCK2 | 13.12.1995

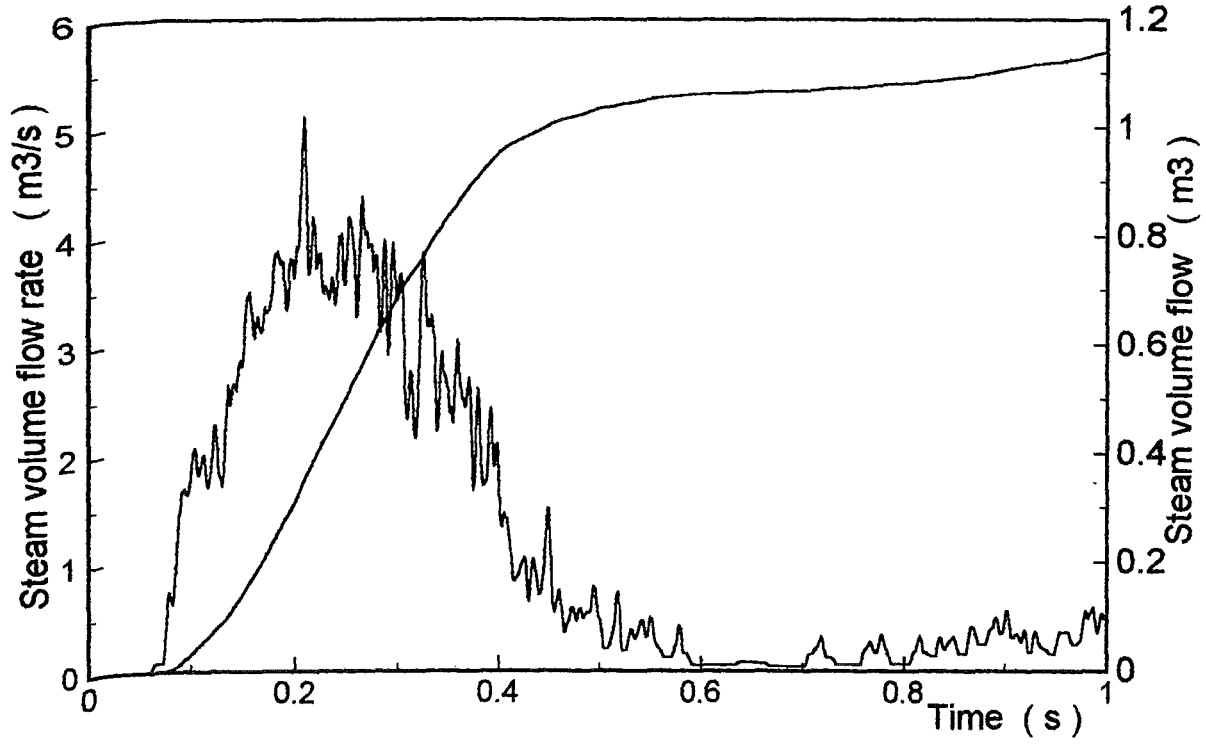

Fig. 3.2;25: PM03, Steam flow rate and integrated volume

DURCH | 13.12.1995

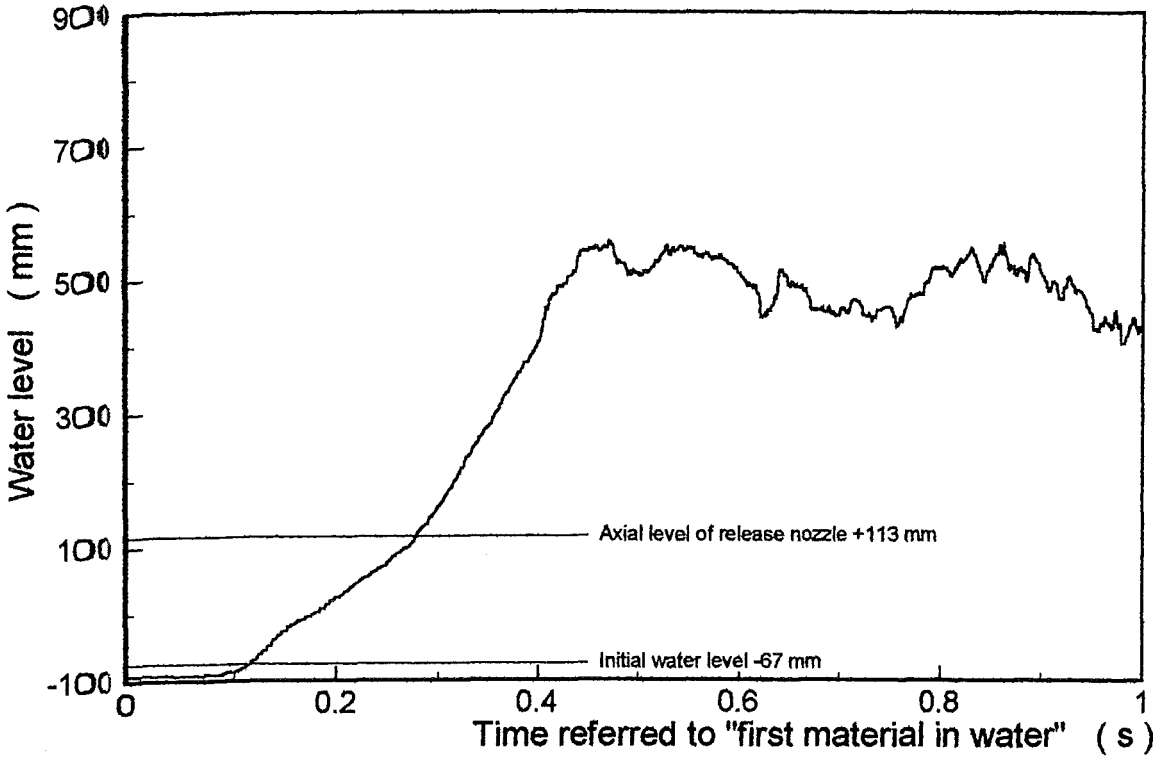

Fig. 3.2;26: PM03, Level measurement

LEVEL | 8.12.1995

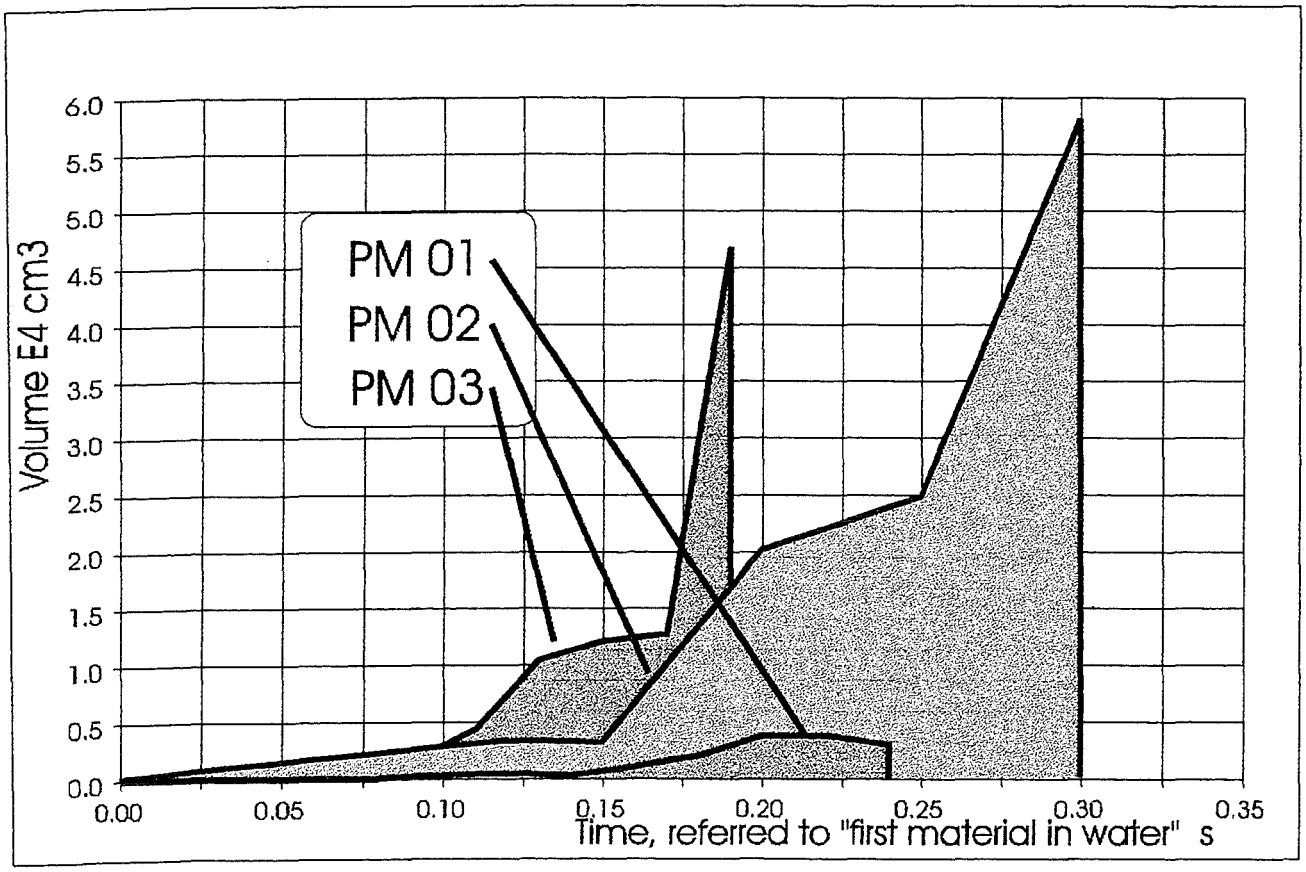

Fig. 3.2;27: PM03 Development of the interaction zone evaluated from video pictures (comparison of PM01 - 03)

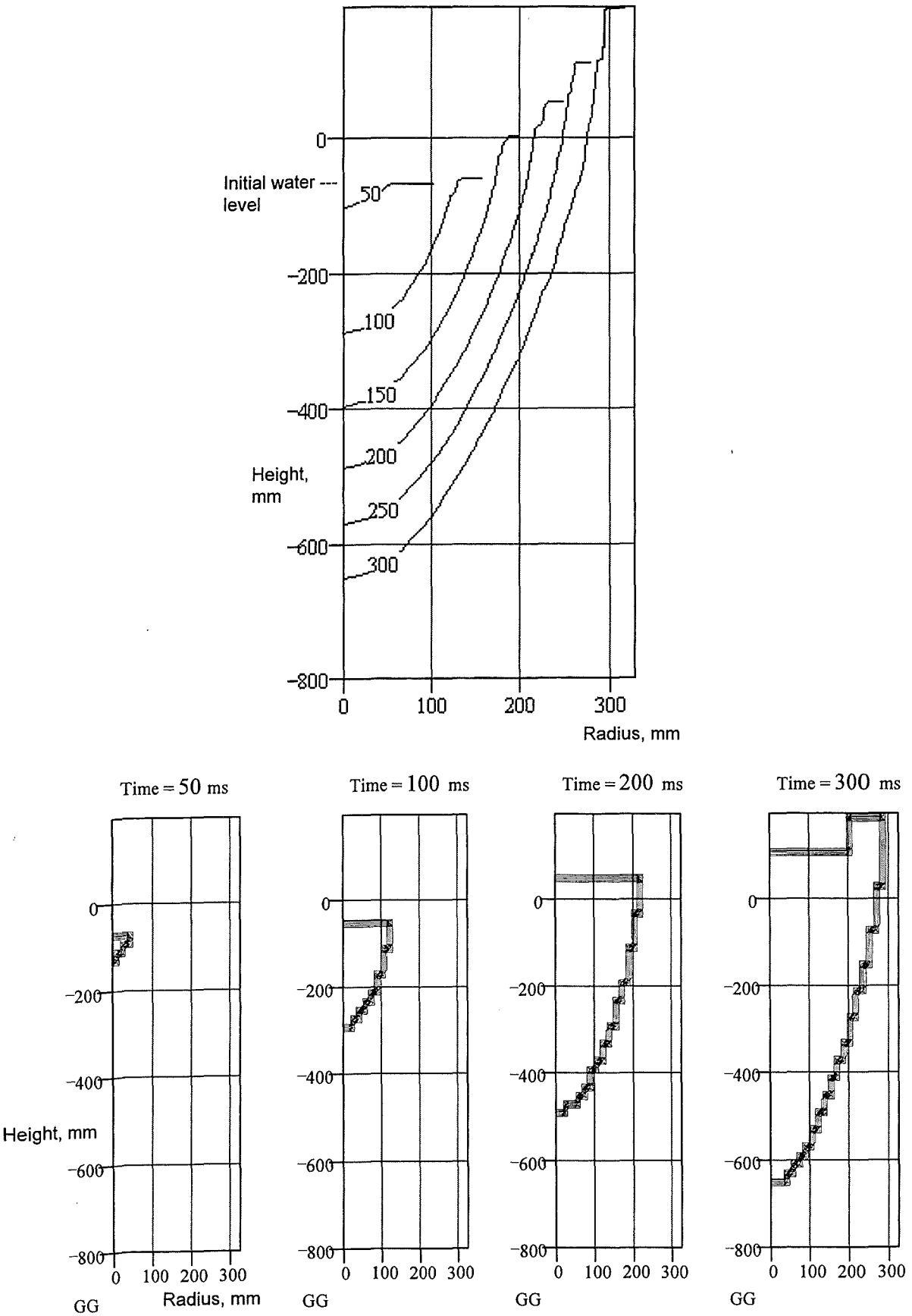

Fig. 3.2;28: PM03. Development of the interaction region with the time as a parameter.

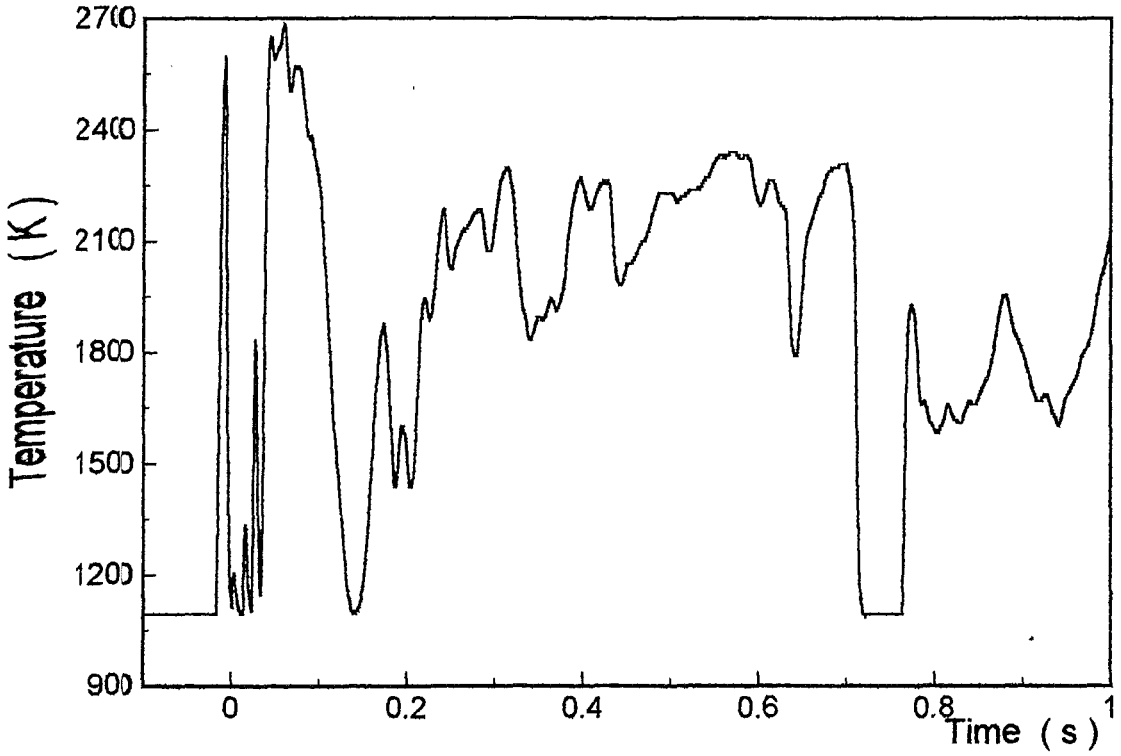

Fig. 3.2;29: PM04 Melt temperature

PYRO | 11.12.1995

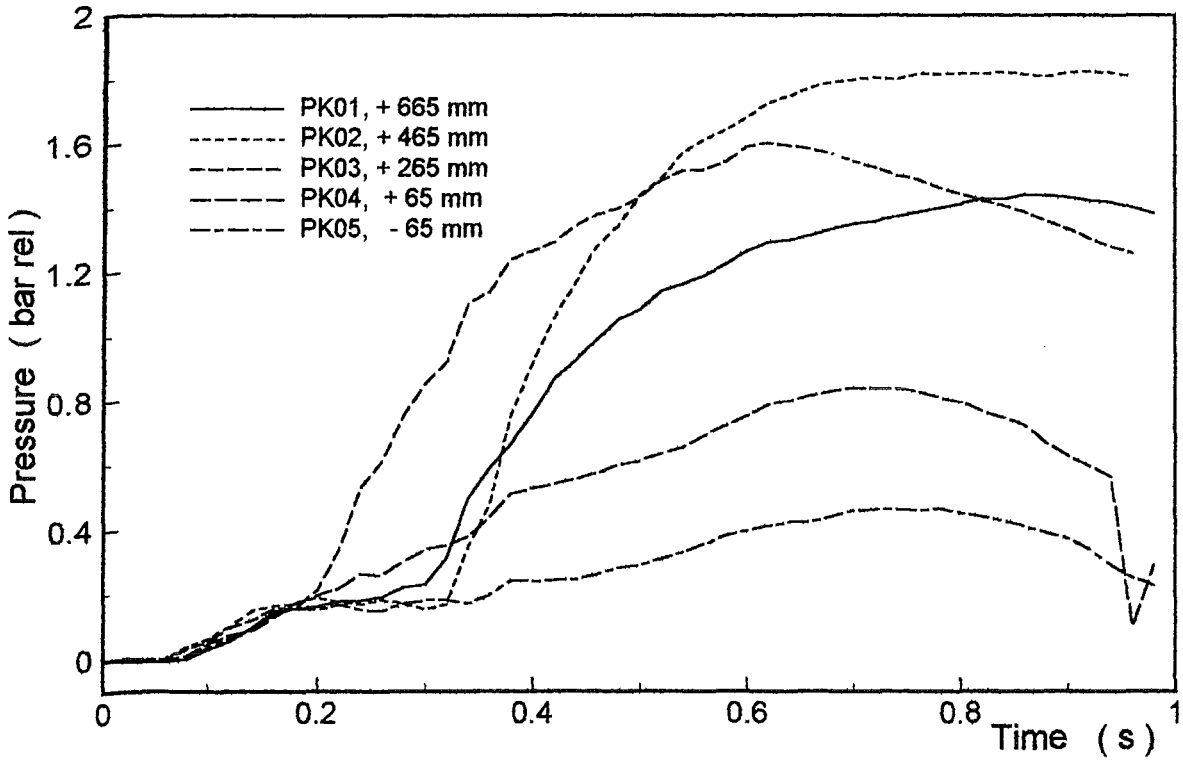

Fig. 3.2;30: PM04, Pressures above the water level

DRUCK1 | 11.12.1995

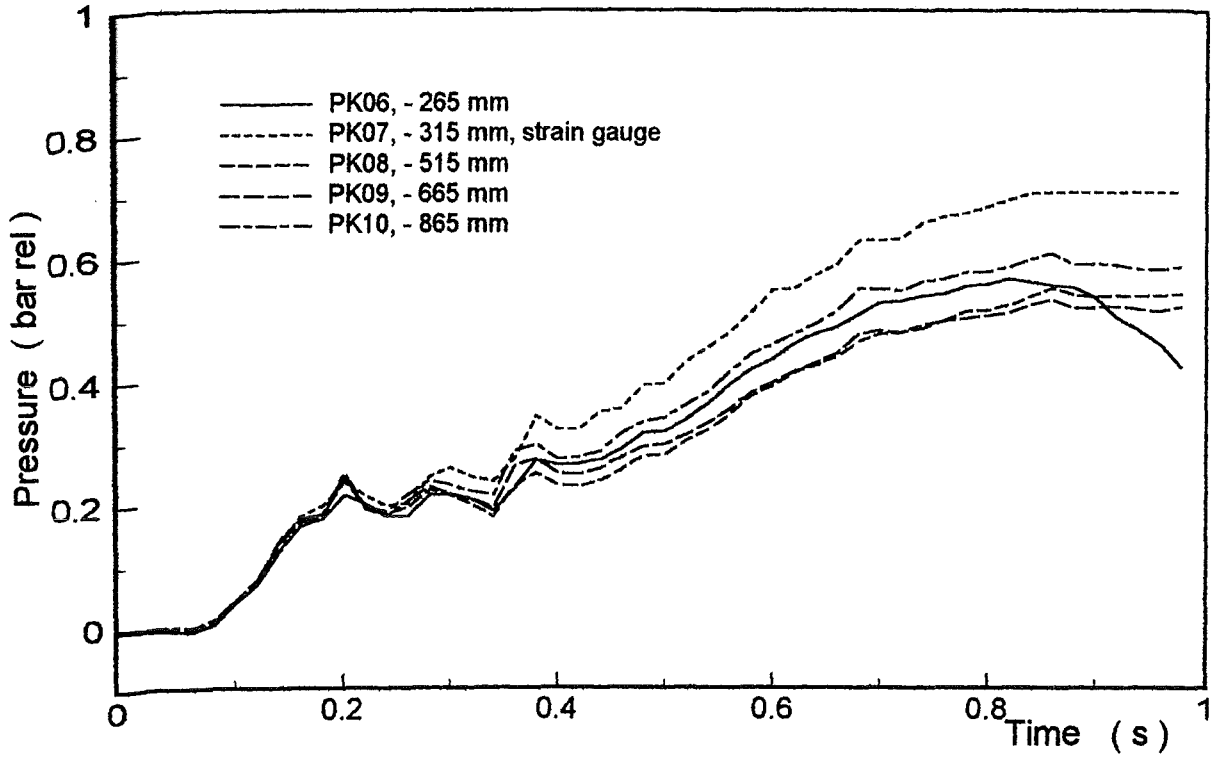

Fig. 3.2;31: PM04, Pressures underneath the water level

DRUCK2 | 11.12.1995

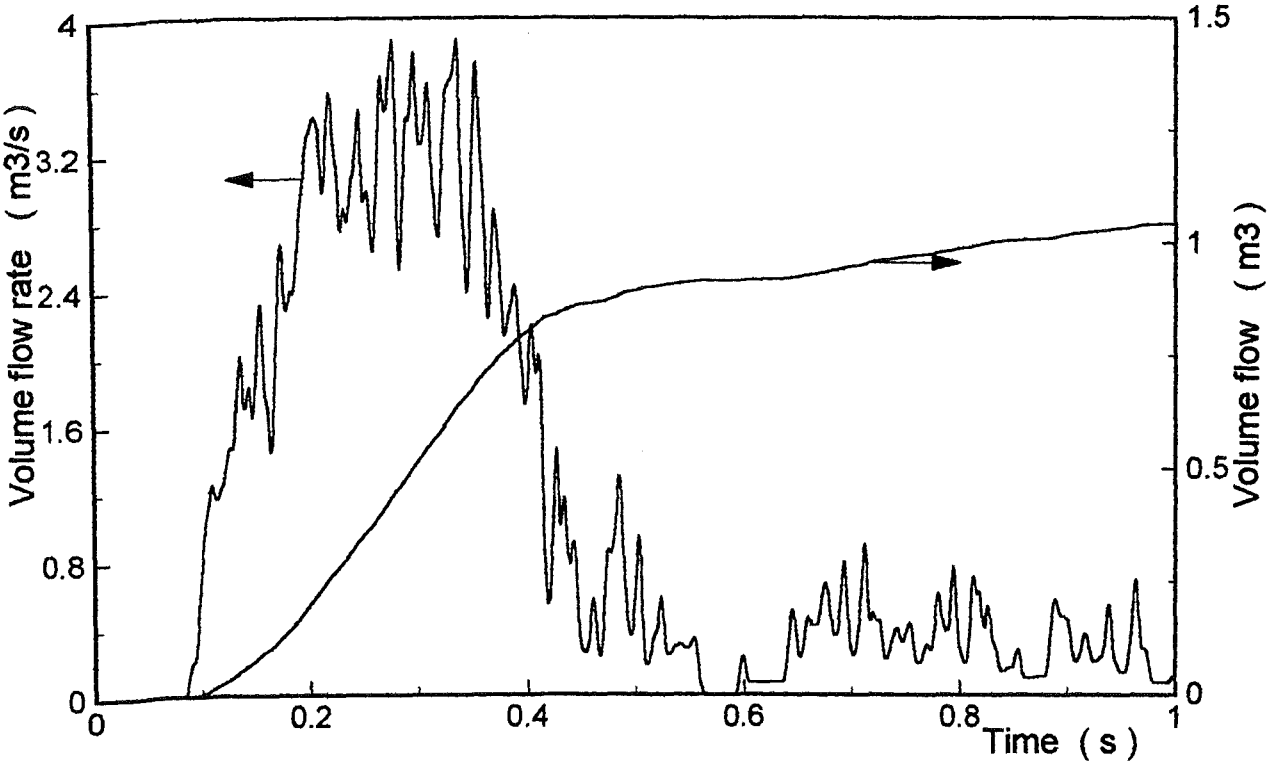

Fig. 3.2;32: PM04 Steam flow rate and integrated steam volume

STEAM | 11.12.1995

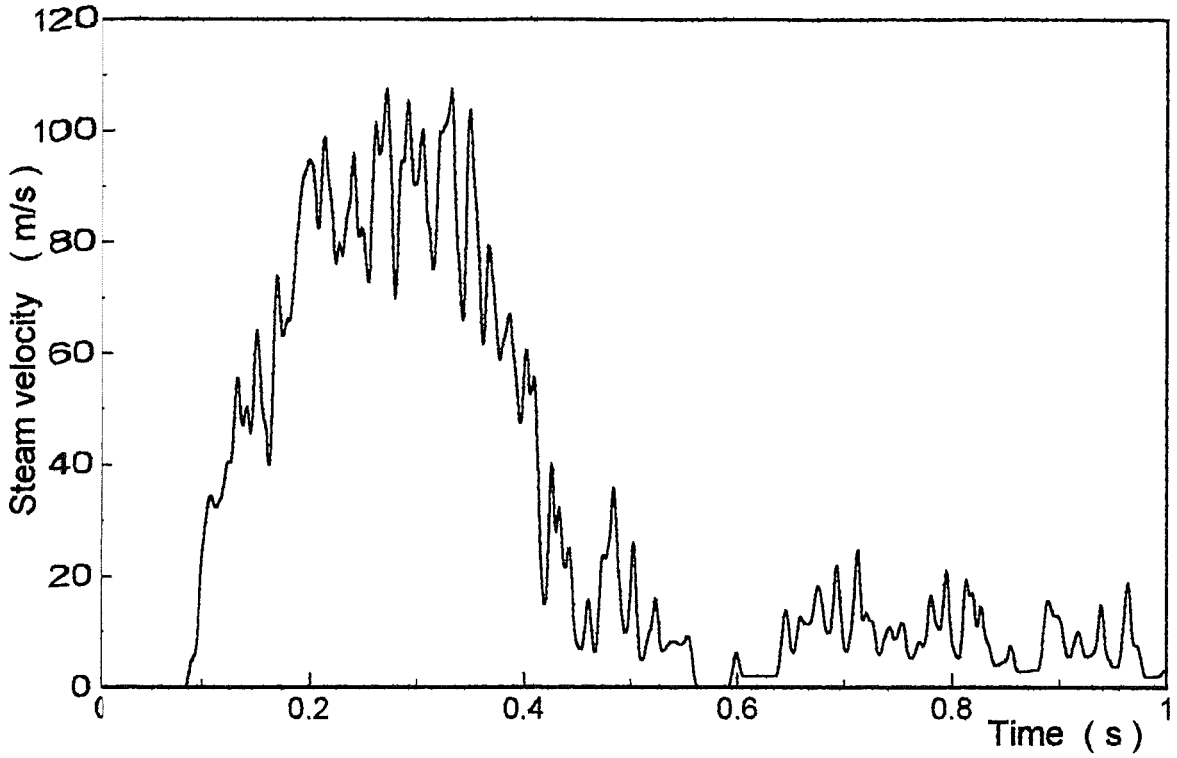

Fig. 3.2;33: PM04, Averaged steam velocity

VELOCITY | 11.12.1995

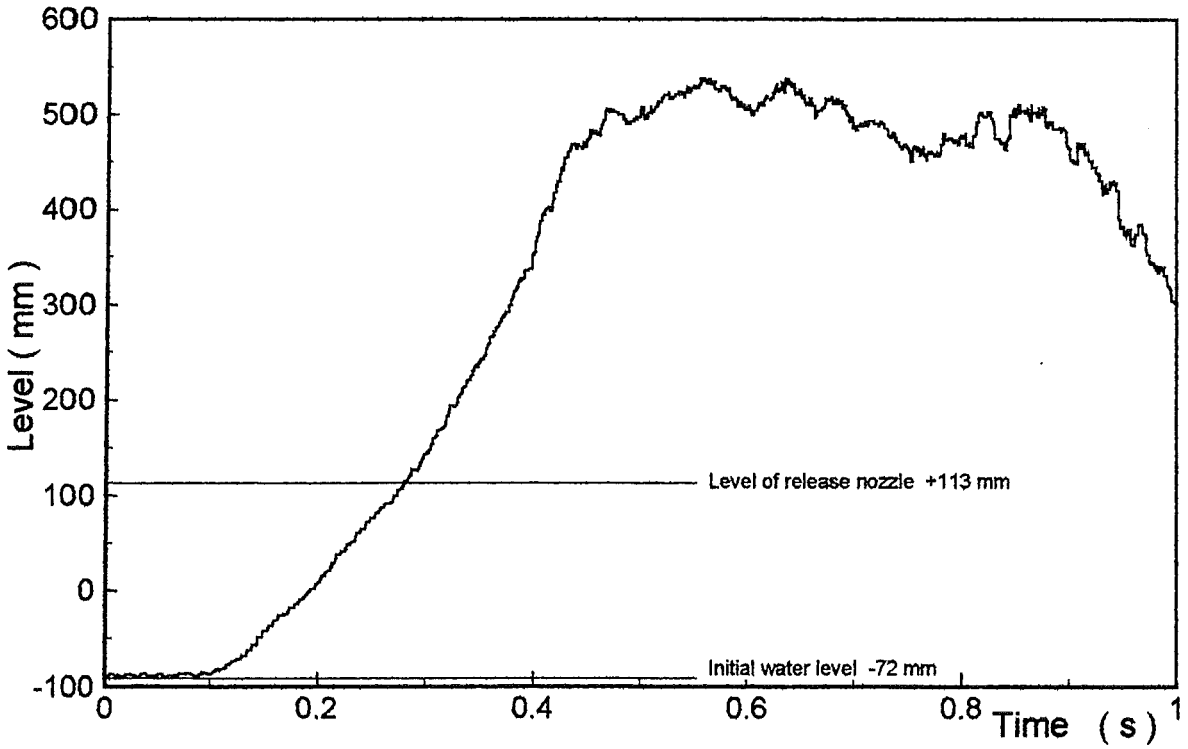

Fig. 3.2;34: PM04 Level measurement

LEVEL | 11.12.1995

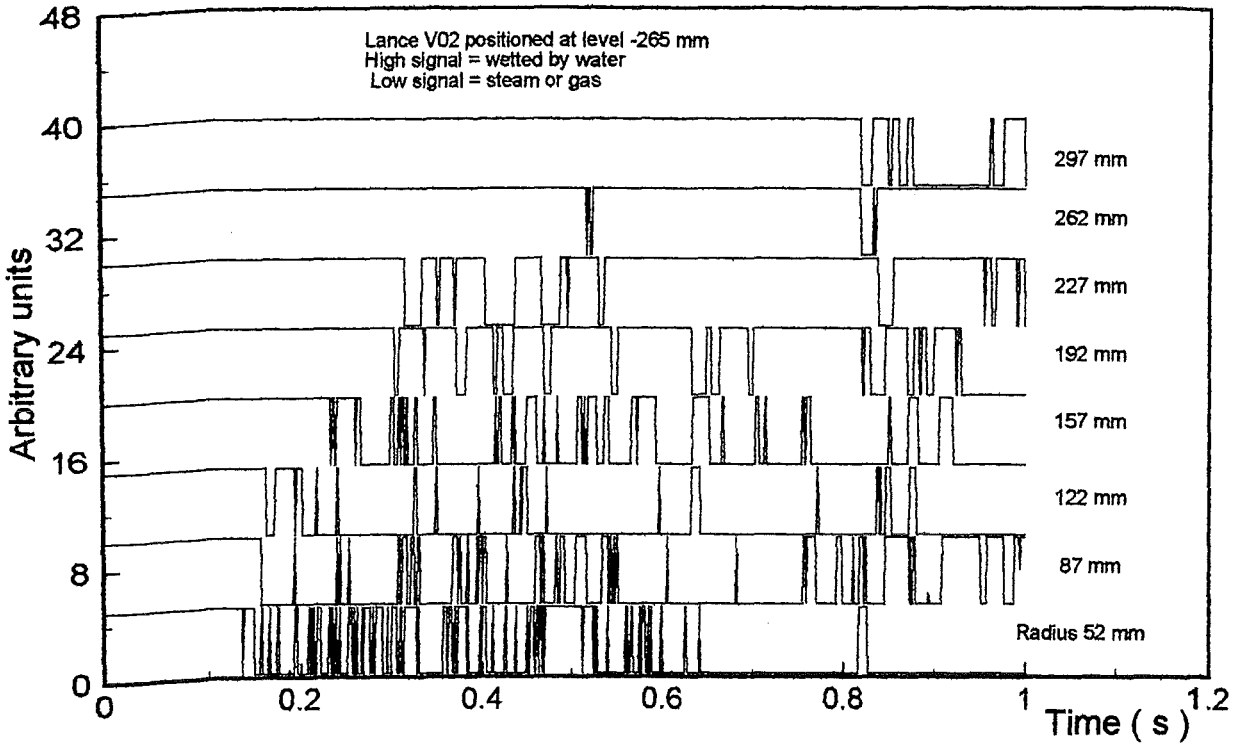

Fig. 3.2;35: PM 04, Void sensor signals

VOID | 11.12.1995

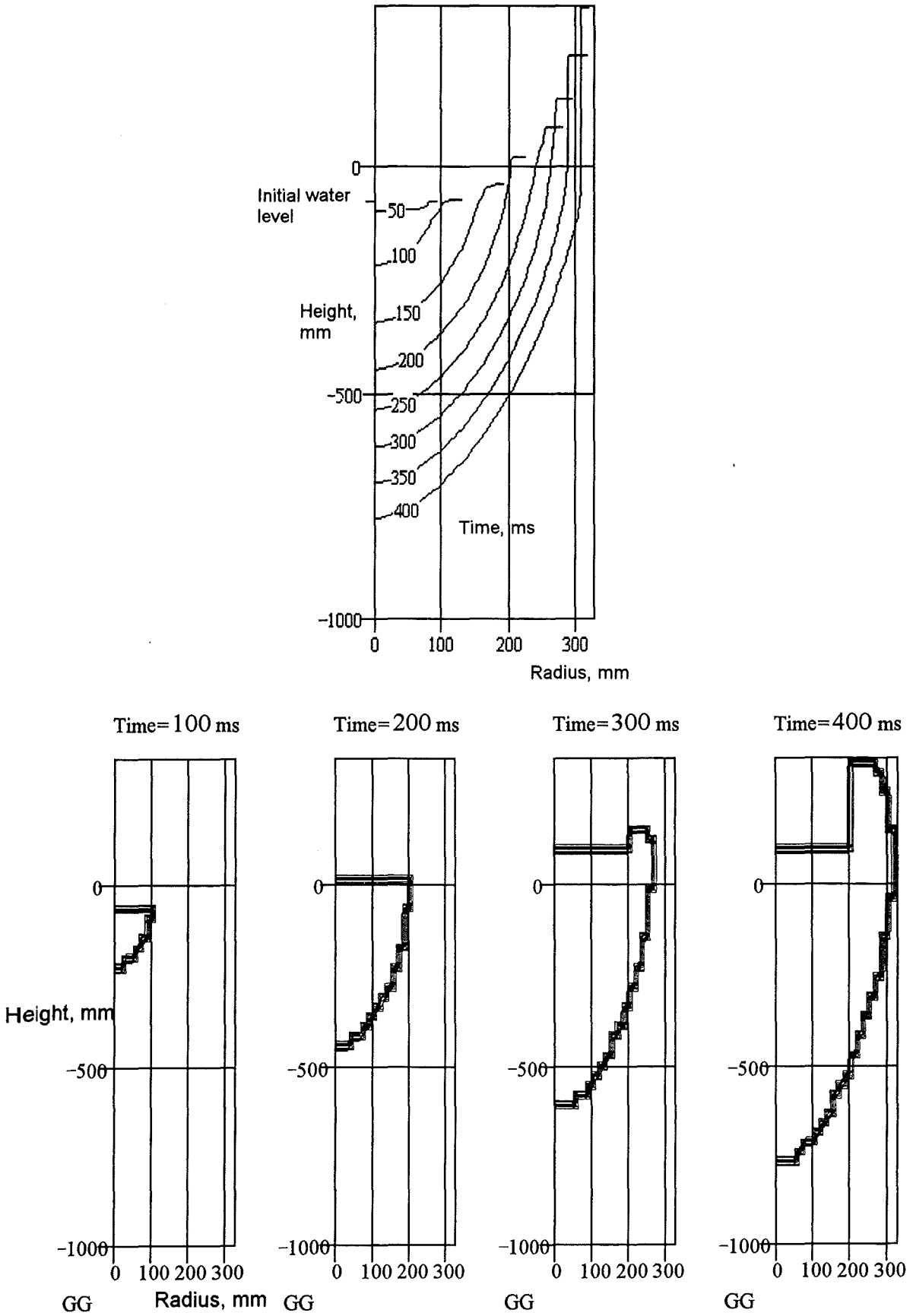

Fig. 3.2;36 : PM04. Development of the interaction region with the time as a parameter. For further description see test PM02, Fig. 3.2;16

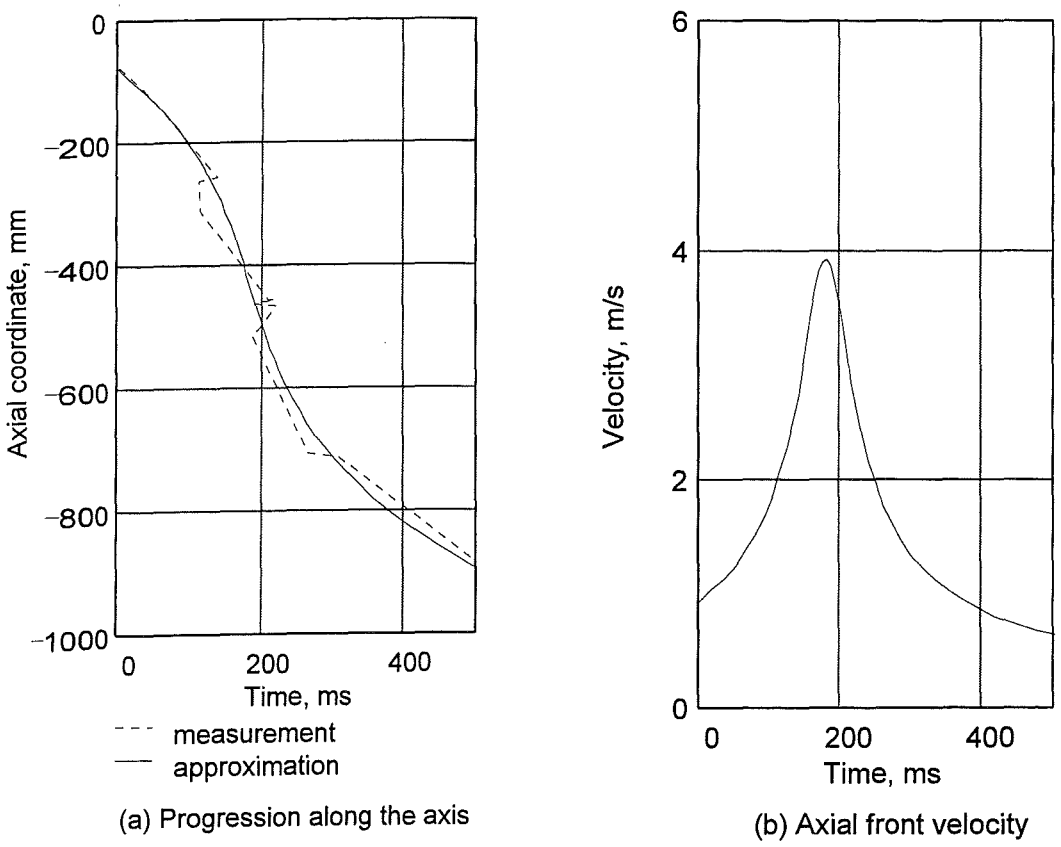

Fig. 3.2;37: PM04: Progression of the interaction region along the vessel axis and derived velocity. The measurements are approximated by a function of third order (method of least squares).

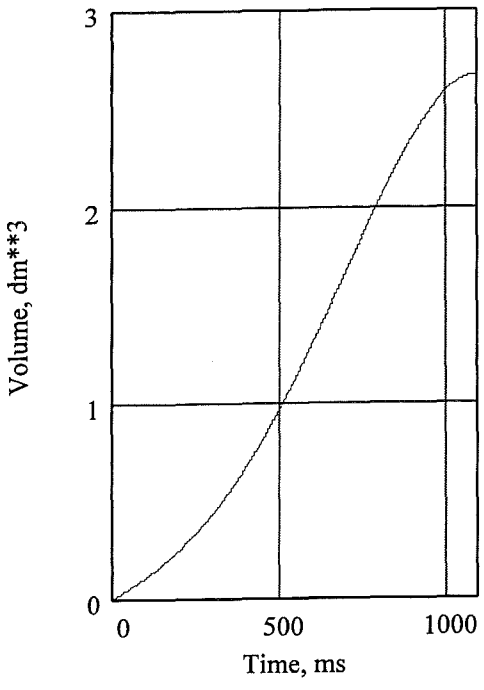

Fig. 3.2;38: PM04. Function assumed to describe the volume flow of the melt entering the interaction region.

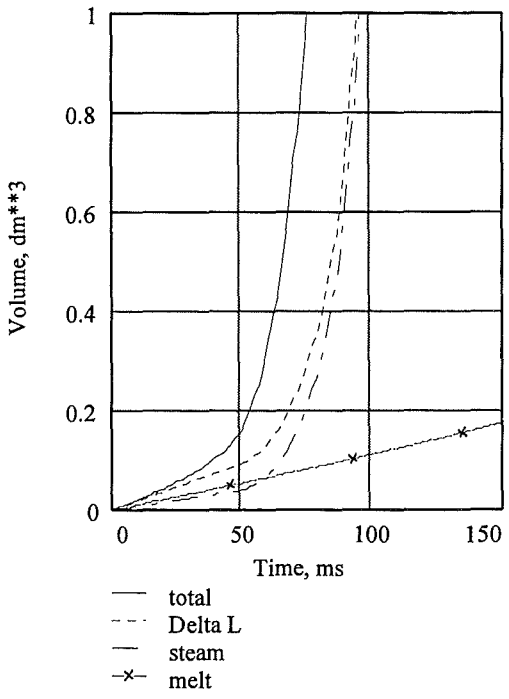

Fig. 3.2;39: PM04. Time histories of some of the partial volumes as approximated for the initial period of time

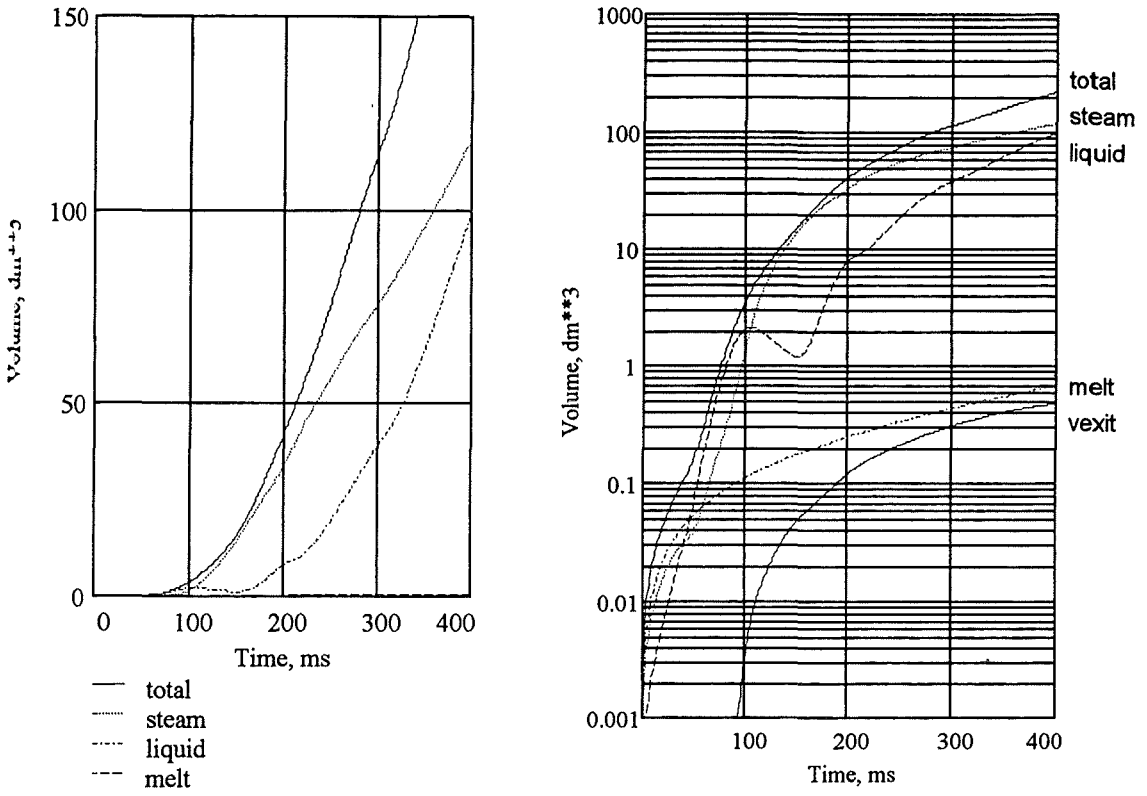

Fig. 3.2;40: PM04. Total volume and partial volumes of the interaction region. The curve labelled with vexit illustrates the small contribution of the outgoing steam.

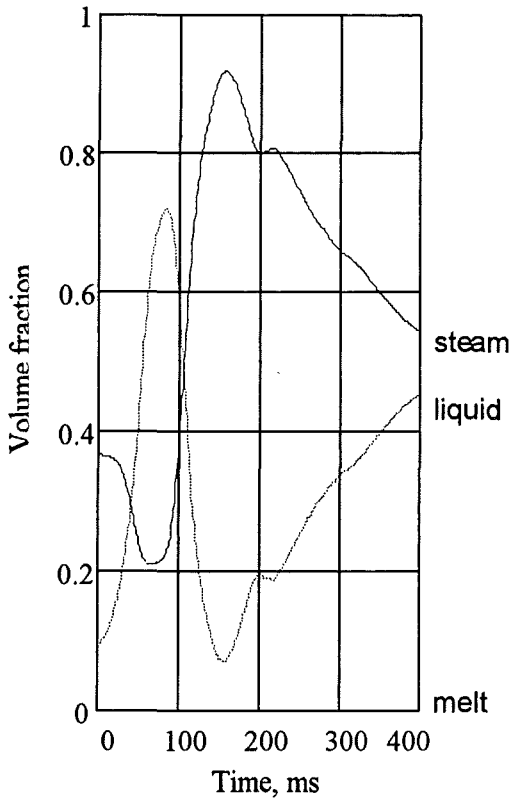

Fig. 3.2;41: PM04. Volume fractions of the three partial volumes

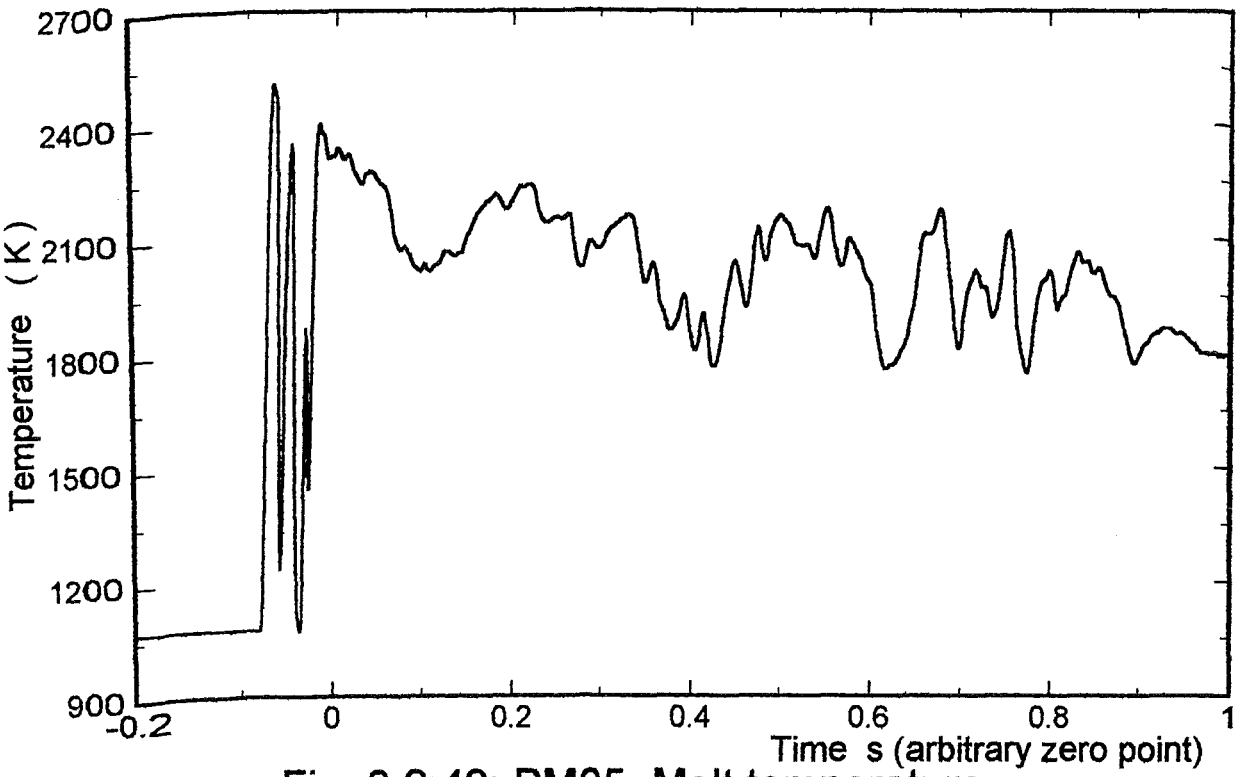

Fig. 3.2;42: PM05, Melt temperature

PYRO | 11.12.1995

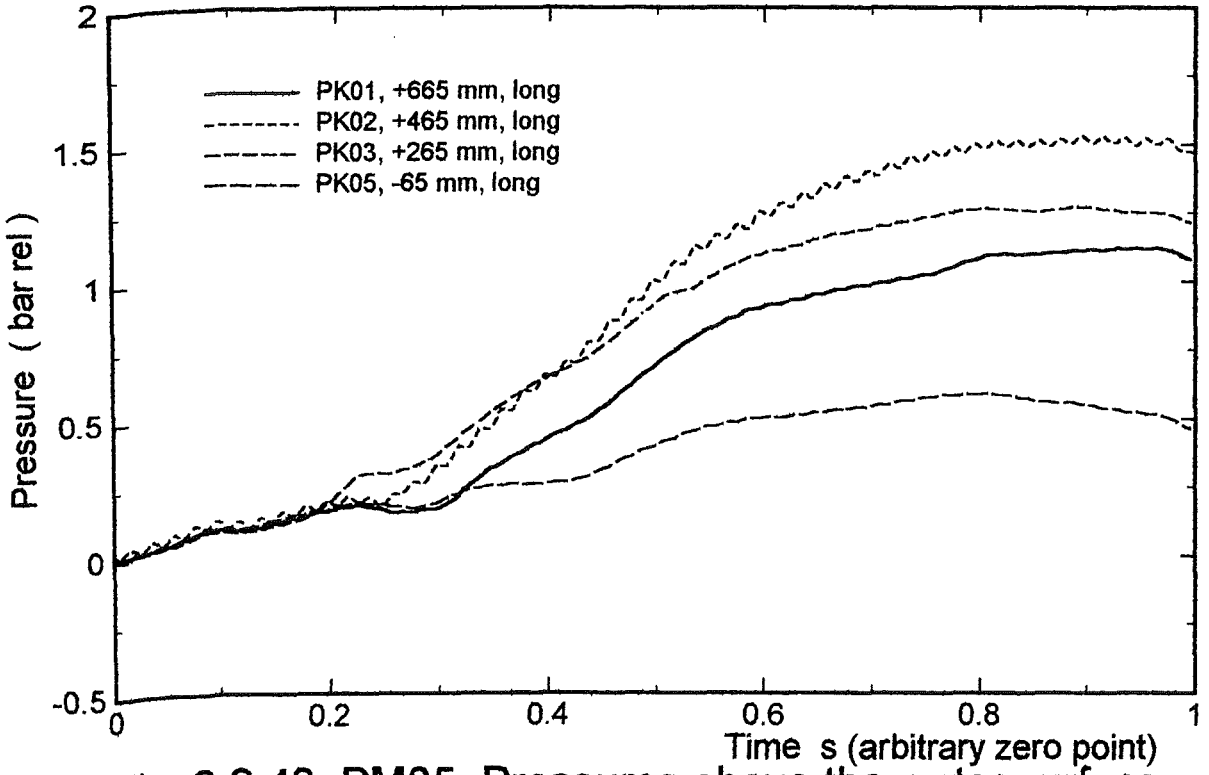

Fig. 3.2;43: PM05, Pressures above the water surface

DRUCK3 | 11.12.1995

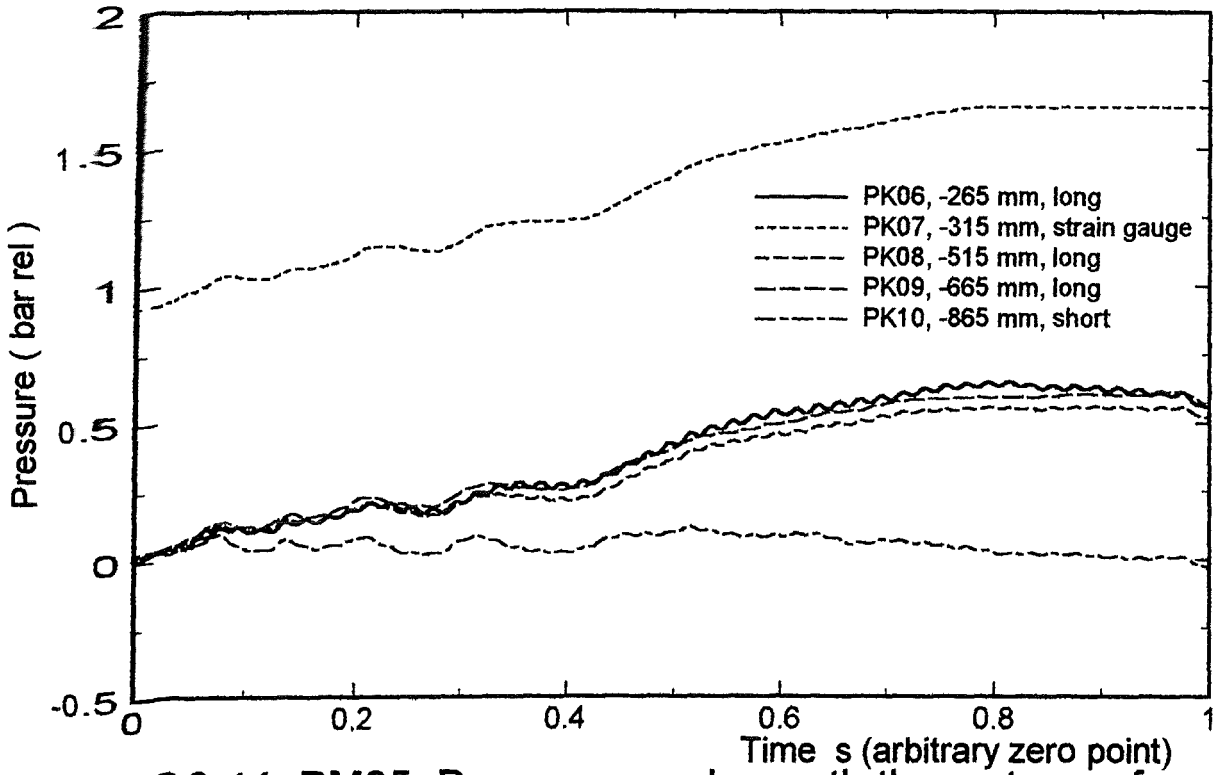

Fig. 3.2;44: PM05, Pressures underneath the water surface
(part 1)

DRUCK4 | 11.12.1995

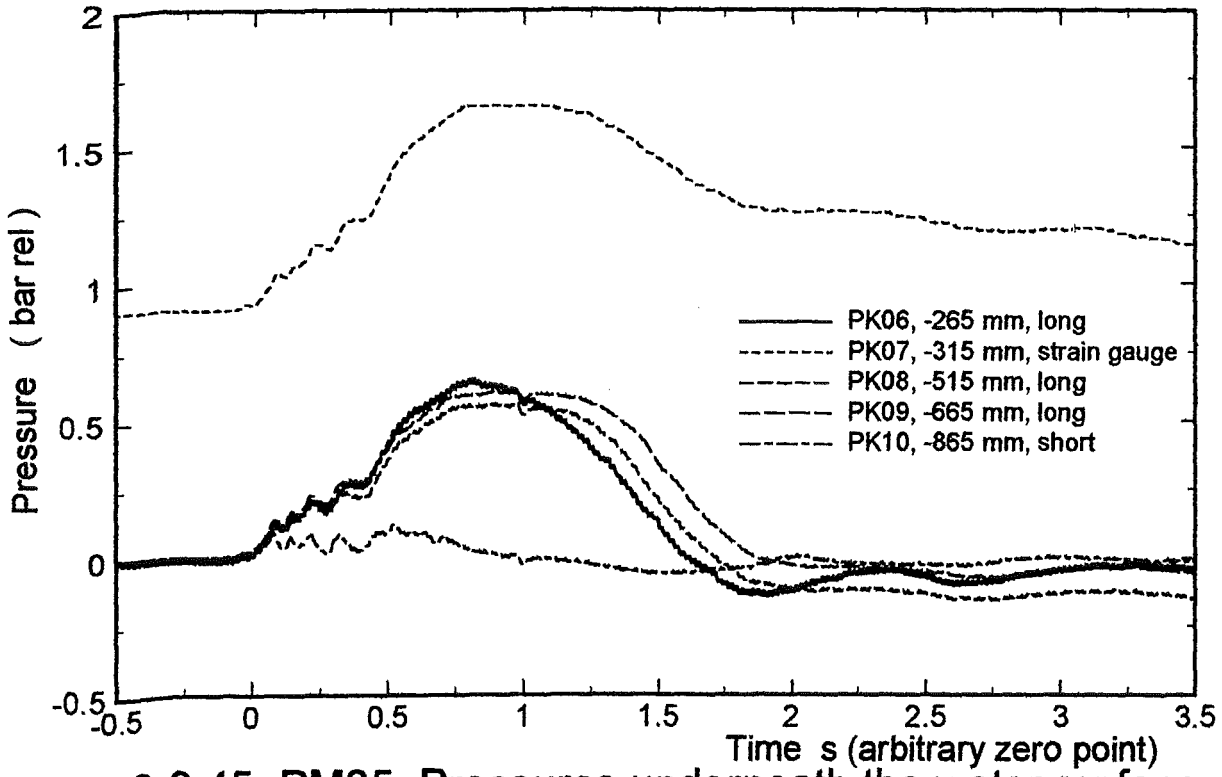

Fig. 3.2;45: PM05, Pressures underneath the water surface
(part 2)

DRUCK5 | 11.12.1995

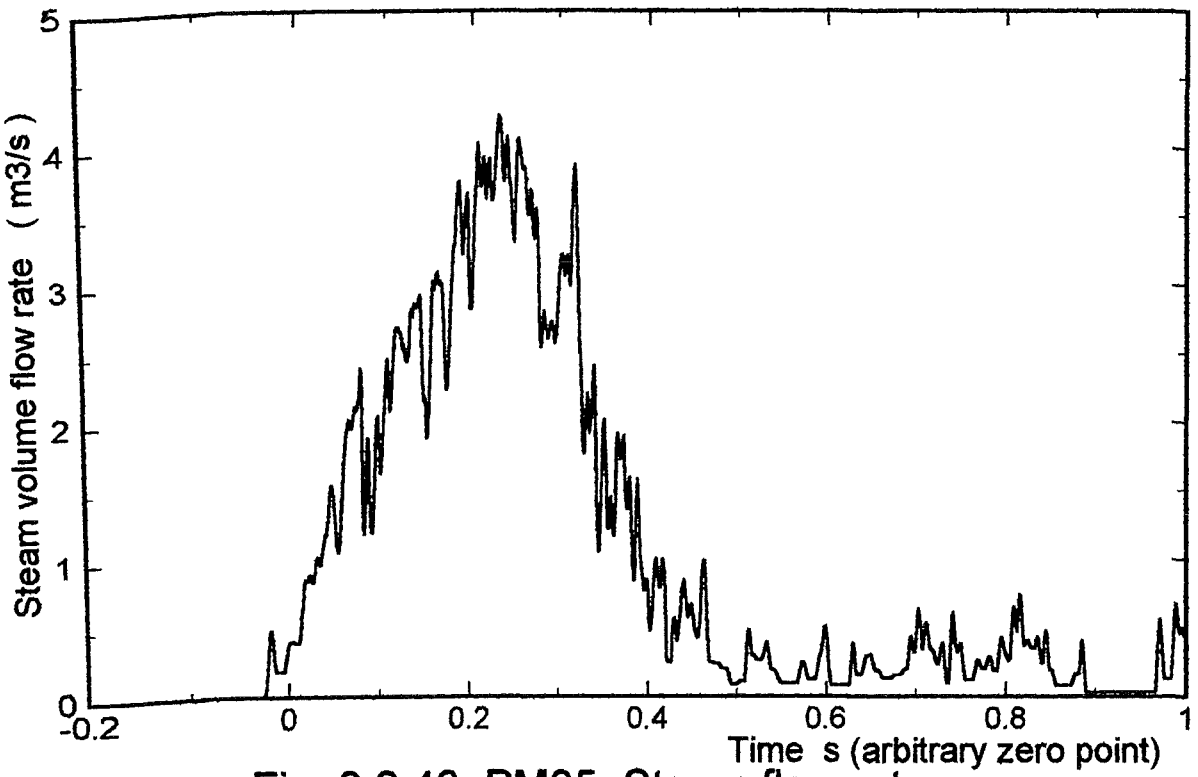

Fig. 3.2;46: PM05, Steam flow rate

STEAM | 11.12.1995

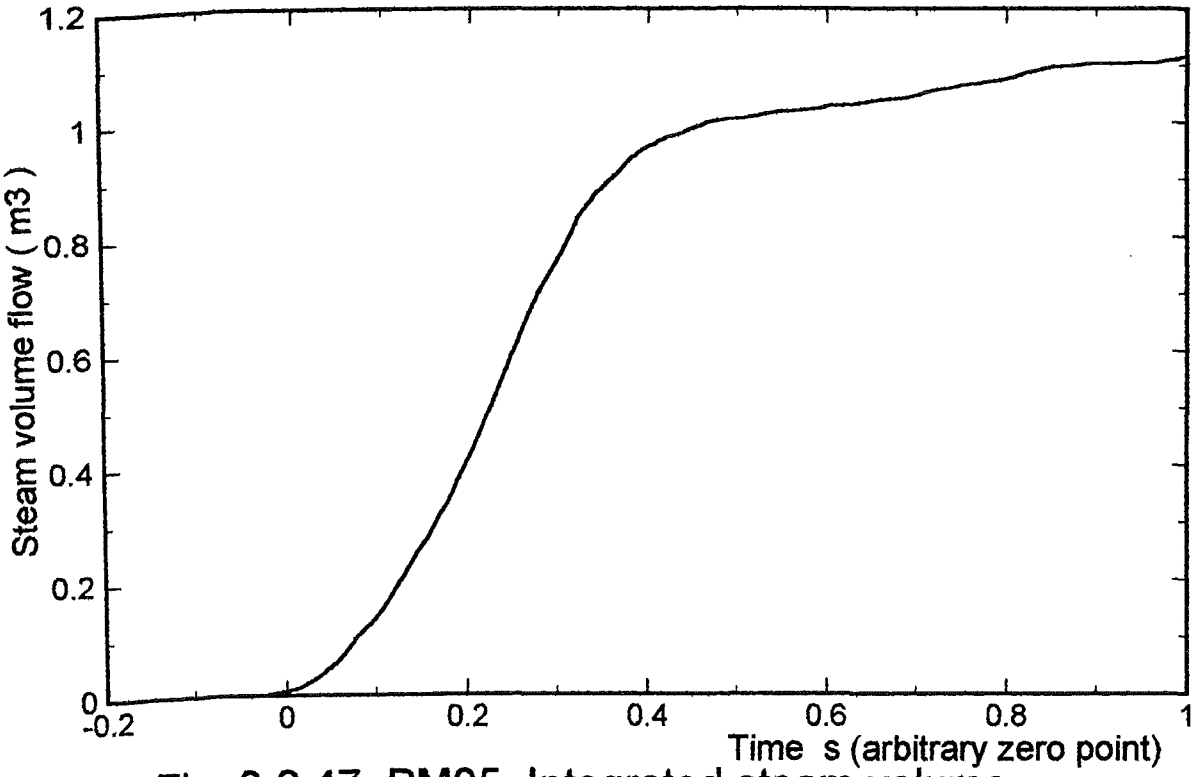

Fig. 3.2;47: PM05, Integrated steam volume

VOLUME | 11.12.1995

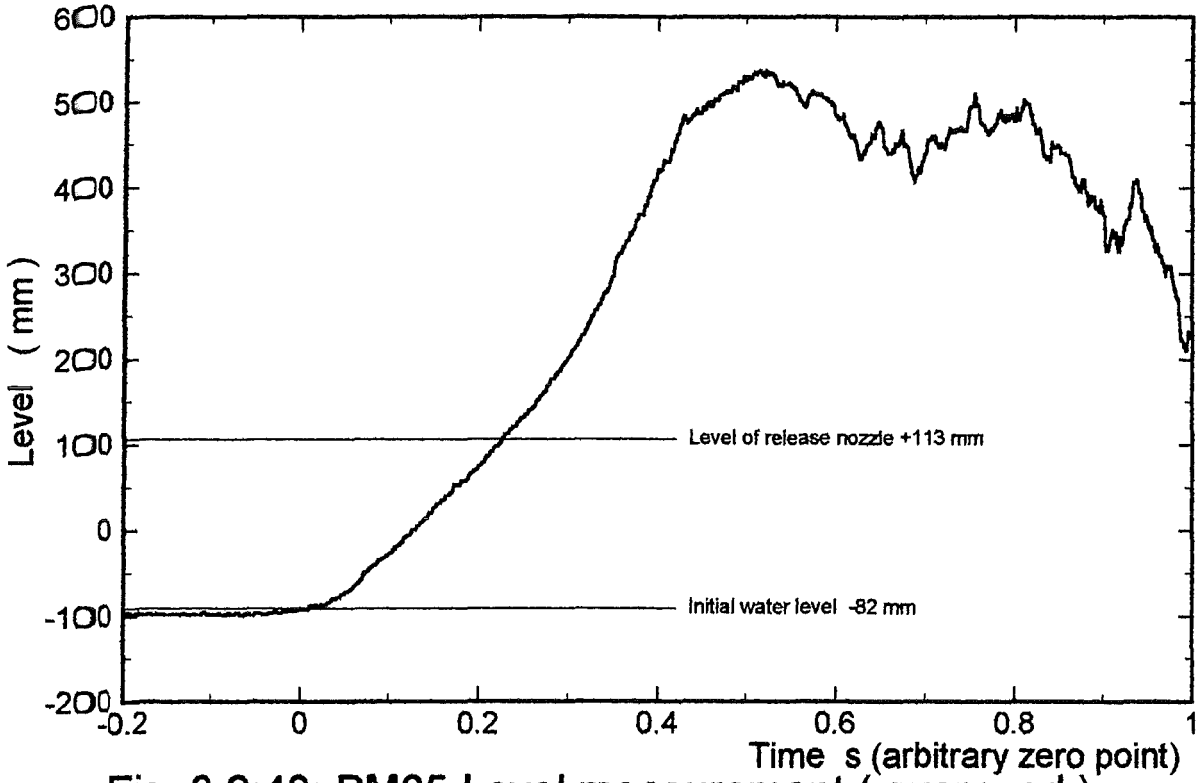

Fig. 3.2;48: PM05 Level measurement (averaged)

LEVEL | 11.12.1995

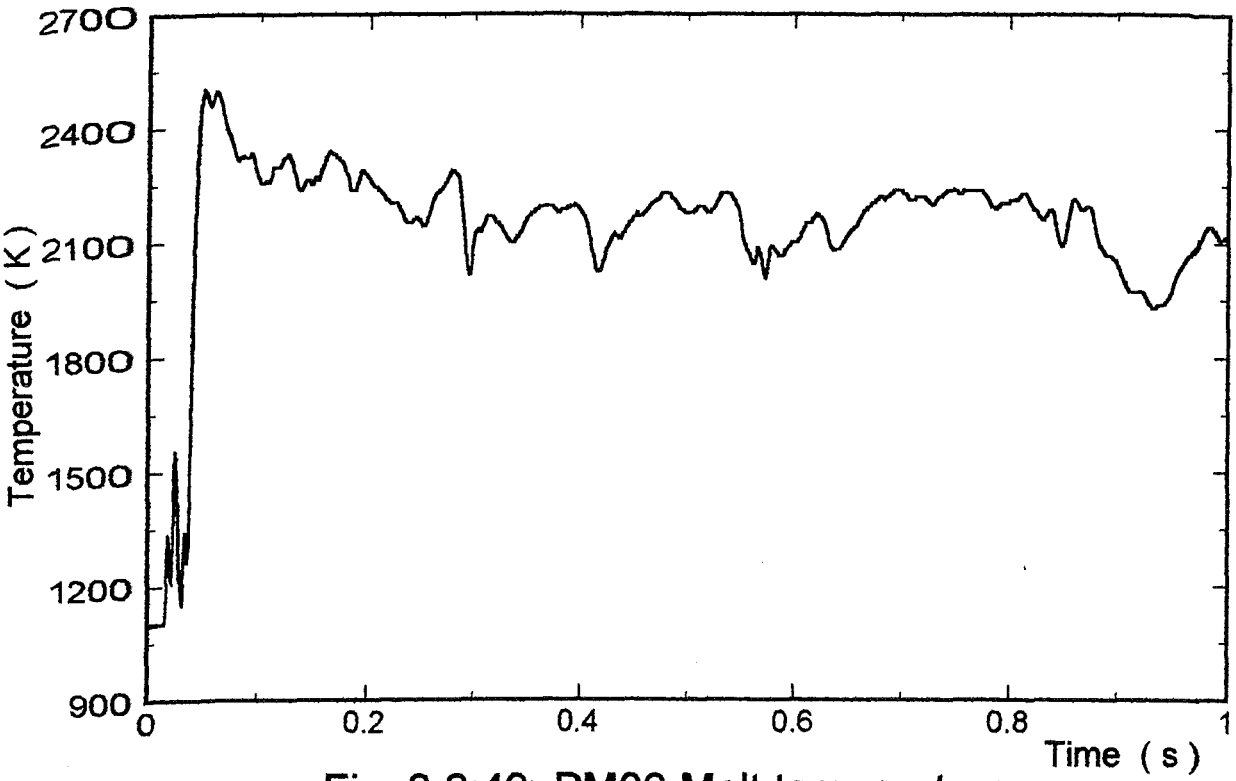

Fig. 3.2;49: PM06 Melt temperature

PYRO | 12.12.1995

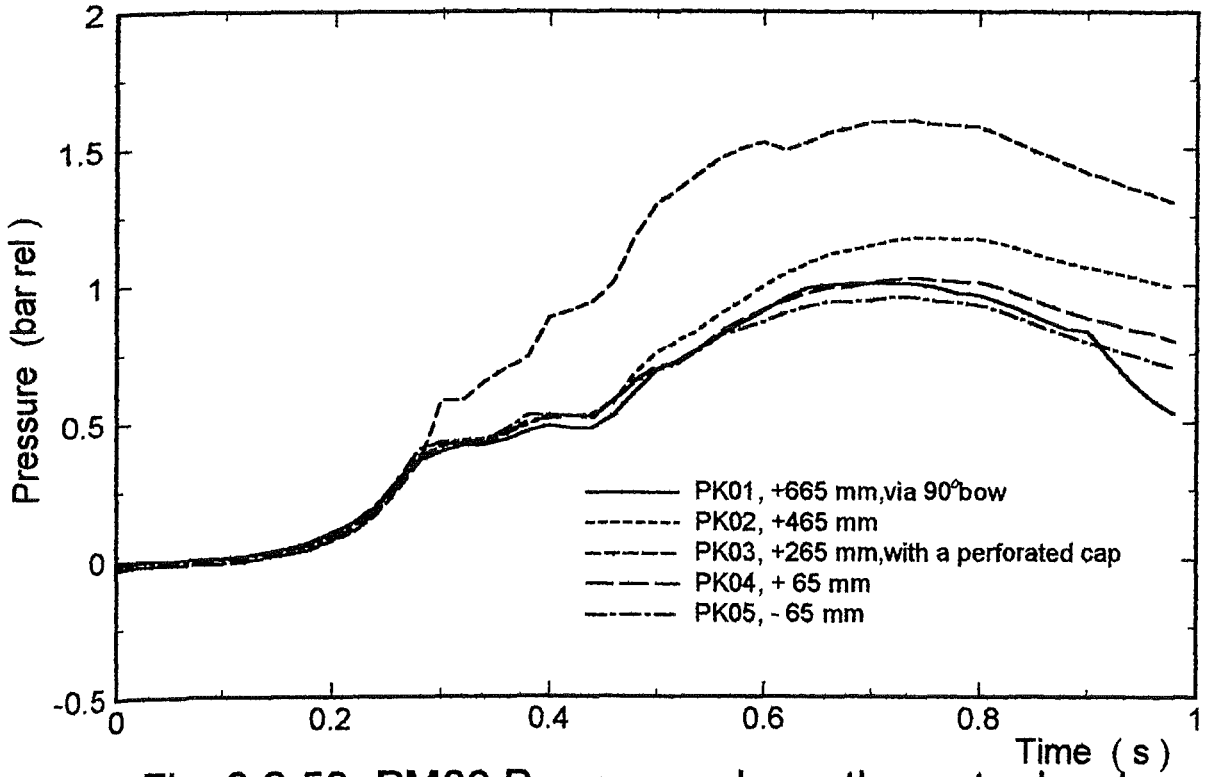

Fig. 3.2;50: PM06 Pressures above the water level

DRUCK1 | 12.12.1995

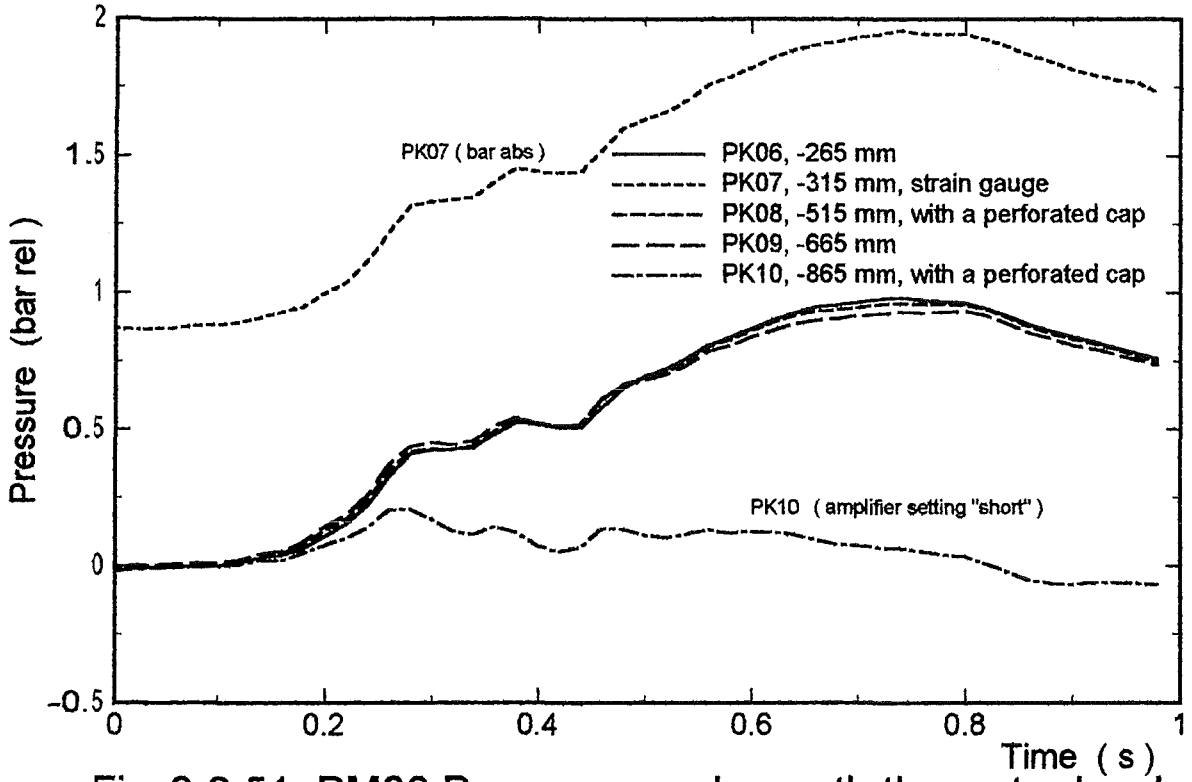

Fig. 3.2;51: PM06 Pressures underneath the water level

DRUCK2 | 12.12.1995

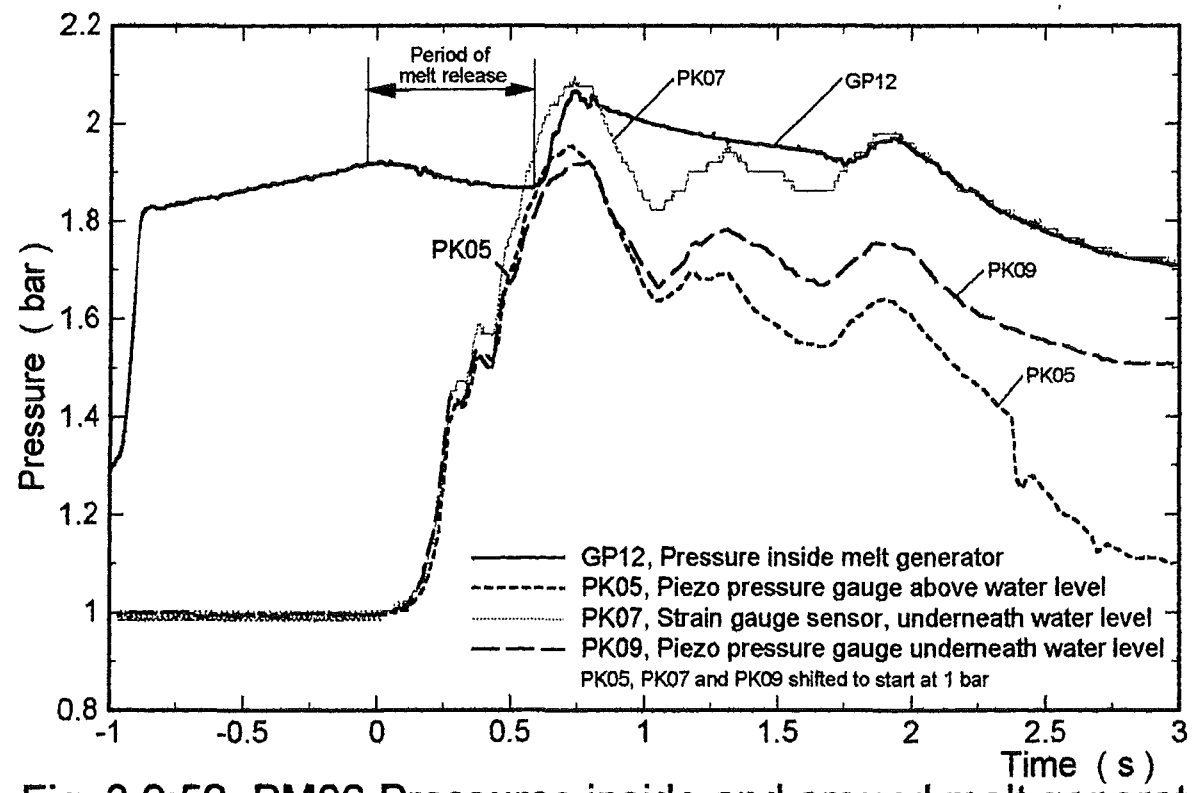

Fig. 3.2;52: PM06 Pressures inside and around melt generator

DRUCK3 | 12.12.1995

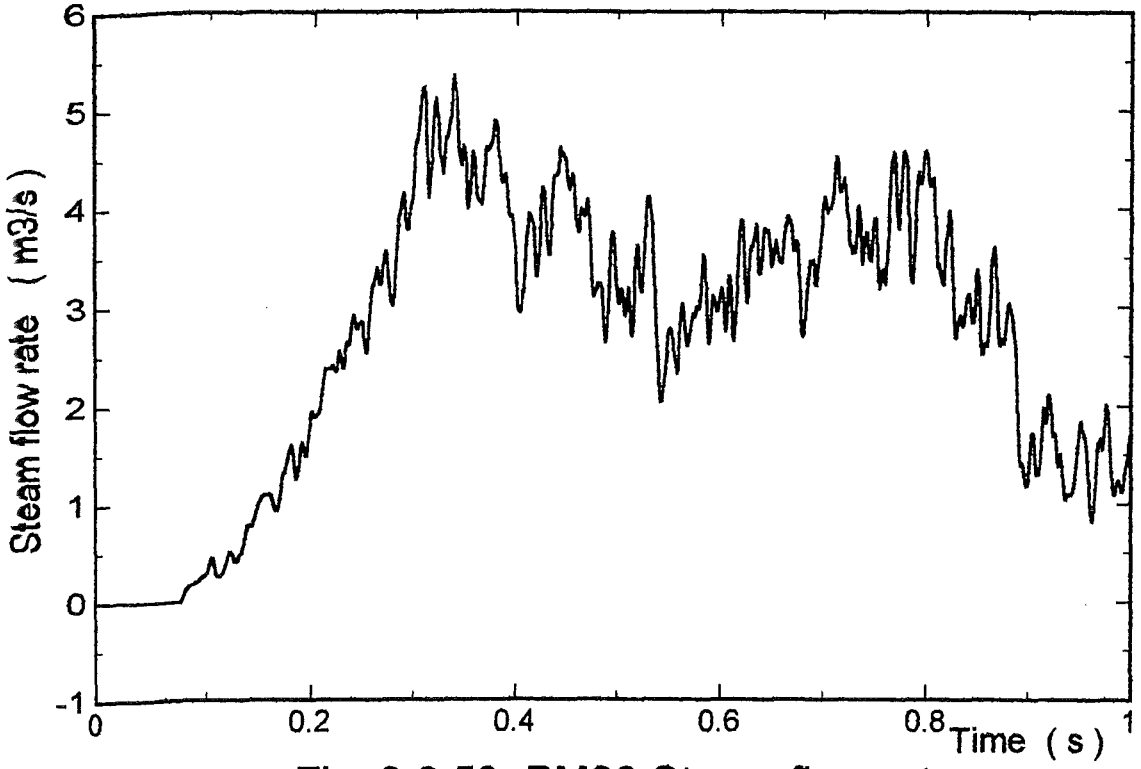

Fig. 3.2;53: PM06 Steam flow rate

STEAM | 12.12.1995

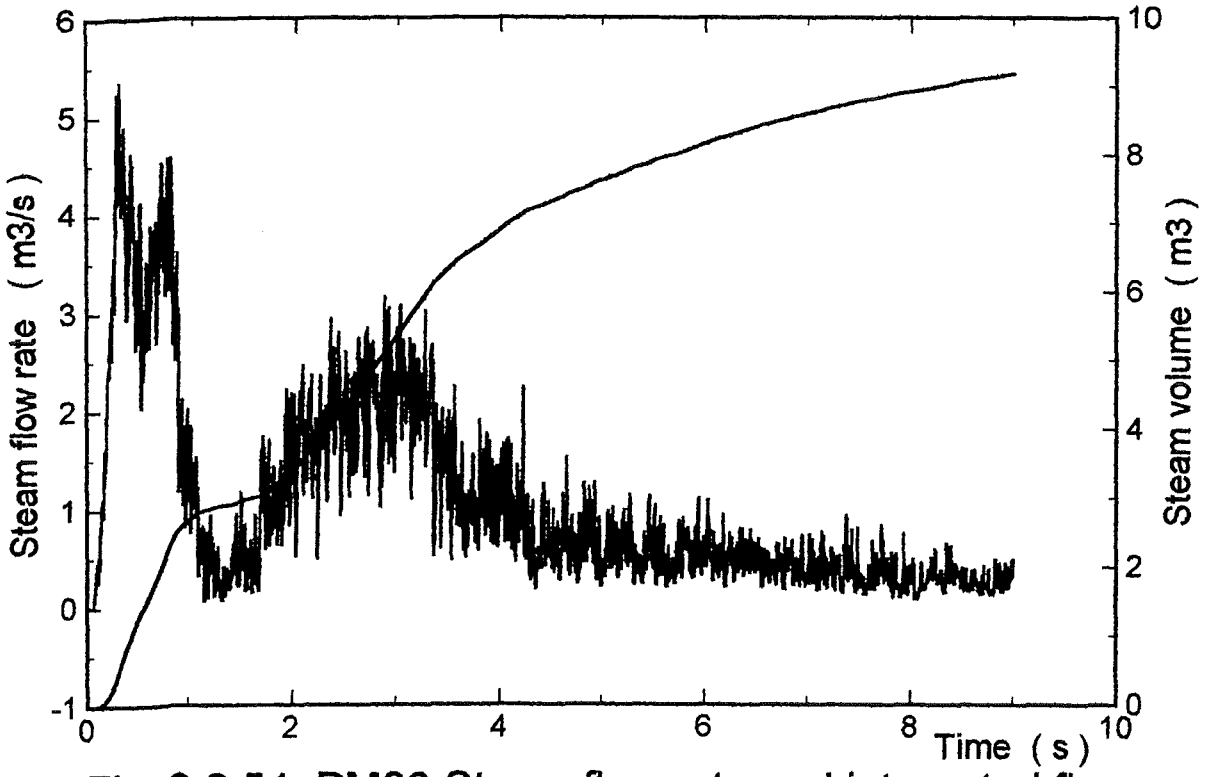

Fig. 3.2;54: PM06 Steam flow rate and integrated flow

STEAM1 | 12.12.1995

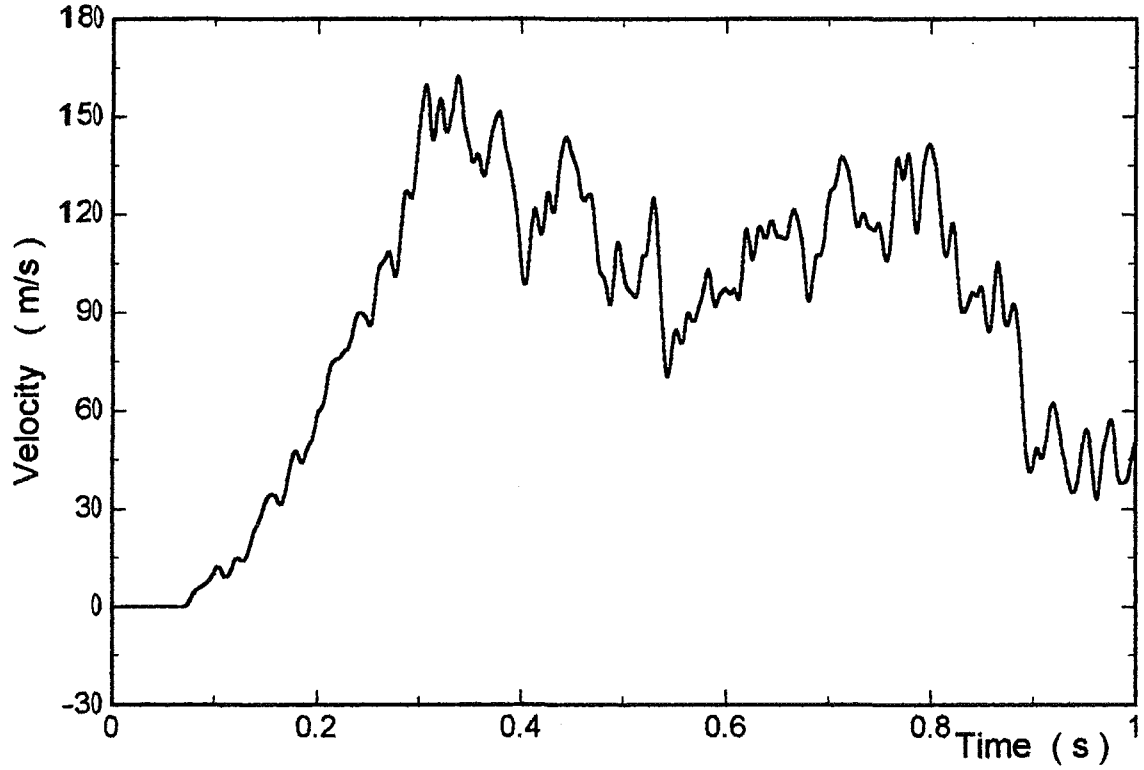

Fig. 3.2;55: PM06 Average steam velocity

VELOCITY | 12.12.1995

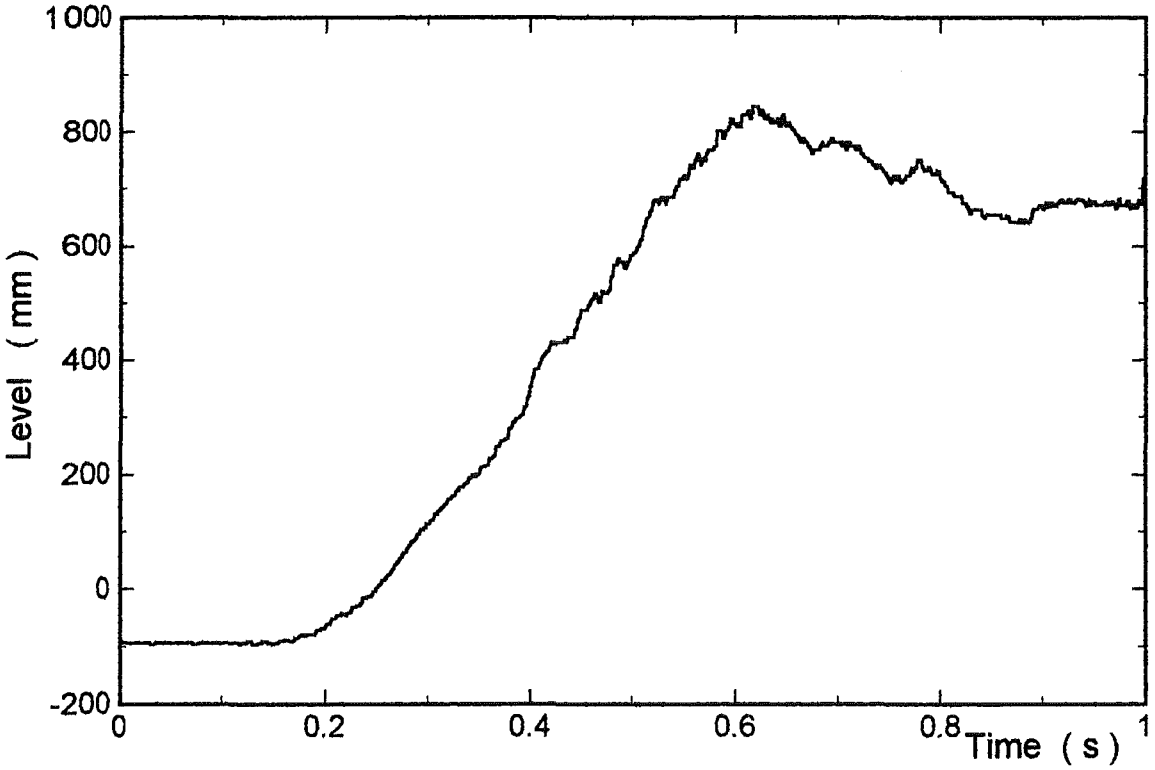

Fig. 3.2;56: PM06 Level measurement (averaged)

LEVEL | 12.12.1995

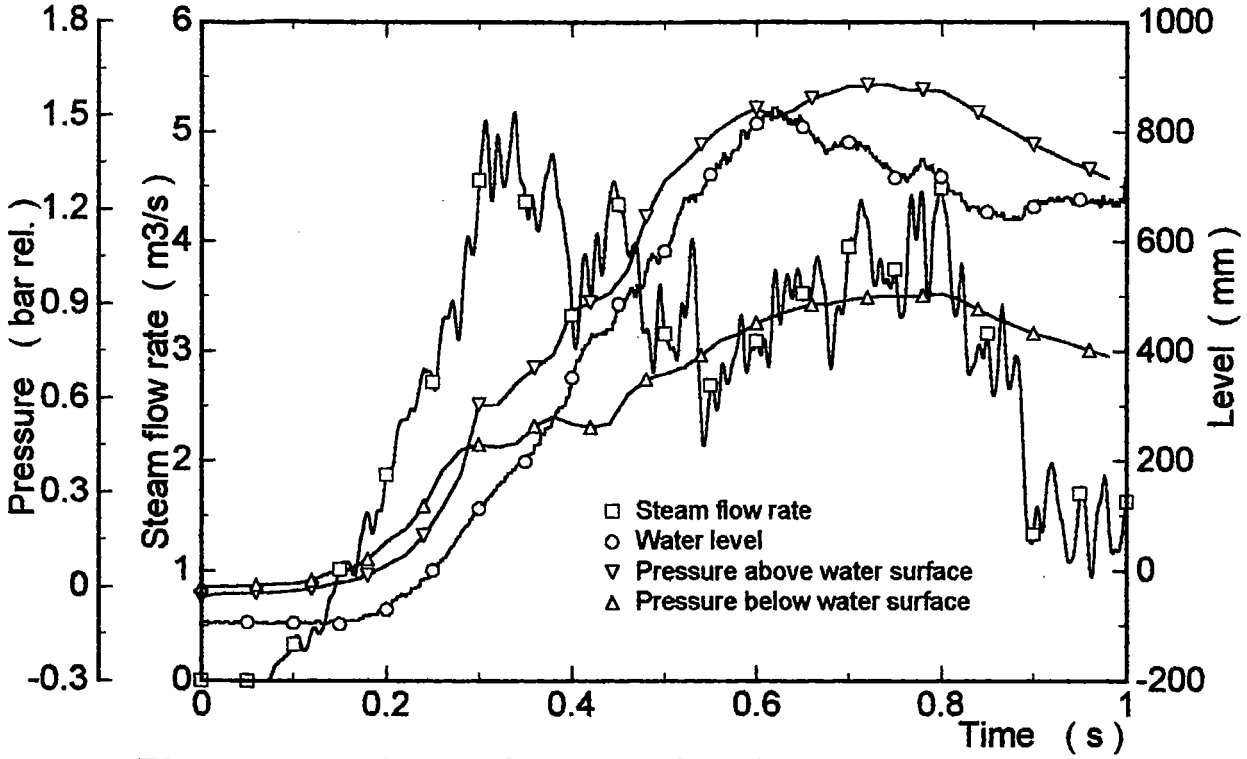

Fig. 3.2.57: PM06 Survey of various measurements

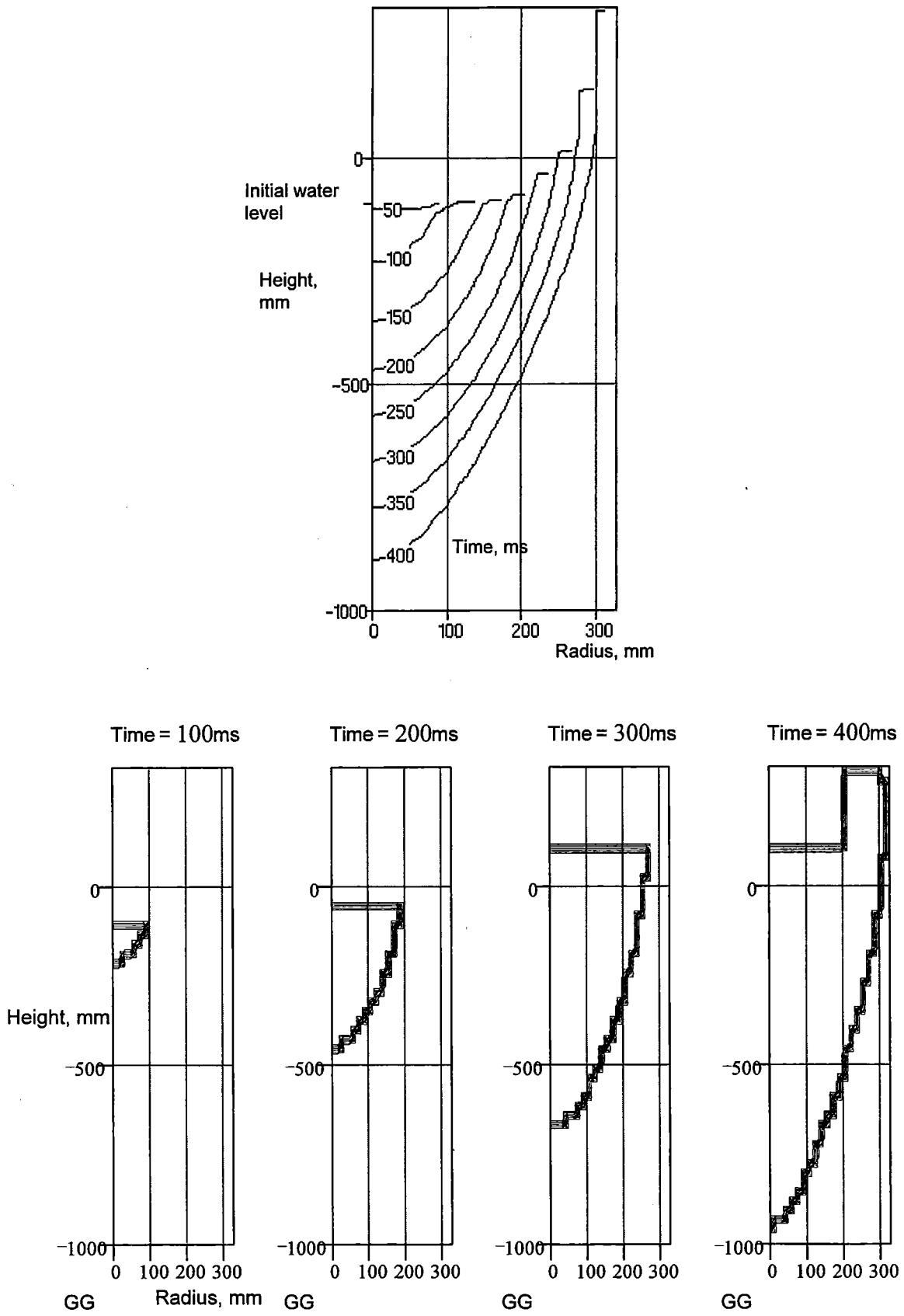

Fig. 3.2;58: PM06. Progression of the interaction region with the time as a parameter. For further description see Fig. 3.2;16, test PM02.

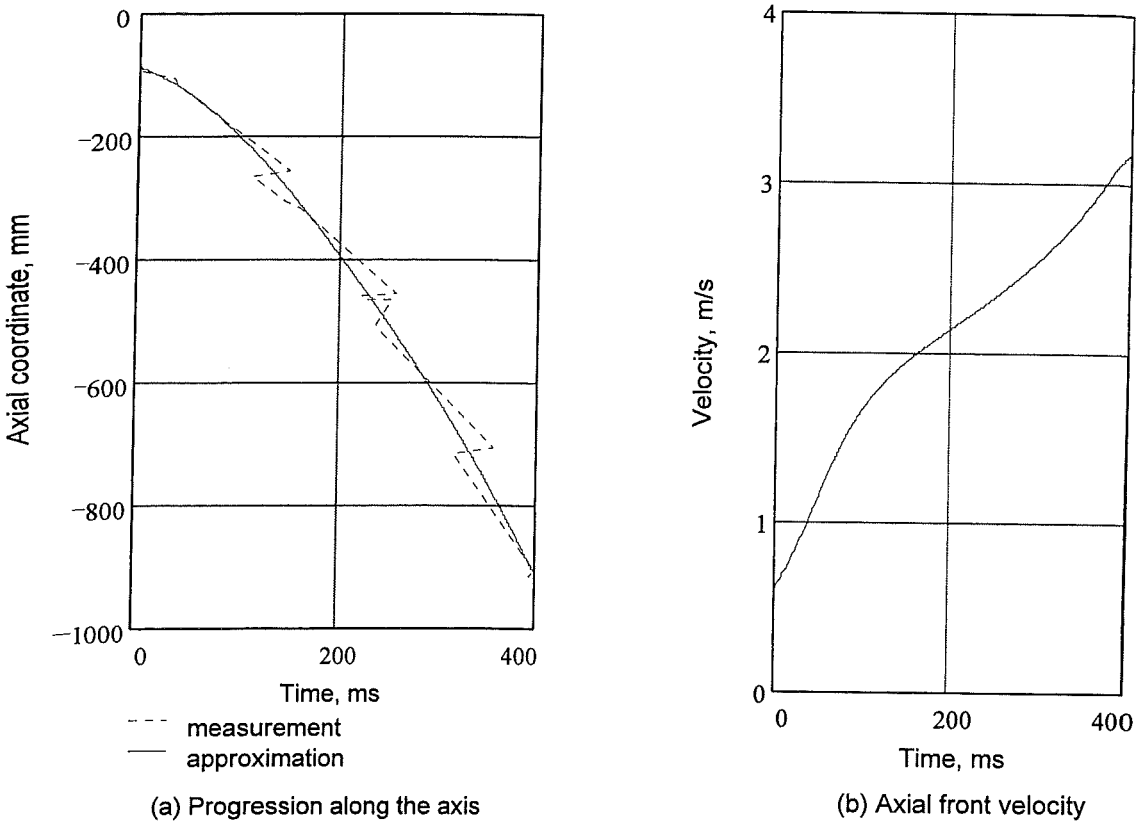

(a) Progression along the axis

(b) Axial front velocity

Fig. 3.2;59: PM06. Progression of the interaction region along the vessel axis and derived velocity. The measurements are approximated by a function of second order (method of least squares).

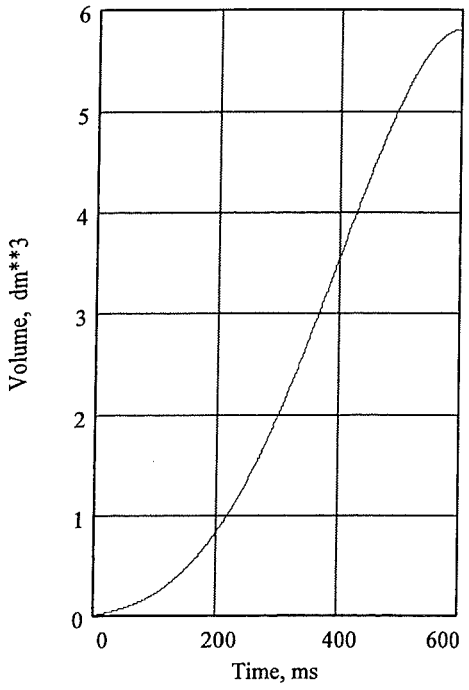

Fig. 3.2;60: PM06. Function assumed to describe the volume flow of the melt entering the interaction region.

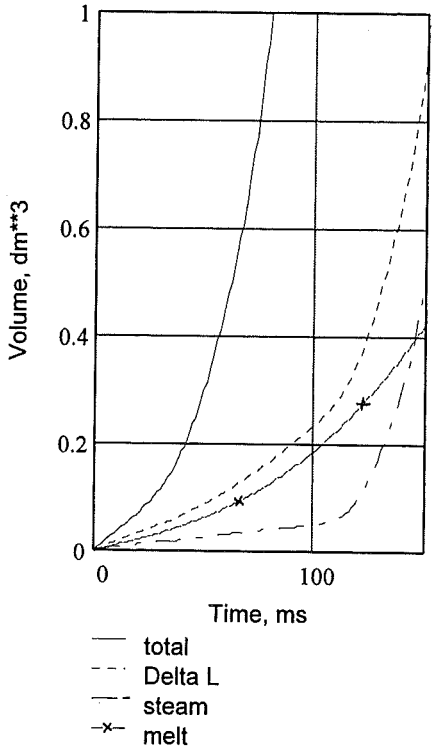

Fig. 3.2;61: PM06. Time histories of some of the partial volumes as approximated for the initial period of time

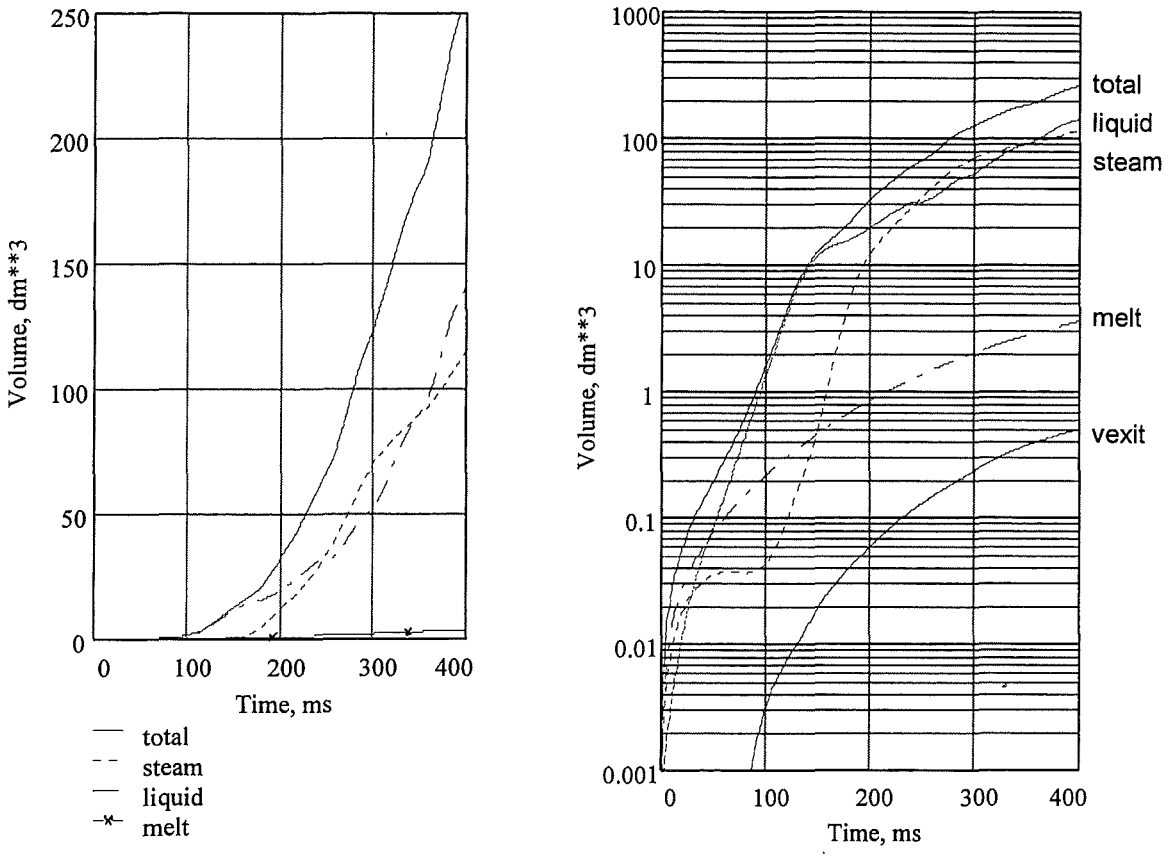

Fig. 3.2;62: PM06. Total and partial volumes of the interaction region

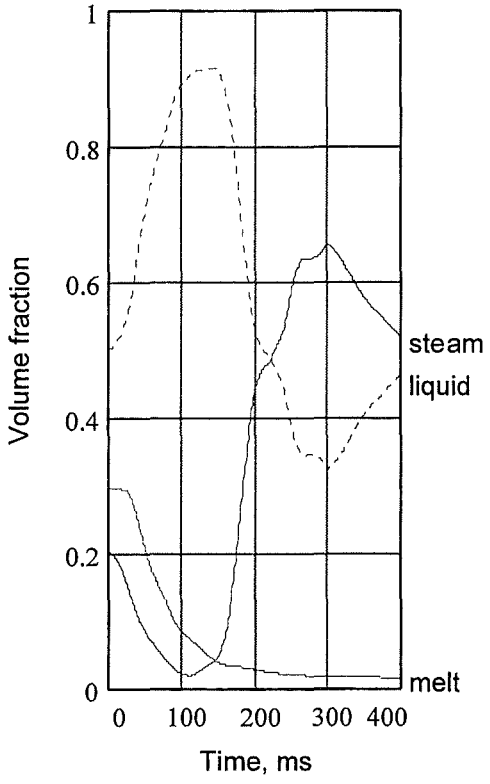

Fig. 3.2;63: PM06. Volume fractions of the three partial volumes.

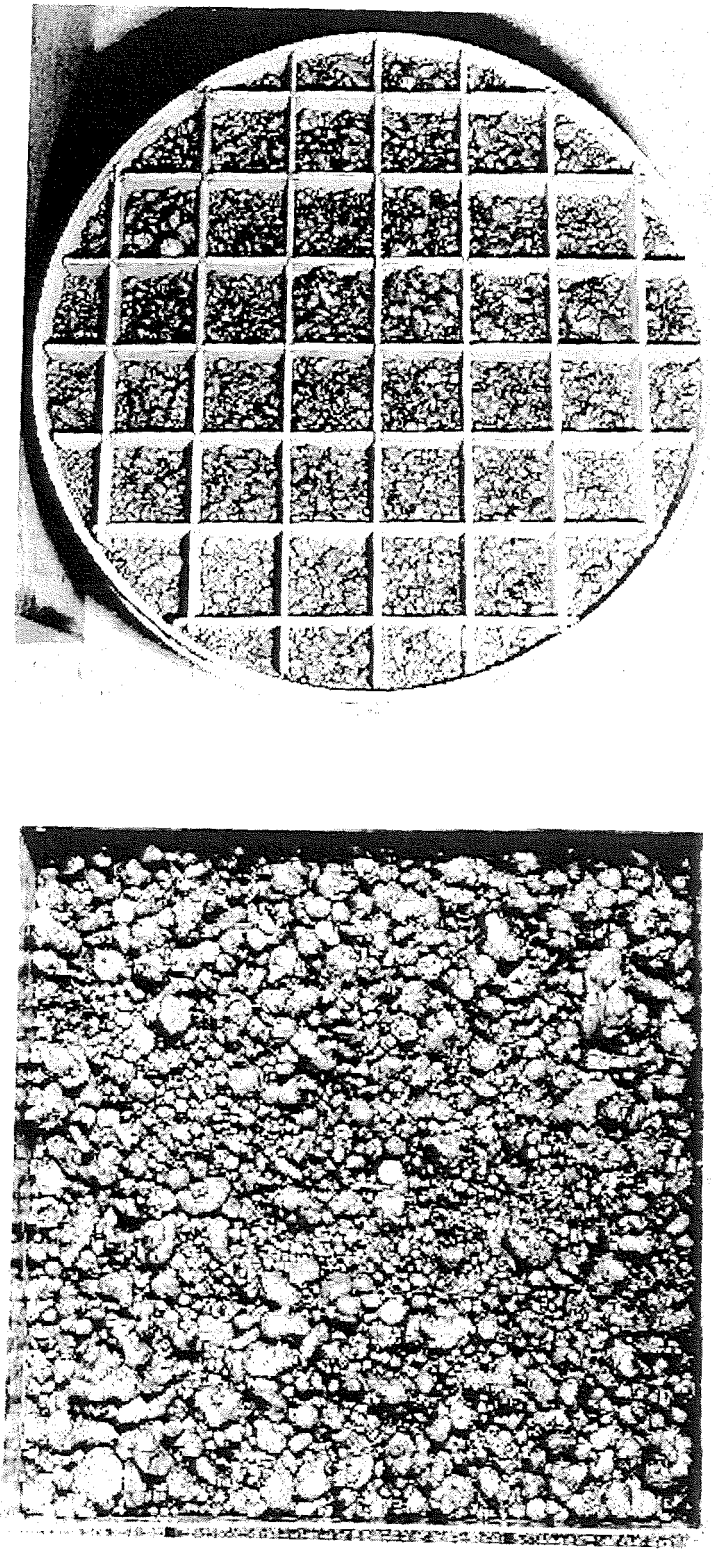

Fig. 3.3;1 PM02: Oxidic Debris after the Test

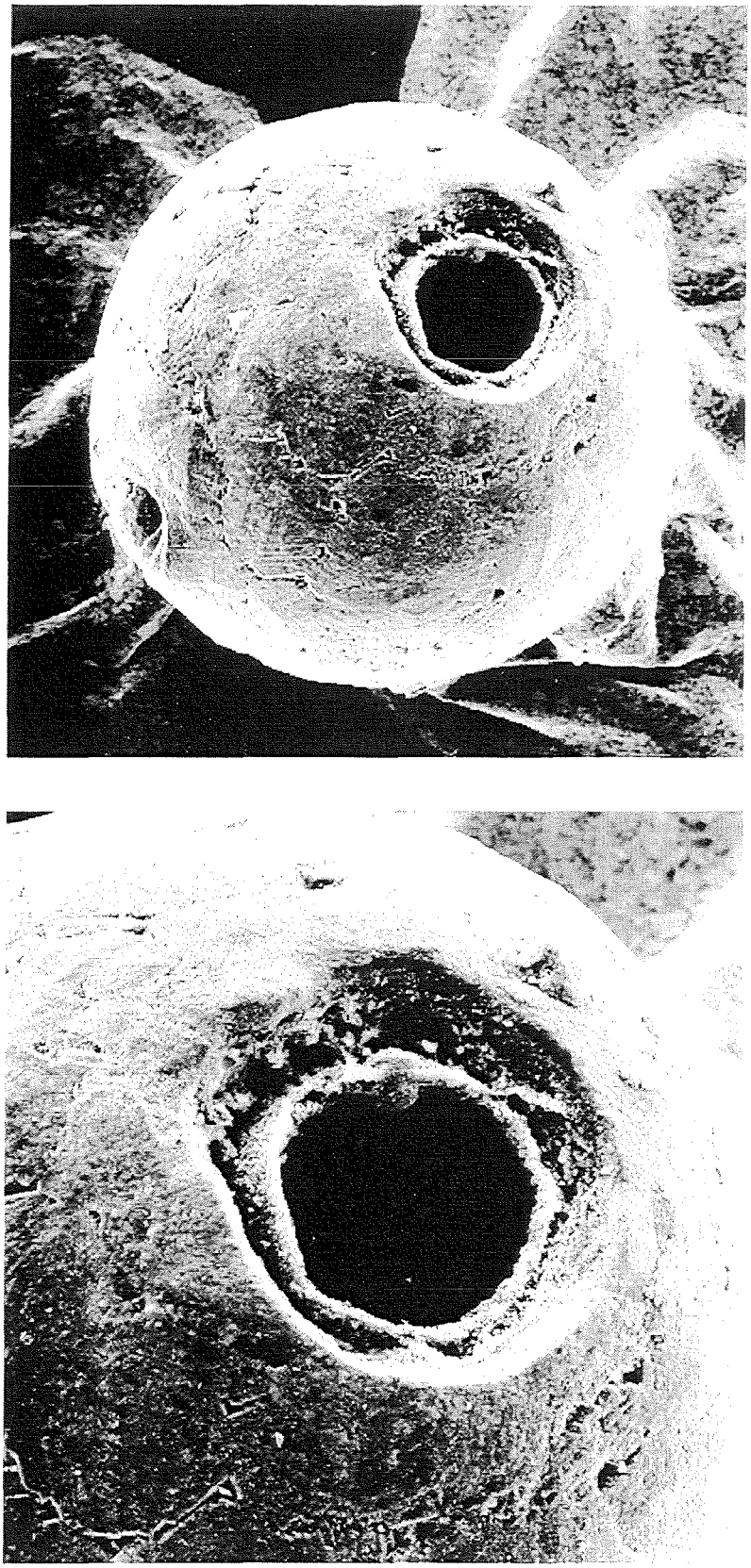

Fig. 3.3;2 PM01: Typical Hollow Particle (Ø 0.8 mm)

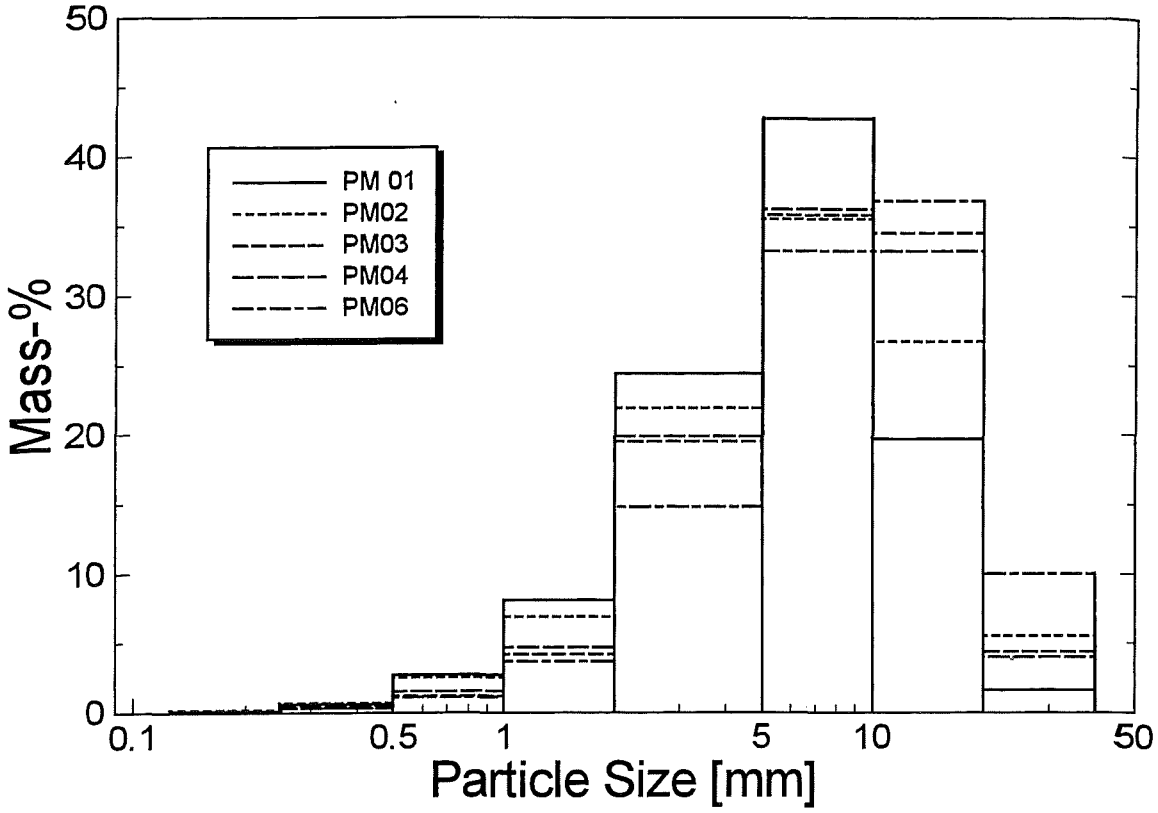

Fig. 3.3;3 Post-test Particle Size Distribution

> 10 mm

5 - 10 mm

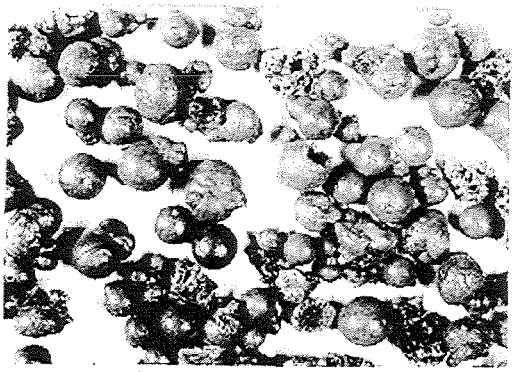

2 - 5 mm

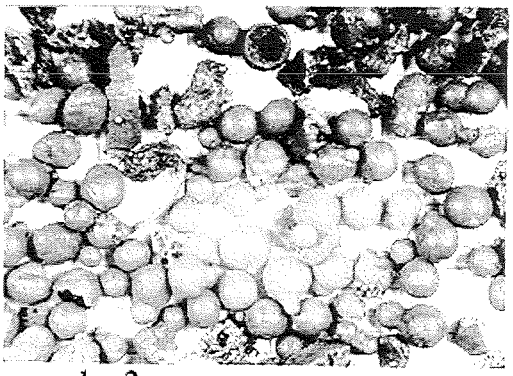

1 - 2 mm

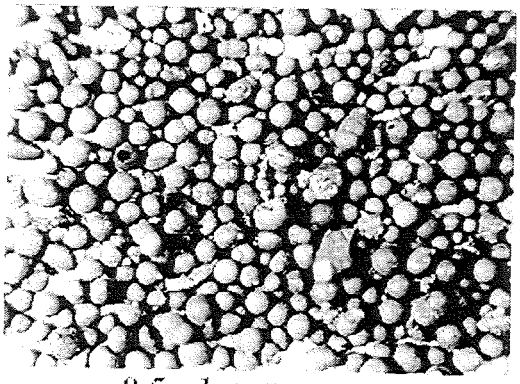

0.5 - 1 mm

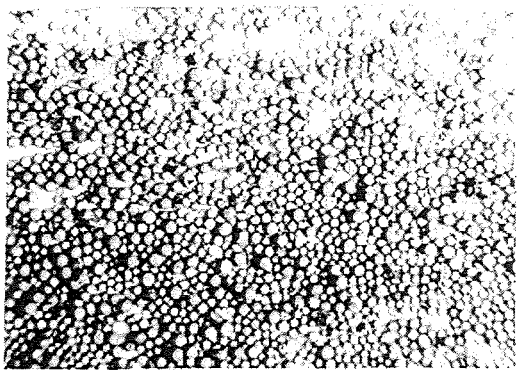

0.25 - 0.5 mm

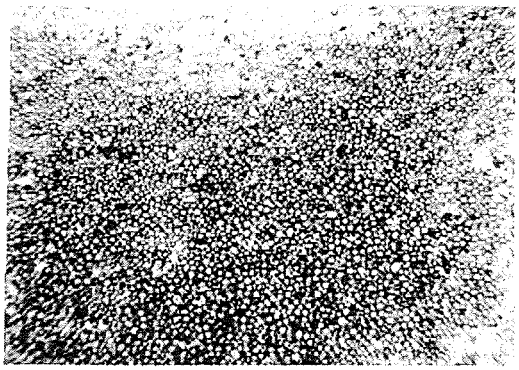

0.125 - 0.25 mm

Fig. 3.3;4 PM01: Debris after Sieve Analysis

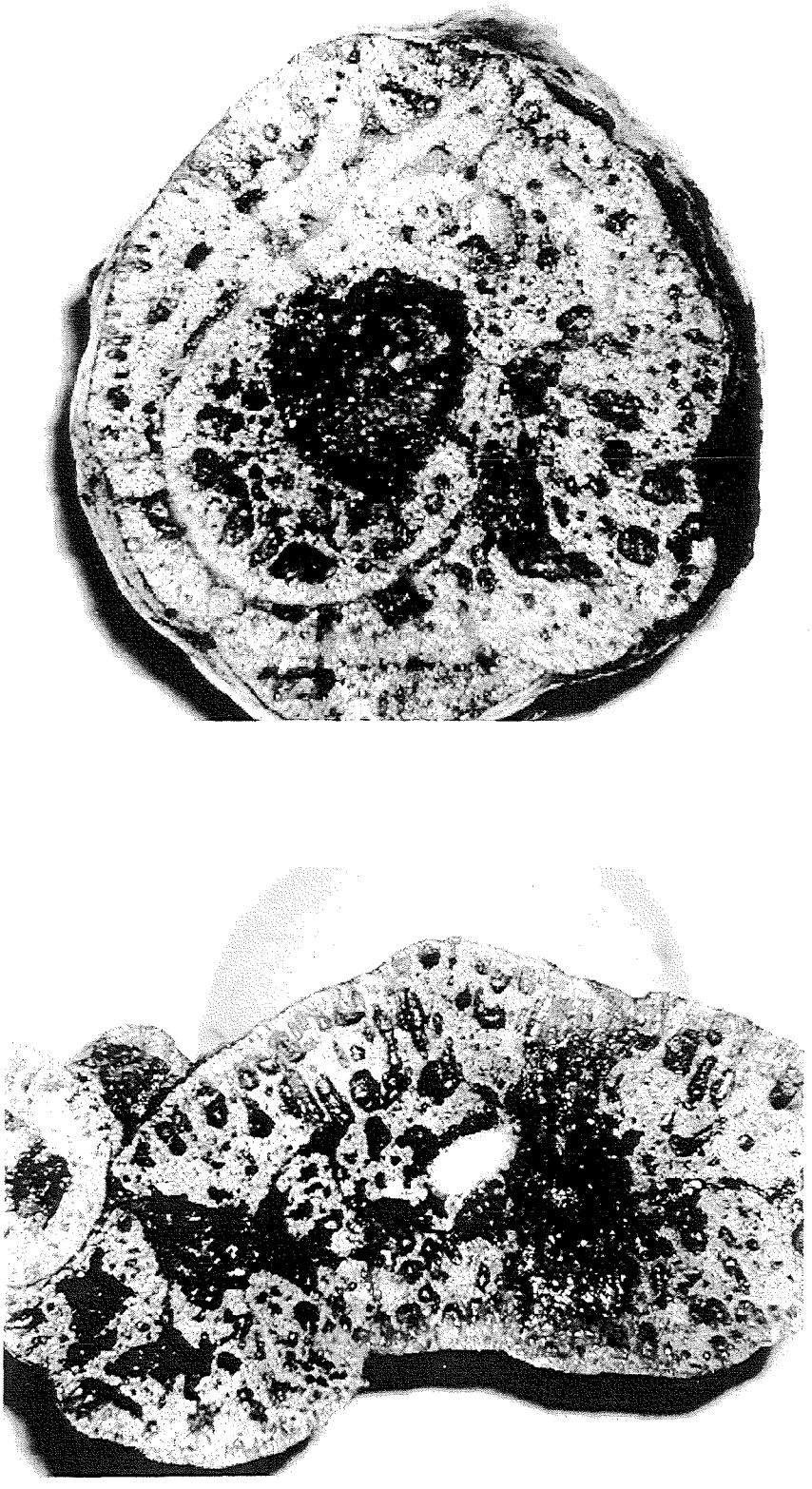

Fig. 3.3;5 Cross-sectional View on Typical Large Debris

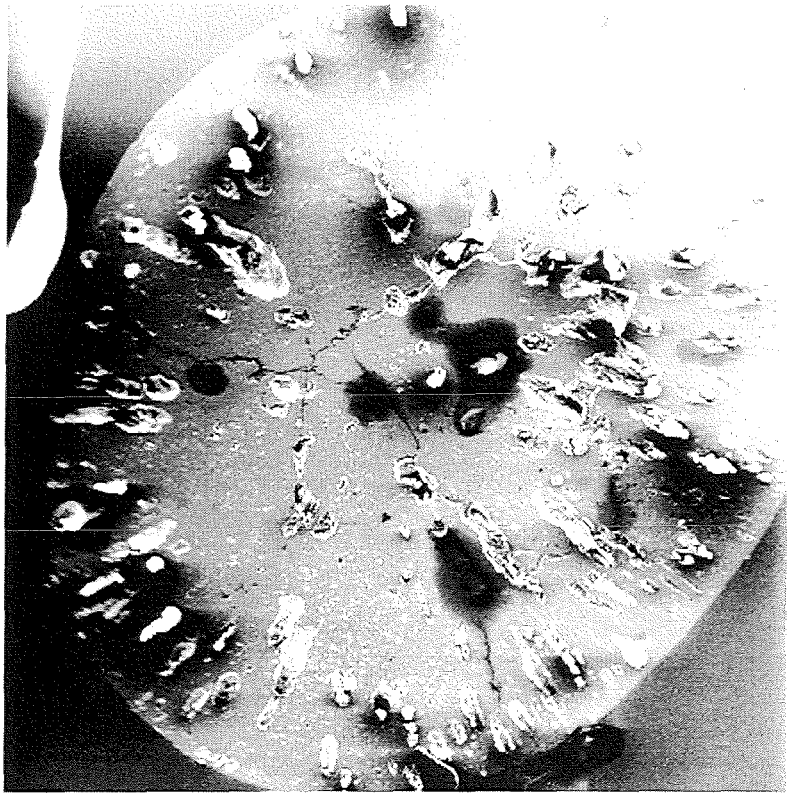

Fig. 3.3;6 Cross-section of a 8 mm Particle

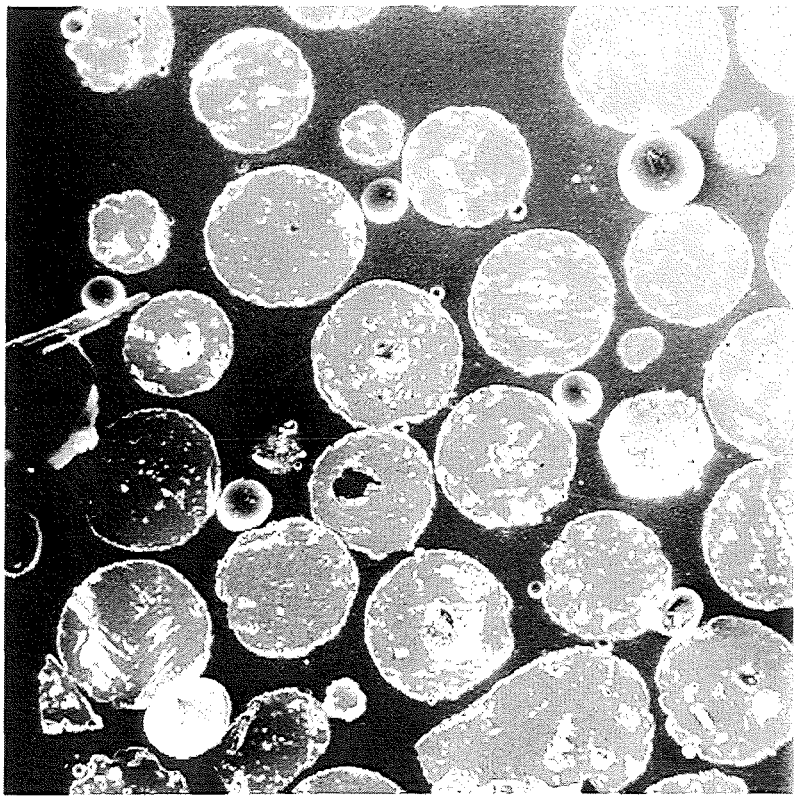

Fig. 3.3;7 Cross-section of 200 µm Particles

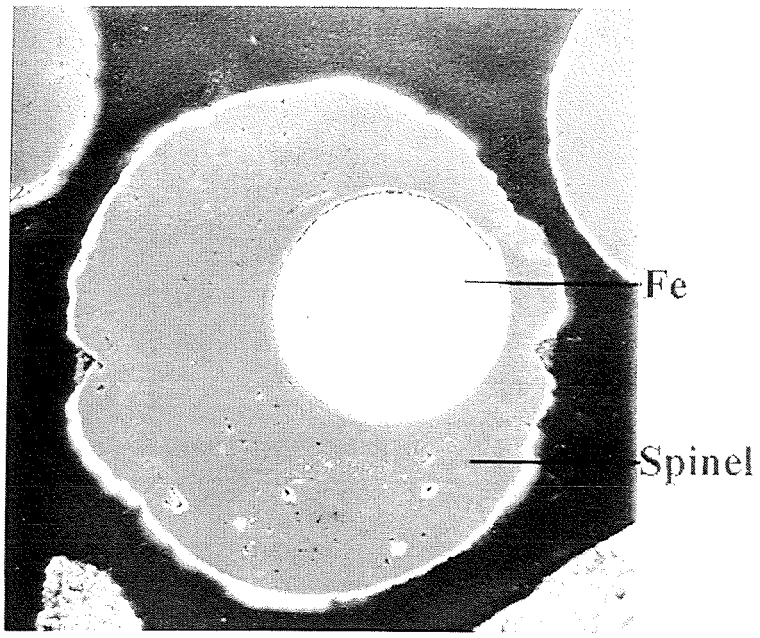

Fig. 3.3;8 Small Debris (180 µm) with Iron Core

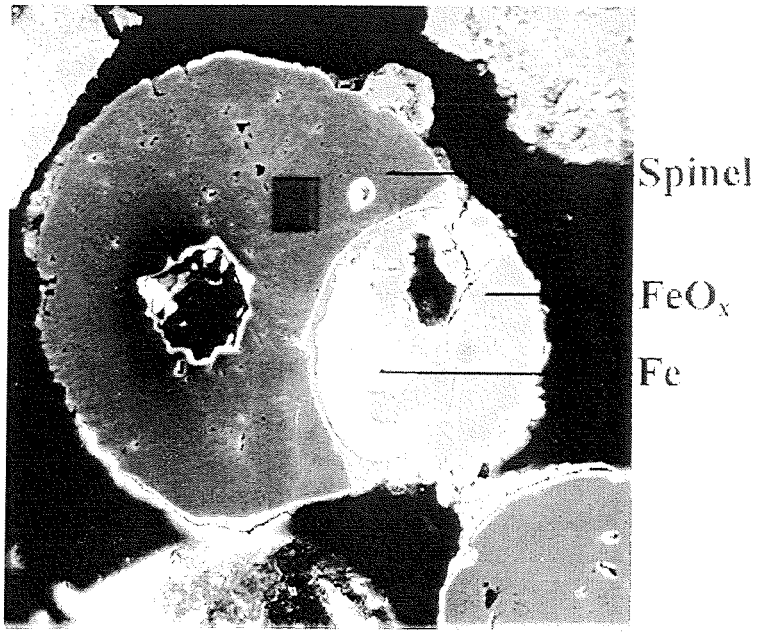

Fig. 3.3;9 Small Debris (180 µm) with partly oxidized iron on the edge

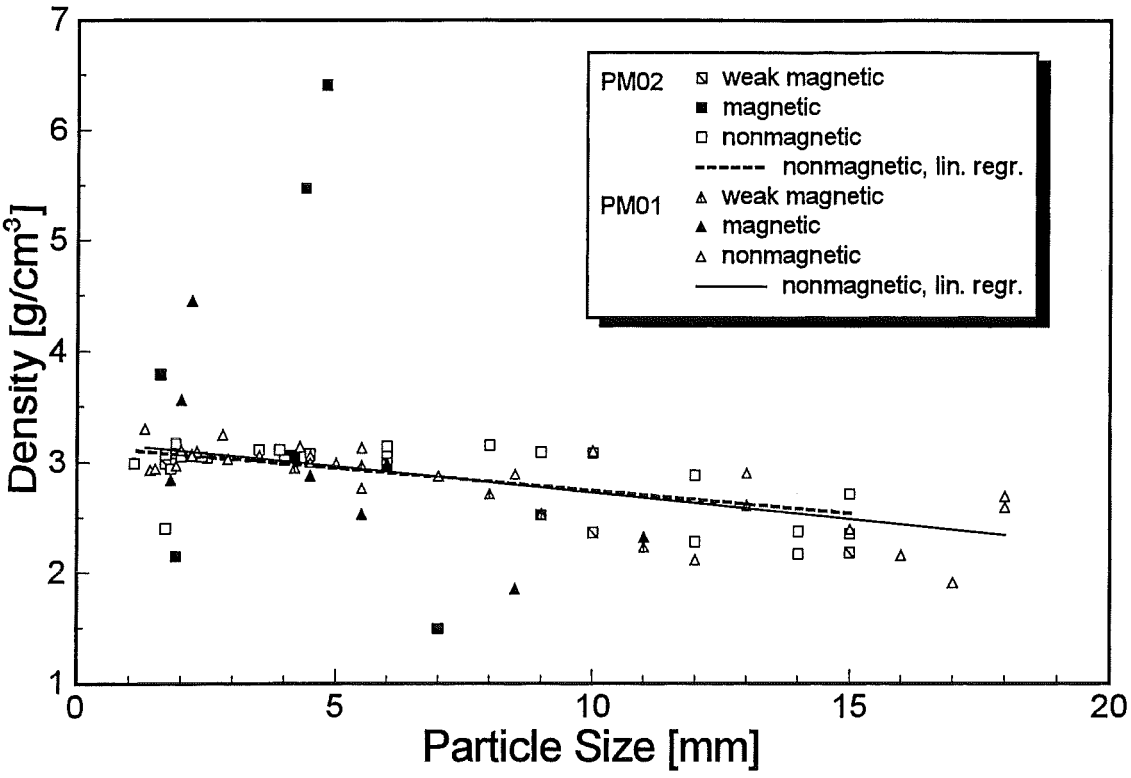

Fig. 3.3;10 PM01/02: Post-test Density of the Debris

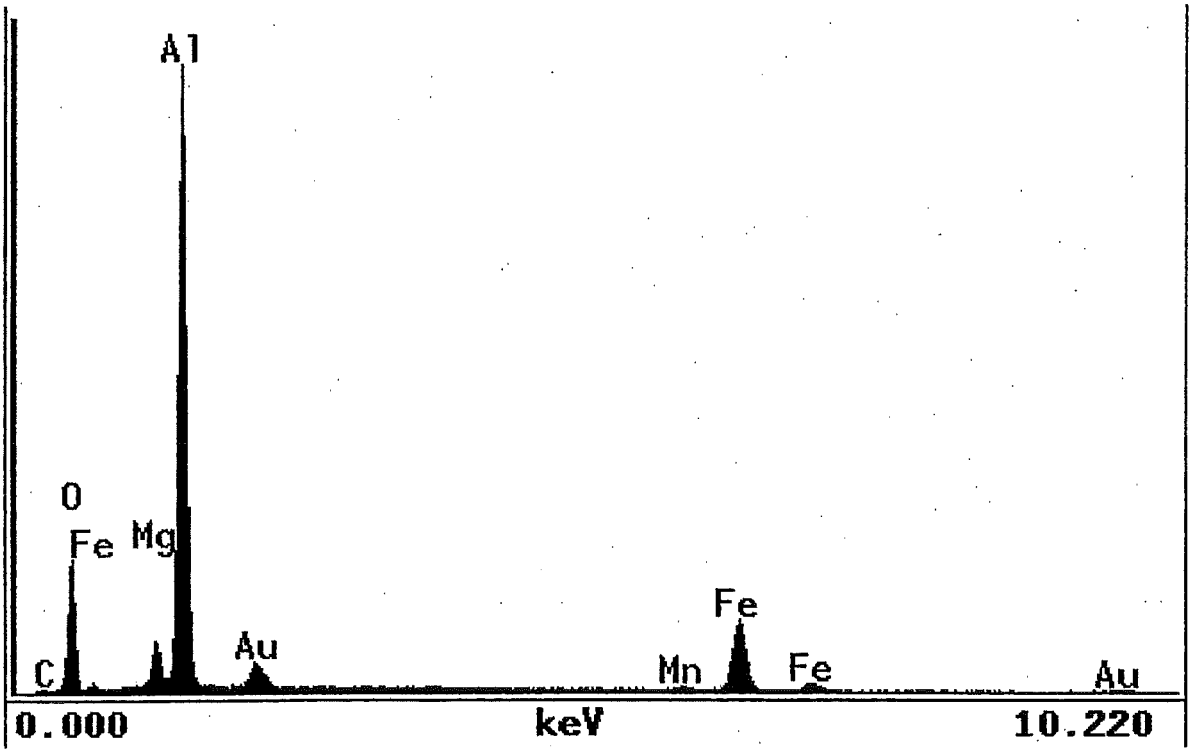

Fig. 3.3;11 EDX Spectrum of PREMIX Debris

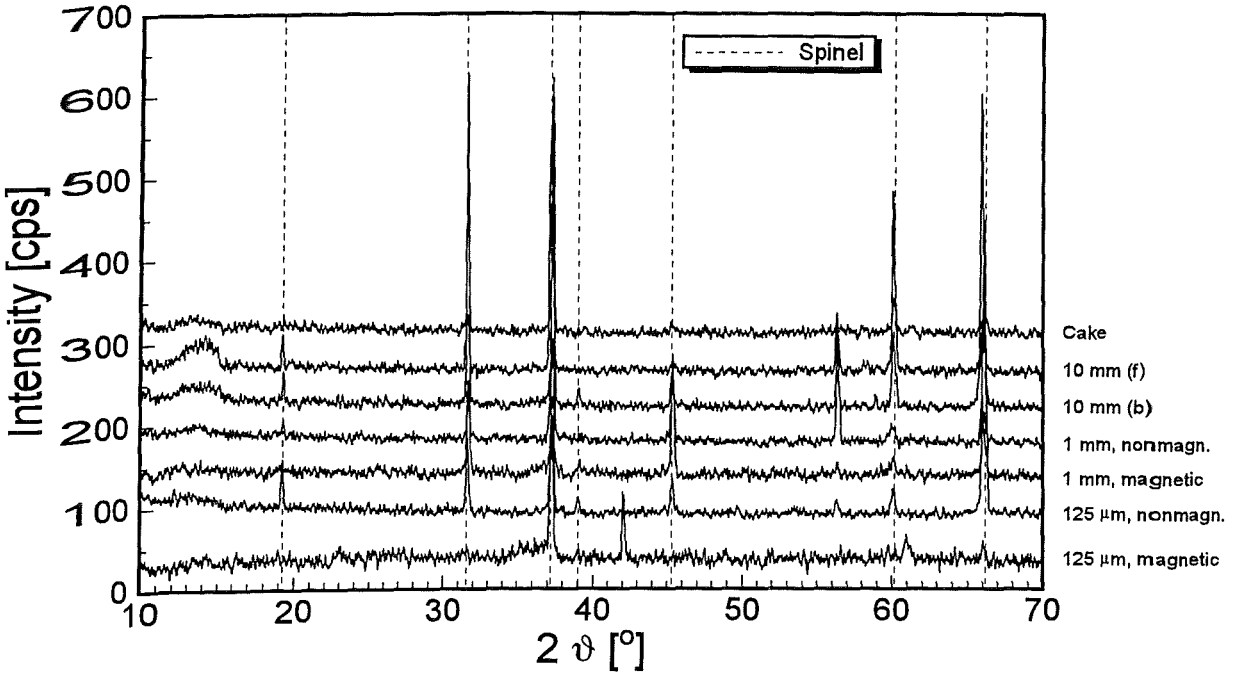

Fig. 3.3;12 PM01: X-ray Diffraction Pattern of Oxidic Debris

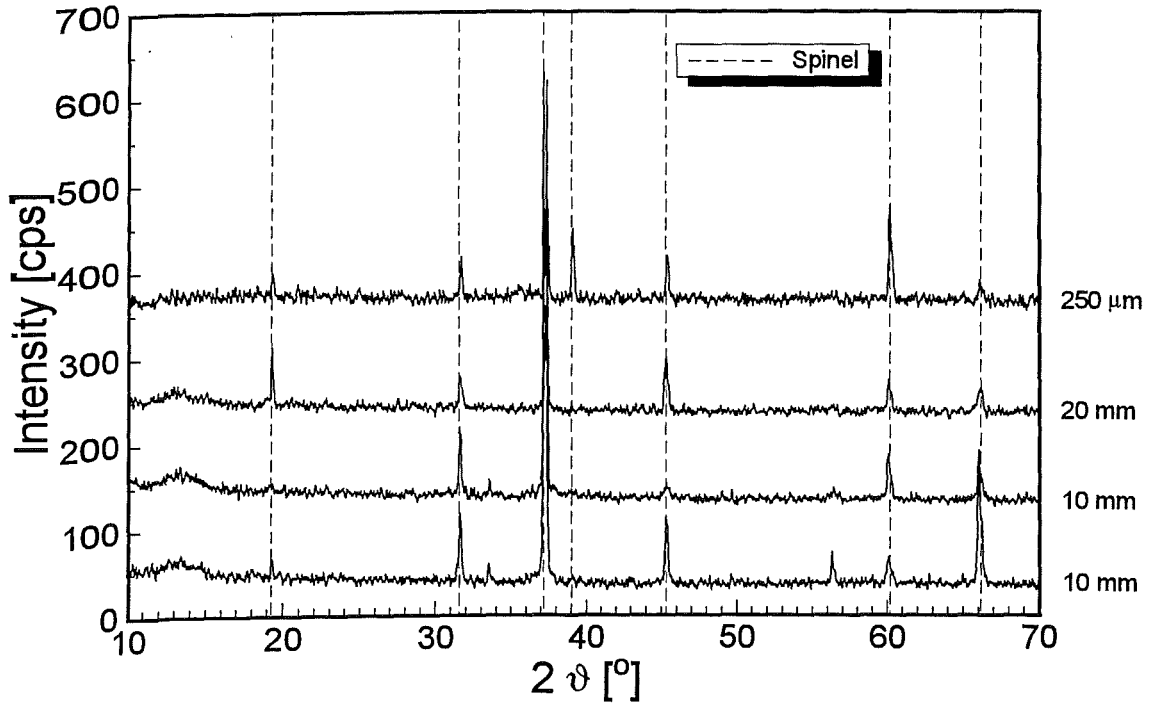

Fig. 3.3;13 PM02: X-ray Diffraction Pattern of Oxidic Debris

Appendix A:

Calibration of measuring devices

1. Flow meter

Flow meters of the vortex type were chosen to measure the steam flow rate in the venting pipes. We believe that this measuring principle has essential advantages:

-It is fast acting;

-it does not matter whether gas, steam, or water is flowing because it is a velocity meter;

-its pressure drop is negligible in case of steam or gas flow.

Unfortunately, it turned out that the measuring principle, i.e. the characteristics of vortexes, is seriously disturbed if a single-phase flow changes into a two-phase-flow.

To check the performance in case of a fast change in flow rate, one of the flow meters was connected to a vessel by a tube of the same diameter as the venting tubes. The tube and the vessel were separated by a burst disk whose rupture pressure was 1 bar.

The pressure of the vessel was increased. When the burst pressure was exceeded, a sudden gas discharge occurred. The respective flow meter signal was integrated over time and compared to the time history of the volume/pressure ratio. The results are reported in reference 7. The error of the flow measurements, under the conditions of the PREMIX tests, is estimated to be within -10%.

2. Level indicator

The four level indicators were calibrated at regular intervals: the water level was increased stepwise and the output was compared to the reading of a ruler. The relation was found to be linear.

3. Pressure transducers:

The pressure transducers generally used in the PREMIX tests are of the piezoelectric type: Pressure changes produce a proportional electrical charge. This implies that static pressures can not be measured. The reason is that the charge is reduced with time due to the finite insulation resistances. Usually, the "short" parameter setting is used. By this setting, a well defined resistance reduces the charge at a rate that also depends on the pressure range setting.

The measurements obtained during the first three tests gave rise to doubts whether the settings were correct to account for the actual test conditions. Consequently, three separate tests on the transient behaviour were performed.

a) Integral test

The pressure transducers were checked in situ and the parameter setting as in test 1-3 was applied. The venting pipes were closed, one of them by a burst disk, and the empty test vessel was pressurised. The pressure time history after burst of the disc was measured and compared with the calculated pressure decrease. The measurement was too low by a factor of 4. This result should be assessed with regard to the larger volume used for the test whose time constant, about 2.4 Hz, is much larger than that given in the PREMIX tests. The research was continued by varying the time constant in a large range (see item b below).

b) Small volume container test

A small container was built and the pressure change was obtained (a) by reducing the setting of a pressure controller, (b) by opening a valve completely, (c) by opening it to about one half. These conditions correspond to three time constants, 5, 0.03 and 0.5 Hz. Three different amplifier settings (long, medium and short) complete the test matrix. The results are listed in the table below:

	5 Hz	0,5 Hz	0,03 Hz
long	perfect	good	sufficient
medium	good	15 % error	20 % error
short	20 % error	insufficient	bad

c) Calibration with pulsating pressures

Another measuring device was built consisting of a small container filled with oil and equipped with a piston, which could be operated by an electric motor. The piston was moved with a frequency that varied between 9 and 40 Hz. For comparison, a strain gauge pressure tranducer was used additionally. It was found, that the "long" and "medium" settings produced satisfactory results for the whole range of frequencies investigated, whereas the "short" setting produced results that were too small by about 20%.

The frequency of pressure measurement in tests PM01 to PM03 was found to be in the size range of 15 Hz. Therefore, it was decided to run the follow-on experiments

with "medium" or "long" settings. One piezo pressure transducer was replaced for comparison by a strain gauge transducer. To get an idea about the error made in the preceding experiments, one of the piezos was operated with a "short" setting. The result for PM05 is given in Fig. A1. Obviously, the pressure readings are equal in size in the initial period of time (the signals were shifted to zero level at time zero). From 0.3 s on, they start to diverge. Part of the differences may be due to the different axial positions. Under the assumption that the strain gauge reading is correct, the piezo gauges will have an error of about 10%.

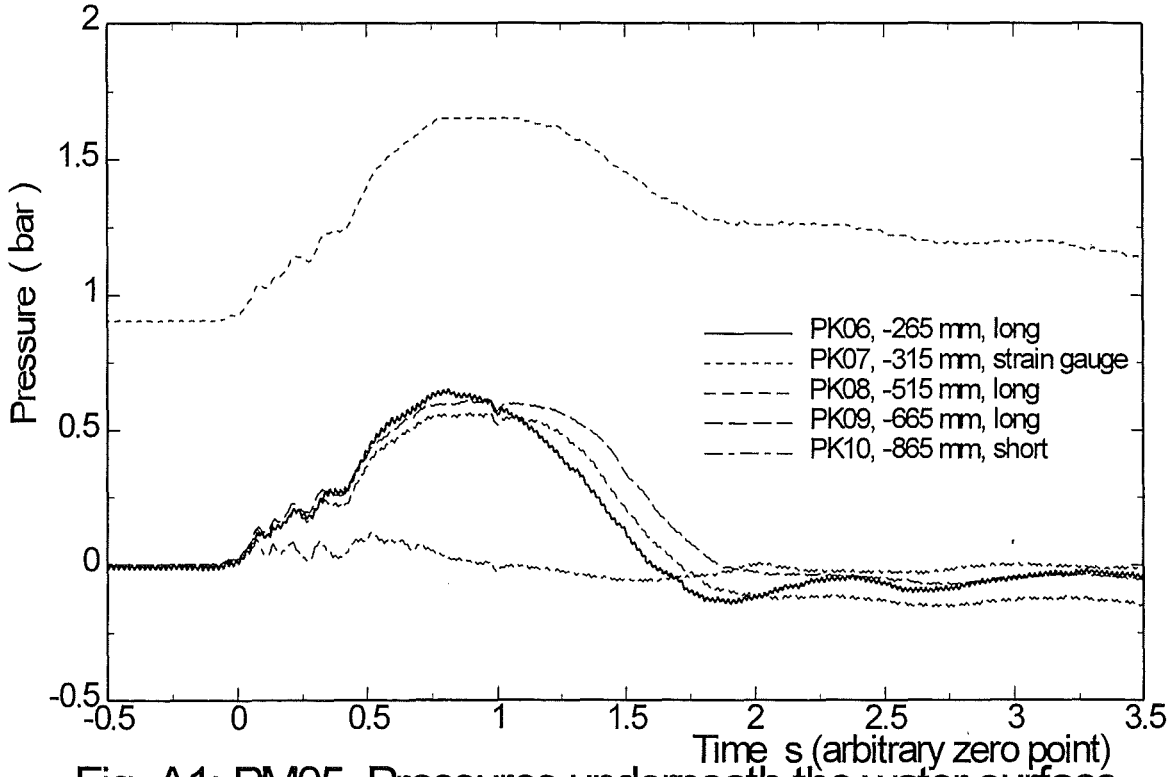

Fig. A1: PM05, Pressures underneath the water surface

DRUCK6 | 8.2.1996

Appendix B:

Balance of the Masses Involved in the Thermal Interaction

This appendix is an extended contribution to the data evaluation procedure described in section 2.6.2. Thereby, a comprehensive deduction of eq. (2) is given.

The interaction region, as defined in the section mentioned before, starts to form in the water pool after the first contact of the melt and water. Its volume can be regarded as composed of three partial volumes:

$$V_I = V_{\ell,I} + V_{v,I} + V_{m,I}. \tag{B1}$$

The partial volumes refer, in the above sequence, to the liquid, the vapour (here: steam), and the melt. The volume of the interaction region, V_I, can be obtained from the measurements. Two of the partial volumes, $V_{v,I}$ and $V_{m,I}$, can be determined from the measurements as described below. Thereby, $V_{\ell,I}$, the partial volume of the liquid, can also be calculated.

The ***partial volume of the vapour***, $V_{v,I}$, is calculated from a mass balance where the masses involved in the interaction are regarded. The control room of the balance comprises the whole water volume, the melt provided by the melt generator, and the steam within the gas compartment. The latter is defined to cover the whole gaseous space above the initial water surface up to the location of the flow meters. The sum of the masses prior to the test is:

$$\sum m = m_\ell^0 + m_{v,G}^0 + m_m, \tag{B2}$$

where the superscript 0 means the condition for t=0. Application of the relation $m = V \cdot \rho$ to eq. (B1) results in

$$\sum m = V_\ell^0 \cdot \rho_\ell + V_{v,G}^0 \cdot \rho_v + V_m \cdot \rho_m. \tag{B2a}$$

For time t>0, part of the water evaporates. Both the masses of the liquid and the steam become a function of time and the mass balance provides the relation:

$$\sum m = m_\ell + m_{\ell,I} + m_{v,I} + m_{v,G} + m_{v,exit} + m_m \tag{B3}$$

The meaning of the summands is:

- m_ℓ is the mass of the water outside of the interaction region;

- $m_{\ell,I}$ and $m_{v,I}$ are the masses of the water and the steam, respectively, inside the interaction region;
- $m_{v,G}$ is the mass of steam in the gas space. It diminishes with time due to the growth of the interaction region;
- $m_{v,exit}$ is the integrated steam mass measured at the venting tubes.

The volume of the mass m_ℓ in eq. (B3) is calculated as the initial water volume plus the water level increase times the vessel cross section minus the interaction volume (compare also Fig. 2.4):

$$V_{\ell,pool} = V_\ell^0 + \Delta L \cdot A_V - V_I . \tag{B4}$$

Introducing the densities in eq. (B3) results in:

$$\sum m = (V_\ell^0 + \Delta L \cdot A_V - V_I) \cdot \rho_\ell + V_{\ell,I} \cdot \rho_\ell + V_{v,I} \cdot \rho_v + V_{v,G} \cdot \bar{\rho}_v + V_{v,exit} \cdot \rho_v + V_m \cdot \rho_m \tag{B3a}$$

Eqs. (B2a) and (B3a) are equated while also considering eq. (B1) and taking into account that the quotient $\rho_v / \rho_\ell << $. One obtains, after some conversions, an equation for the partial volume of the vapour:

$$V_{v,I} = \Delta L \cdot A_V - V_{m,I} + V_{v,exit} \cdot \frac{\rho_v}{\rho_\ell} + \left[V_{v,G} \cdot \frac{\bar{\rho}_v}{\rho_\ell} - V_{v,G}^0 \cdot \frac{\rho_v}{\rho_\ell} \right] \tag{B5}$$

The two terms summarized in brackets constitute the change in steam volume in the gas room. The value of the difference is comparatively very small and, therefore, eq. (B5) is reduced to the following equation:

$$V_{v,I} = \Delta L \cdot A_V - V_{m,I} + V_{v,exit} \cdot \rho_v / \rho_\ell , \tag{B5a}$$

The (total) melt volume, V_m, disappears during the above conversions. Instead, the ***partial volume of the melt***, $V_{m,I}$, comes into consideration in eq. (B5a). Since the melt flow rate can not be measured in the experiments, it is approximated in the evaluation by an analytical function of time of fourth degree. This function which gives the integrated volume of the melt that has entered the interaction region is used in the MATHCAD evaluation procedure (see Appendix C).

The partial volume of the vapour in the interaction region can now be calculated by use of eq. (B5a) and thereby also the ***partial volume of the liquid water*** from eq. (B1).

Appendix C:

The MATHCAD evaluation procedure

The evaluation program was written by use of the MATHCAD computer software in the frame of MS Windows. The input data which originate from a multitude of fast measuring probes are being processed by algorithms and finally combined to gain information of a higher grade. Thereby, the following information is evaluated:

(1) Progression of the boundary of the multi-phase interaction zone into the water pool, drawn in r-z coordinates with the time as a parameter.

(2) The time histories of the (total) volume of the interaction region, of the partial volumina, and of the respective volume fractions.

(3) The velocities of the axial and radial fronts (the latter taken at maximum radius) of the interaction region.

(4) The time history of the mechanical work $\int pdV$.

(5) The local (vapour) void distribution within the interaction region for constant times (optional).

The following measurements are used as input data: void and temperature signals, the water level increase, the flow rate of the steam escaping through the venting pipes, and the pressure obtained in the water pool. The melt flow rate can not be measured in the tests. Instead, various other measurements and pieces of information, like the mass of the debris collected after the test, the course of the driving pressure, and film pictures, are considered in the construction of an approximated function which is taken as an input. The procedures concerning items 1 and 2 which provide the most important information are explained in the following sections.

1. Development of the multi-phase interaction zone. The void signals are checked for indicating the first changes in phase, i.e. from water to steam in the water pool and, vice versa, in the gas space. This is made in a separate procedure advancing the main evaluation procedure. By that, a matrix is formed which contains three columns: the r-z coordinates and the "switch" times of the void sensors. From these data, a p(r,z) function is calculated by use of the regression method. A third order polynominal expression is obtained, whose coefficients are determined by the least square method. The p(r,z)

function and the water level function L(z) are combined in a third S function which provides contour plots in an r-z diagram with the time as a parameter as shown in Fig. C1(a). In a first approximation, all measurements are taken into account. In fact, three of the eight lances considered in the evaluation are mounted at different azimuthal positions. By omitting the data of the one or the other of these lances in the evaluation, one obtains a measure for the unsymmetry in the development of the interaction region. This work is part of an error analysis which has not been completed yet.

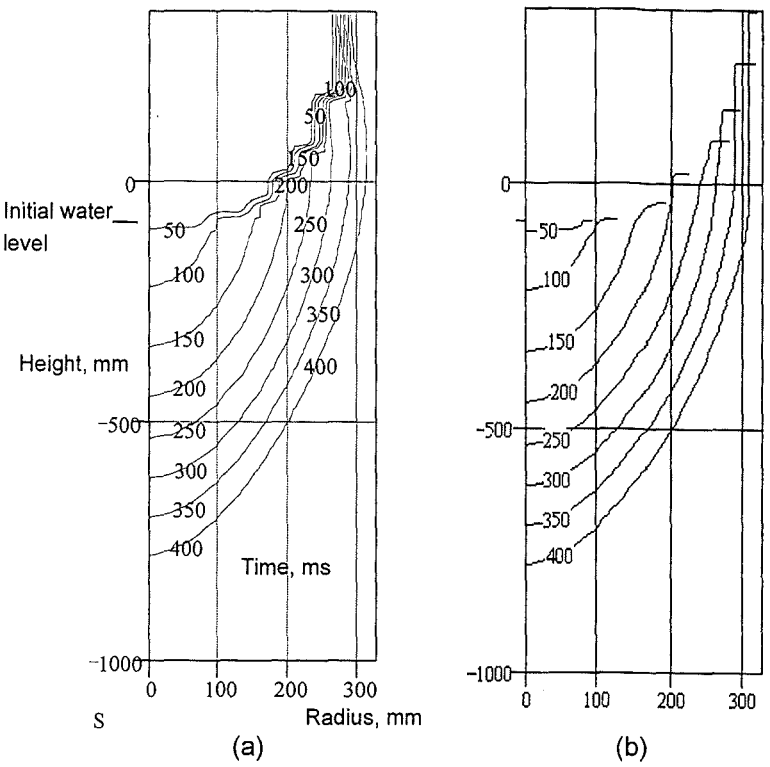

Fig. C1: Development of the interaction region (PM04); (a) MATHCAD graph, (b) corrected version.

As one can see in Fig. C1 (a), the outcome gives a partly incorrect picture of the interaction boundary lines, namely in the parts that proceed from the actual water level into the gas space. This behaviour lies in the evaluation procedure that does not allow for an intersection of lines. A correction was made by use of the PAINTBRUSH software. The upper ends of the isochrones were made consistent with the actual coordinate of the water level which is sketched as a short horizontal line (Fig. C1 (b)). Because this procedure is rather time consuming, we prefer another procedure which also uses both the p(r,z) function and the water level measurement and provides single diagrams in r-z coordinates for constant times (cf. Fig. C2). The goal of the effort is to put together the various boundary lines in one diagram.

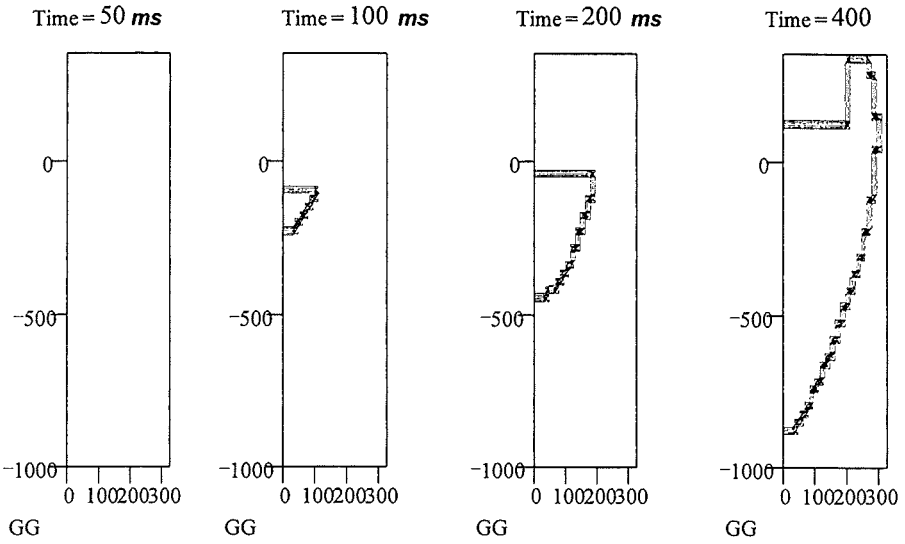

Fig. C2: Development of the interaction region depicted in a series of single pictures

2. Volumes of the interaction region. The development of the (total) volume of the interaction region, V_I, is calculated from the function p(r,z) taking also into account the water level rise. Considering rotational symmetry, the volume of the interaction region is calculated at discrete times $t = t_k$ (k = 1 ... 20) as follows:

$$V_{I,k} = 2\pi \int_{H_{max}}^{Z_{max}} \int_{0}^{R_{max}} p_k(r,z) \cdot r \cdot dr \cdot dz ,$$

where H_{max}, Z_{max}, and R_{max} are the coordinate of the water level at time t_{max}, the depth and the maximum radius of the water pool, respectively. In the evaluation procedure, the double integration is replaced by a double summation across the numerical model which consists of i = 10 radial and j = 50 axial nodes. Time t_{max} is the maximum evaluation time (here: 400 ms); the function p_k is unity if the respective geometrical conditions (position inside the interaction region) is satisfied.

The partial volumes of the interaction region, $V_{v,I}$, $V_{\ell,I}$, and $V_{m,I}$, are calculated as outlined in Section 2.6.2. The procedure is illustrated in the following.

The *partial volume of the vapour (here: steam)*[1] in the interaction region, $V_{V,I}$, is calculated using to the following equation:

$$V_{v,I} = \Delta L \cdot A_V - V_{m,I} + V_{v,exit} \cdot \rho_v / \rho_\ell ,$$

[1] the index "v" for vapour is used here to meet common practice

(cf. eq. (2.2) in section 2.6.2). The summand that accounts for the gas room volume is not taken into consideration here because its contribution to the mass balance is negligible. The three summands on the right hand side of the above equation are calculated as follows:

(1) $\Delta L \cdot A_V$ is the product of the water level increase and the cross section of the test vessel.

(2) *The melt volume,* V_m. Since the melt outlet flow rate can not be measured in the experiment, an approximation is used in the evaluation. An analytical function of fourth degree gives the (integrated) volume of the melt that enters the interaction region (see Fig. C3). The characteristics of this function are largely in agreement with the information gained from the experiments: (i) a small inclination at the beginning ($f'(0) > 0$) that accounts for the spray-type of melt release; (ii) the total volume released at time $t = t_e$; (iii) the reversal point is at about half of the time of outflow.

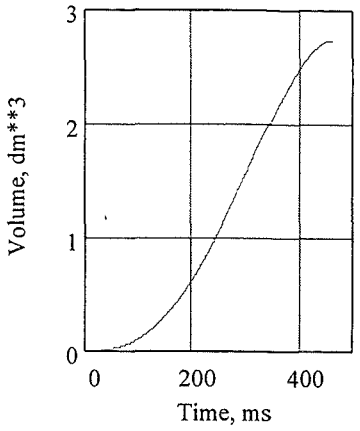

Fig. C3: Flow of the melt

(3) *The volume of the vapour that has left the test vessel.* The volume is obtained by integrating the flow rate. It is multiplied by the density ratio.

The *partial volume of the liquid* contained in the interaction region, $V_{\ell,I}$, is calculated as the difference between the total volume and the sum of the vapour and melt volumes:

3. Volume fractions The (average) volume fractions are obtained by relating the respective partial volumes to the total volume of the interaction region. An example is given in Fig. C4. Note that all curves shown start at time 1 ms.

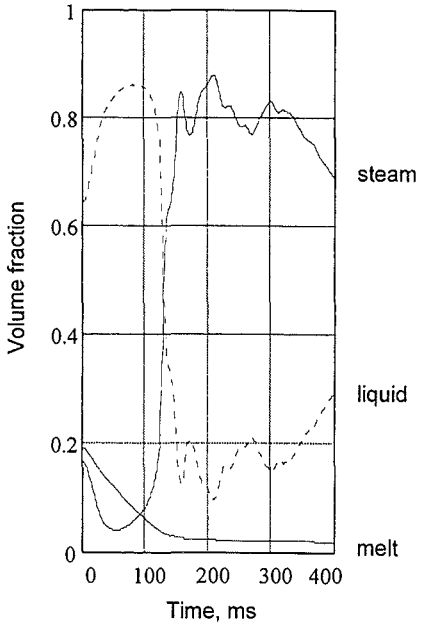

Fig. C4: Volume fractions inside the interaction region (PM02)

Appendix D:

Some aspects of the melt generation procedure

As already mentioned in section 2.1, there are three melt detectors positioned along the axis of the melt release nozzle (D1 - D3, see Fig. 2.2), whose signal rises are used to trigger various actions, such as operating the valves of the gas supply system or starting the high-speed cameras and the transient recorders. Two detector positions are somewhat above the foil which separates the thermite compartment from the gas space, one position is at the lower end of the melt release nozzle. In tests PM01 to PM05, each of the detectors consisted of a pair of thermocouples.

Normally, a time lag of 1 to 2 seconds is expected to occur between the trigger signals of D2 and D3. This happened in tests PM01 to PM04. In test PM05, the trigger signals occurred within only 1 ms. It was therefore concluded that, in this case, the front of chemical reaction did not progress evenly across the nozzle length. Probably, the front was both funnel-shaped and non-symmetric and its peak passed the melt detectors some distance apart. As a result of this, the D2 trigger signal came delayed and the high speed cameras, which have a starting time of about half a second, could not record the initial phase of thermal interaction. Moreover, the video recording failed in test PM05, too.

This chain of unexpected events initiated several small separate tests in which thermite reactions were performed in glass tubes. These tests confirmed the probability of a channelwise progression of the thermite reaction. At the same time, improvements were tested to prevent such an incident. As a first consequence of this investigation, the thermocouples of the D2 and D3 detectors were replaced by an improved detecting system consisting of a grid of wires that covered the whole nozzle cross section.

Our experience can be summarized as follows: The new detector device ensures the punctual starts of the high-speed cameras and transient recorders. In case of a funnel-shaped progression of the melt front, which can not be excluded to occur, the foil in the outlet nozzle melts locally and unreacted thermite may be discharged together with the melt. Presumably, this was the case in test PM04 also; the reason could not be recognized at that time.